STRUCTURAL AND MAGNETIC STUDIES OF SELECTED RARE EARTH INTERMETALLICS

Duane Ray McNeely
B.S., University of Puget Sound, 1970
M.S., Oregon Graduate Center, 1972

A thesis submitted to the faculty
of the Oregon Graduate Center
in partial fulfillment of the
requirements for the degree
Doctor of Philosophy
in
Physics

October, 1976

This thesis has been examined and approved by an Examination Committee:

Hans Oesterreicher, Thesis Advisor
Associate Professor
University of California San Diego - La Jolla

Douglas F. Barofsky
Associate Professor

Thomas M. Loehr
Associate Professor

Lynwood Swanson
Professor

ACKNOWLEDGEMENT

I respectfully acknowledge the guidance of my advisor Dr. Hans Oesterreicher and my examining committee chairman Dr. Douglas F. Barofsky. Since Dr. Oesterreicher moved to the University of California, San Diego, Dr. Barofsky has provided unlimited assistance and encouragement throughout the completion of this manuscript.

The literary and professional guidance of Dr. Thomas M. Loehr and Dr. Lynwood W. Swanson was also greatly appreciated.

I would like also to thank the other members of my examining and ad hoc committes. Drs. Richard A. Elliot, George P. O'Leary, Gerald J. Throop, Roger Eiss and Michael A. Gray.

I lovingly thank my wife, Victoria J. McNeely for her encouragement and endless hours of typing on the original drafts of this manuscript.

My final thanks is to Mrs. Beverly J. Kyler for preparing this manuscript in its final form.

TABLE OF CONTENTS

LIST OF FIGURES

LIST OF TABLES

ABSTRACT

Various $R_x(T,E)_y$ and $(R,E)_xT_y$ alloys are studied, where R is Yttrium or a rare earth element, T is a 3d transition metal and E is an element to be substituted for either R or T. These alloys were studied with respect to structural stability, magnetic hardness and saturation magnetization. In the case of $Sm_{.105}Fe_{.895-x}Al_x$ with x = 0.0 to 0.5, the Curie temperature (T_c) versus composition was investigated.

The ternary compound $Sm_{.167}Co_{.683}E_{.15}$ showed highly energetic domain walls of atomic dimensions when E is Si. The coercive field in this material (H_c) at 4.2°K is 30 kOe for bulk materials and 28.5 kOe for powdered materials. The substitution of Ni or Cu for Co in $SmCo_5$ yielded relatively high values for H_c while substitution of Ag or In produced low values of H_c. E = Pt or Au failed to stabilize the $CaCu_5$ structure. Replacing Sm in the lattice of $R_{.167}Co_{.633}Al_{.20}$ by Ce and Tb produced low values of H_c. Partial replacement of Sm by Zr according to $Sm_{.167-x}Zr_xCo_{.833}$ to x = .134 showed both a decrease in H_c and the anisotropy field (H_a).

Within the Dy-Fe-Al ternary system, $Dy_{.25}Fe_{.75-x}Al_x$ to x = .30, $Dy_{.207}Fe_{.793-x}Al_x$ to x = .20 and $Dy_{.105}Fe_{.895-x}Al_x$ to x = .4475 were studied. A Curie type low dependence of H_c versus temperature was observed in the $Dy_{.25}Fe_{.75-x}Al_x$ compounds. At high Al

substitution for T in these materials increasingly energetic, thin domain walls were observed from the 1:3 to the 2:17 alloys. The highest H_c was found in $Dy_{.105}Fe_{.4475}Al_{.4475}$. Through extrapolation this field was estimated to be ~ 60 kOe. The pseudobinary $Dy_{.25}Fe_{.75-x}Al_x$ indicated a phase transformation at x = .15 from the $PuNi_3$ isotype to the $CeNi_3$ structural type. The Th_2Ni_{17} structural type showed a narrow region of stability in the $Dy_{.105}Fe_{.895-x}Al_x$ pseudobinary with the Th_2Zn_{17} isotype stable on both sides of this region.

The two pseudobinaries, $Sm_{.105}Fe_{.895-x}Al_x$ to x = .5 and $Sm_{.105-x}Zr_xCo_{.895}$ to x = .04 were also studied. These both stabilized the Th_2Zn_{17} type structure. As in the case of $SmCo_5$ with Sm replaced by Zr, the 2:17 alloys exhibited disappointingly low values of H_c. The $Sm_{.105}Fe_{.895-x}Al_x$ alloys, on the other hand, showed a tendency towards moderately energetic domain walls, and an H_c = 15 kOe in both the bulk and powdered materials was observed. Investigation revealed an initial increase in T_c up to 20 atomic percent of Al in $Sm_{.105}Fe_{.895-x}Al_x$ with a subsequent decrease in T_c upon further Al substitution.

The structural stabilities of the compounds investigated were considered on the basis of geometrical and deformable sphere packing factors. The nearest neighbor diagram is developed with respect to these factors. The role of the Ruderman, Kittel, Kasuya and Yosida (RKKY) exchange interaction in describing the magnetic properties of these alloys is also considered.

CHAPTER I

INTRODUCTION

This study is concerned with structural and magnetic parameters in multicomponent systems based on elements of the rare earth and 3d transition metal groups. Emphasis is mainly given to questions of phase stability, magnetic exchange and magnetic hardness. Some aspects of this work have relevance towards improving the technology of modern permanent magnets.

Interest in the rare earth based alloys began when it became technically possible to obtain the rare earth elements in pure form. Although some work was done with the rare earth elements prior to the late 1950's, the major contributions towards their alloy development began in 1959. The pioneering work of Nesbitt et al.[1] pointed out the antiparallel spin alignment of Gd and Co in the various Gd-Co alloys of their investigation. This antiparallel spin coupling is referred to as a ferrimagnetic coupling since the magnitude of the total Gd and Co magnetic moments are different. Hubbard et al.[2] in 1960 noted a high coercive field for $GdCo_5$ which they attributed to a large anisotropy field. In 1966 Hoffer and Strnat[3] confirmed the technological potential of the RCo_5 compounds and, thus, initiated the pursuit of the rare earth, hard, magnetic alloys.

With these new materials many possible applications are being found, including permanent field motors and generators, cavities for

microwave devices, memory storage in computers and magnetic tapes. Since some of these devices may be operated at cryogenic temperatures, accumulation of information about the low temperature characteristics of magnetic materials is of interest.

A compound is considered a stable phase when it is identified as being of one structural type. Phase stability is not completely understood, and one must rely on the guidelines of experience and intuition. The metallic phases encountered in this study are strongly influenced by the electron concentration (e.c.) per atom as related to the conduction bands and to a lesser extent by the electrons below the Fermi surface. The e.c. is related to cohesion occurring in these alloys, and when the e.c. is coupled with the relative size of the atoms present, a nondirectional bonding effect is seen as the controlling factor. The influence of the 3d transition metals' (T) and the 4f rare earth metals' (R) electrons below the Fermi surface are of a directional nature. The combined effects of the nondirectional and directional bonds and the influence of an electron rich third constituent on these bonds are exemplified in the following chapters.

With regard to magnetic hardness and exchange there are three important properties to be considered: (1) the coercive field (H_c), (2) the saturation magnetization (M_s) and (3) the ordering or Curie temperature (T_c). Each of these parameters will be considered individually and then they will be discussed collectively from the point of view of simultaneously optimizing all three within a given alloy.

The coercive field, (H_c), is that shown in Figure 1 where the magnetization of a previously saturated material is zero. This is more an empirical than a fundamental parameter. The anisotropy field, (H_a), however, is of a fundamental nature. This parameter is a measure of the field necessary to rotate the magnetic moments from their aligned axis within a given structure by 90°. In a material where the nucleation of a domain or Block wall is not possible, H_c may be equivalent to H_a.

Recent discoveries in this laboratory have shown that substitution of an electron rich, nonmagnetic element in a magnetic lattice can increase H_c.[4,5] For instance, substitution of Al for Co in $SmCo_5$ results in a material of higher H_c while also maintaining a high value of H_a.[4] Such materials are known to have very thin and highly energetic domain walls.

The saturation magnetization, (M_s), is also shown in Figure 1. M_s is the asymptotic value of the magnetization (M). It is found experimentally by an extrapolation of M to infinite fields. This procedure is discussed further in Chapter 2. M_s is also found through neutron diffraction studies. None of the materials studied in this work were subjected to neutron diffraction; however, reference to it in other investigations will be made where comparisons are of value.

The magnitude of M_s relates to the coupling scheme of atoms within the solid. There are three principal classes of interactions consistent within the alloys of the current study: (1) R-R, (2) R-T

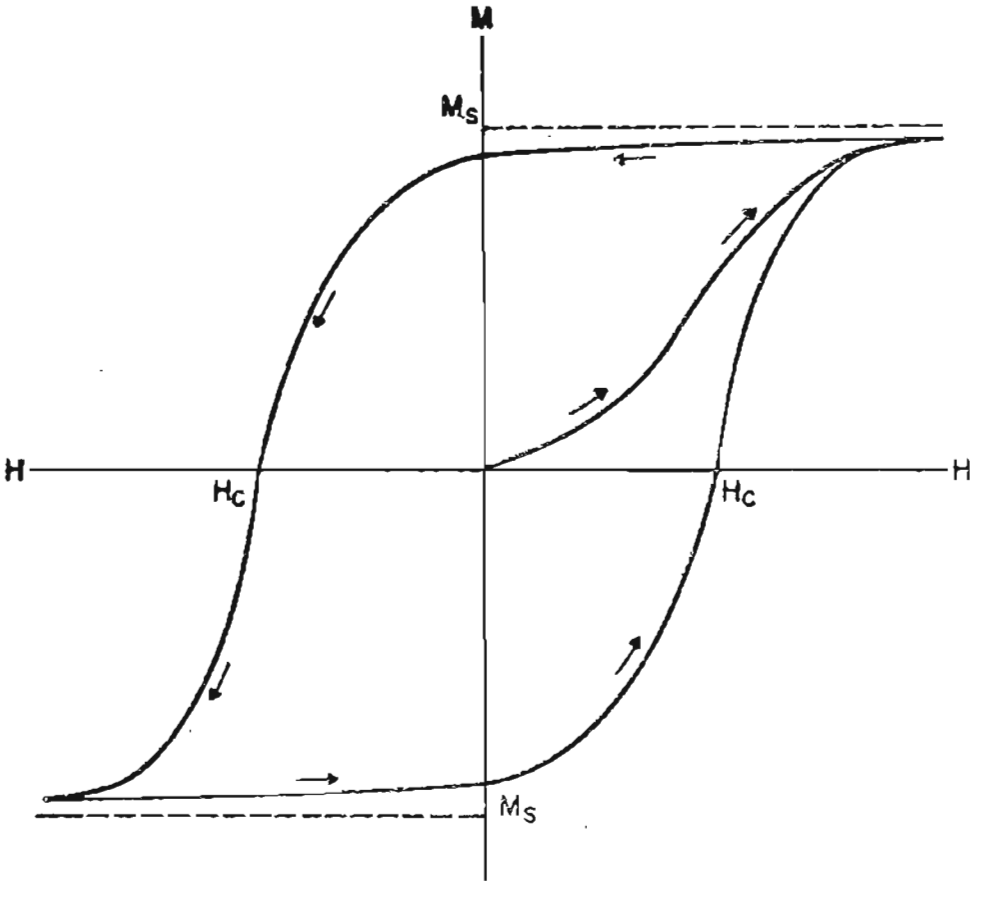

Figure 1. Typical hysteresis loop of a hard magnetic material

and (3) T-T. Since the 4f electrons are confined to a radius of 0.4A[6] about their respective nuclei there are few direct interactions in the first two classes above. Instead an indirect exchange interaction through the conduction electrons is responsible for their couplings. This is referred to as the Ruderman, Kittel,[7] Kasuya,[8] and Yosida[9] (RKKY) exchange interaction. The T-T interactions are of a direct nature due to overlapping of the 3d electron wave functions. The exact nature of this direct exchange interaction is poorly understood.

Empirical evidence to date supports the notion that R-R and R-T couplings are principally controlled by an RKKY interaction. In the systems of the present study, R-R spins couple parallel with one another while the R-T spins couple antiparallel. The T-T magnetic moments appear to couple parallel with each other with, in some cases, partial filling of the d band. The net effect of coupling in the alloys of this study is that two sublattices are formed of the R-R and T-T types. These sublattices then couple either parallel or antiparallel to each other. The first half of the R elements, ending with Eu, couple parallel with the T sublattice, which is referred to as ferromagnetic coupling. This is due to the Russell-Saunders coupling of the spin ($\overline{S}$) and orbital ($\overline{L}$) angular momenta giving a total angular momentum of $\overline{J} = \overline{L} + \overline{S}$. The second half of the R elements, beginning with Gd, have a total angular momentum of $\overline{J} = \overline{L} - \overline{S}$ and, therefore, couple antiparallel with the T sublattice.

If the R and T sublattices have magnetic moments of the same magnitude, the coupling is referred to as antiferromagnetic. If, however, the two sublattices are different in magnitude, the coupling is considered ferrimagnetic. Since RKKY exchange is unaffected by any change in lattice parameters but is affected by e.c., especially in the conduction bands, the addition of an electron rich element can possibly change the coupling of the R and T sublattices. If such a change in coupling were to take place, the heavy R elements (those from Gd to Lu) could produce alloys with very high M_s. As of yet no coupling change between the R-R and T-T sublattices has been observed. However, in the alloy $GdAg_{1-x}In_x$, where the GdAg R-R sublattice of Gd couples antiferromagnetically, this coupling is changed to ferromagnetic as the concentration of In is increased.[10] Also in the compound $Eu_{1-x}La_xAl_2$, where the two different R elements couple ferrimagnetically to $x = 0.4$, a change to ferromagnetic coupling occurs related to the RKKY sums and the change in e.c.[11]

The Curie temperature, (T_c), is defined as that temperature where the spontaneous magnetization of a magnetically ordered material vanishes. In the cobalt rich compounds RCo_x with $x \geq 3$, the T sublattice is the main controlling factor on T_c. For instance pure Co has $T_c \sim 1400°K$[12]; Gd_2Co_{17} has $T_c \sim 1200°K$[13]; and $GdCo_3$ has $T_c \sim 600°K$.[14] The R elements in these compounds tend to lower T_c through the weaker coupling of the indirect exchange of the RKKY type. In the RFe_x compounds with $x \geq 3$ the reverse is true, i.e. an increase

in the Fe content (up to $x = 8.5$) results in a decrease in T_c. For instance Dy_2Fe_{17} has $T_c \sim 380°K$[15,16]; Dy_6Fe_{23} has $T_c \sim 520°K$[15,17]; and $DyFe_3$ has $T_c \sim 600°K$.[17] Since Fe has $T_c \sim 1040°K$[12] and the ordering temperature of the R-R systems are relatively low, the R-T couplings are apparently effective in the reduction of T_c for the rare earth iron alloys. Further evidence of this effect is shown by the two Curie temperatures of RFe_3 where R is a heavy rare earth element. The first of these temperatures is referred to as the compensation temperature, (T_p), and the second T_c. T_p occurs in ferrimagnetic alloys of this study when two oppositely directed sublattices of the R and T elements cancel each other as shown in Figure 2. The coupling of magnetic moments in the RFe_x with $x \geq 3$, therefore, appears to be controlled by both the T-T and R-T interactions.

As in the case for M_s, T_c is also influenced by the e.c. where R-R and R-T couplings are concerned. In the case of T-T coupling, which is characterized by a very high T_c, the effects on changing e.c. and its relation to T_c can only be understood empirically.

Appendices I and II are included at the end of this work to illustrate trends in the stability of structures. Appendix I is a compilation of structural data taken from the work of other researchers. Appendix II is a compilation of structural data of the present study. These two accumulations of data include elemental composition, lattice parameter(s), c/a relation where pertinent, method of preparation and references.

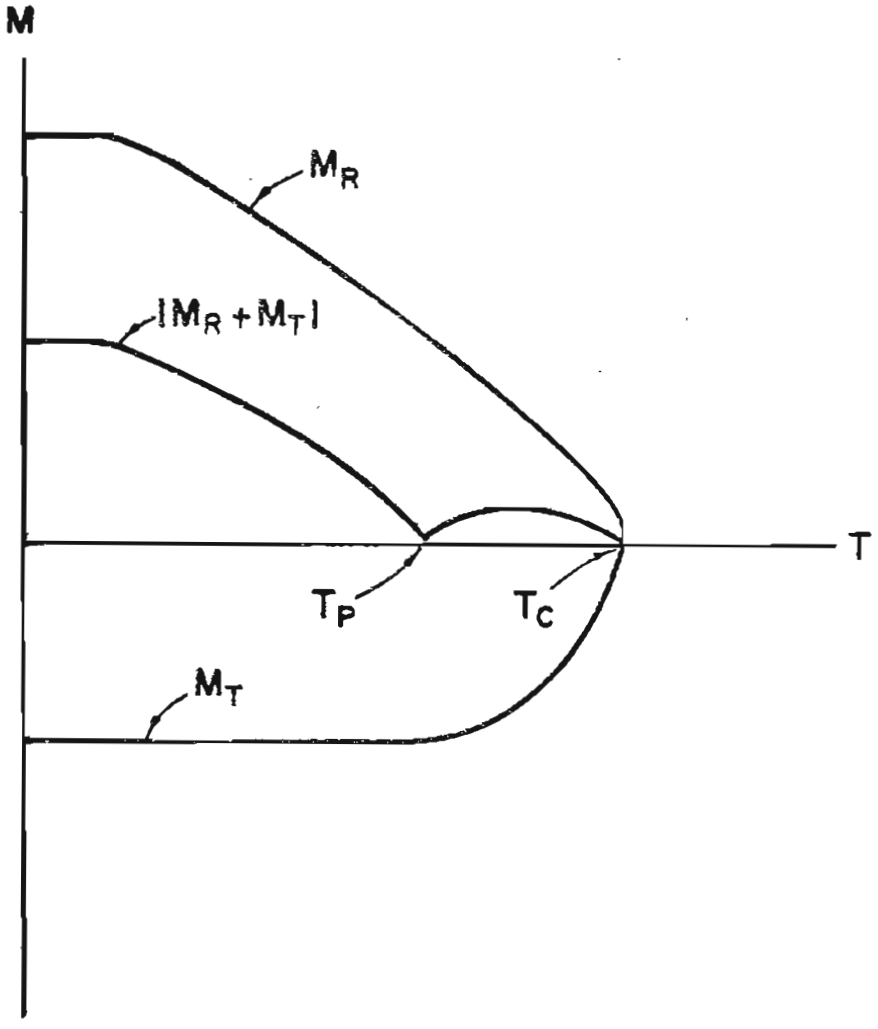

Figure 2. Typical M versus T curves of a ferrimagnetic material showing T_p and T_c.

Appendices III and IV are compilations of pertinent magnetic data taken from the work of other researchers and the present study respectively. These compilations include composition, T_c, T_p where pertinent, H_c, H_a, M_s, type of ordered state and references.

In view of the above considerations of magnetic hardness and exchange, and the anticipated effects of the e.c. on them, certain choices were made of binary R_xT_y compounds in which a third component was used to replace T or R. Since single phase materials were desired, questions of phase stability were also considered.

As mentioned above, $Sm_{.167}Co_{.833-x}Al_x$ shows very high values of H_c and H_a.[4,5] Since Al is an electron rich substituent for Co, Si and Cu were also anticipated to have a similar effect on H_c. Other substitutions considered for Co were; Ag and Au because of their low e.c. and same relative size as Al; In and Sn because of their large size and high e.c.; and finally Pt because of the relatively high H_c in the PtCo alloy.[18] Zr was substituted for Sm in the $SmCo_5$ lattice because of its high e.c. and relatively close size to Sm.

Besides the RT_5 alloys listed above, studies were done on several RT_3, R_6T_{23} and R_2T_{17} pseudobinary systems. The results for these systems are given in Appendices II and IV. Of these systems, the DyFeAl ternary system has also been studied structurally by Russian researchers with similar results.[19]

CHAPTER 2

STATE-OF-THE-ART

One of the principal objectives of any solid state study is an ability to calculate the total energy of a given system. Having accomplished this, one need only extract the appropriate terms for specific interactions of interest, such as phase stability, specific heat, magnetic interactions, electrical conductivity, lattice dynamics, etc. As pointed out by Tinkham,[20] the Hamiltonian of a solid system would include the kinetic and potential energy terms of all the electrons and nuclei. The potential energy terms would include nuclei-nuclei, nuclei-electron, electron-electron, spin-orbit, spin-spin, hyperfine structure and external field couplings. To calculate an exact solution for such a system is impossible. Therefore, the current approach employs a combination of symmetry considerations, various approximation methods and correlations in empirical data to explain and predict effects. Examples of this will be given in the following discussions of phase stability, magnetic interactions, and magnetic hardness.

In order to understand the energy within a solid system, the atomic positions as well as identities of the elements occupying these positions are essential information and relate to the potential energy terms of the Hamiltonian.

Although magnetic interactions do occur within systems of randomly distributed atoms this investigation is limited to structurally ordered materials. Such solids exist as homogeneous, single phase materials whose Gibbs free energy, as a function of composition of the constituents, is at a minimum. The number of possible phases depends on the number of degrees of freedom of the system as given by the Gibbs phase rule[21] which relates to the number of intensive variables in the system.

There are two current theoretical approaches to predicting phases. The first is to consider the heats of formation of the binary compounds and in turn to use these to predict the ternary and multicomponent phase formations.[22] The main difficulty with this method is that the calorimetry data of the binary compounds must be known quite accurately in order to predict the stability of multicomponent compounds. Since accurate calorimetry data within the rare earth intermetallic binaries are sparse, the need for further work is indicated.

A second approach is to determine all the interactional terms comprising the free energy from first principles. The free energy is given by:

$$G = H - TS,$$

where H is the enthalpy, T the temperature and S the entropy. The environmental factors of temperature and pressure are associated with the TS term of the free energy. The enthalpy, on the other hand,

is related to the geometrical, energy band and chemical bond factors resulting from the properties of the component atoms. The differences in the electrochemical factors of the component atoms are also reflected in the enthalpy.

The enthalpy in metals is mainly affected by the nearest-neighbor interactions or chemical bond factor. In the 3d T metals and 4f R metals there are unfilled energy bands below the Fermi surface which control the chemical bond factor. The electron concentration on or very near to the Fermi surface (i.e. the conduction band electrons per atom) are related to the next nearest and further neighbor interactions. The effect on the enthalpy by these conduction band electrons is usually an order of magnitude smaller than the chemical bond factor. The interplay between the nearest neighbors or chemical bond factor, the further neighbors or conduction band factor and the geometrical factor is very complex in alloys. The net effect of these factors dictates the formation of a lattice of compressible atoms which can best fill space.

Since the alloys of this study are analogs to known binary compounds, the electronegativity difference of the constituent atoms is not of great importance in most instances. For example, the electronegativity difference between the R and T metals is ~ 0.8 and the atomic size difference is ~ 0.4 Å. These size and electronegativity factors indicate a very limited solubility between the R and T metals which is observed for the alloys in this study. However,

other structural types have been found to form stable metallic compounds in the binary systems, such as the RT_3, R_6T_{23}, RT_5 and R_2T_{17} metallic phases. Unless a large difference in size and electronegativity factors is shown on the basis of a third element replacement in the known compounds, solid solubility arguments based on these two factors are not considered important.

Since the electronegativity difference in the alloys of this study is of little importance, the metallic bond based on the packing of the constituent atoms to fill space is considered of great importance. The original work of Laves[23] and later work of Parthe[24] treated hard sphere packing. Pearson[25] has extended this concept to include nonrigid, deformable spheres. He introduced the concept of the near neighbor diagram (n.n.d.). This is a plot of the strain parameter versus radius ratios of the constituents in a given structure. Such a plot helps in considering the stability of metallic phases.

Along with the near neighbor diagram, consideration of the coordination polyhedron surrounding each atom is important. The coordination polyhedra have been discussed by Pearson[25] in addition to the relations of different structures on the basis of stacking sequences of triangular, hexagonal and Kagomé nets. The structures discussed in this study, with one exception (Th_6Mn_{23}), are a combination of the Laves ($MgCu_2$) and Hauke ($CaCu_5$) type stacking sequences. There have also been explanations of these structures by various

authors[26-29] on the basis of the stacking sequences of $CaCu_5$ sub structures.

The structural isotypes investigated in this work ($CeNi_3$, $PuNi_3$, $CaCu_5$, Th_2Ni_{17}, Th_2Zn_{17} and Th_6Mn_{23}) can be discussed on the basis of the above approaches to interpret structural stability. Consideration of stacking sequences, coordination polyhedra and interatomic distances are included in the discussion of each isotype.

Structural considerations will begin with the very common $CaCu_5$ structural type. Not only is this the structure of several technologically important materials but it also can be considered the basis of most of the structural phases to follow. The structure is hexagonal primitive with six atoms per unit cell (hP6), an average base of 5.0 Å, an average height of 4.0 Å, and a c/a value of 0.8. The only exceptions to this c/a ratio among $CaCu_5$ isotypes are the platinum binaries and the boride ternaries. In terms of Pearson's stacking of hexagonal and Kagomé nets its sequence is $[\underline{A}a]\alpha$,[25] where the underline represents the large atom (Ca) sites in that phase. To explain Pearson's stacking sequences Figure 3 is included. Figure 3a, taken directly from Pearson,[25] shows the various triangular, hexagonal, and Kagomé nets. Whenever a group of these nets is surrounded by square brackets i.e. [Aa], the nets are coplanar. Figure 3b is an example of this type of sequence. However, when a group of nets is surrounded by round brackets i.e. (BAC), the nets, although not coplanar, are considerably closer to each other than the

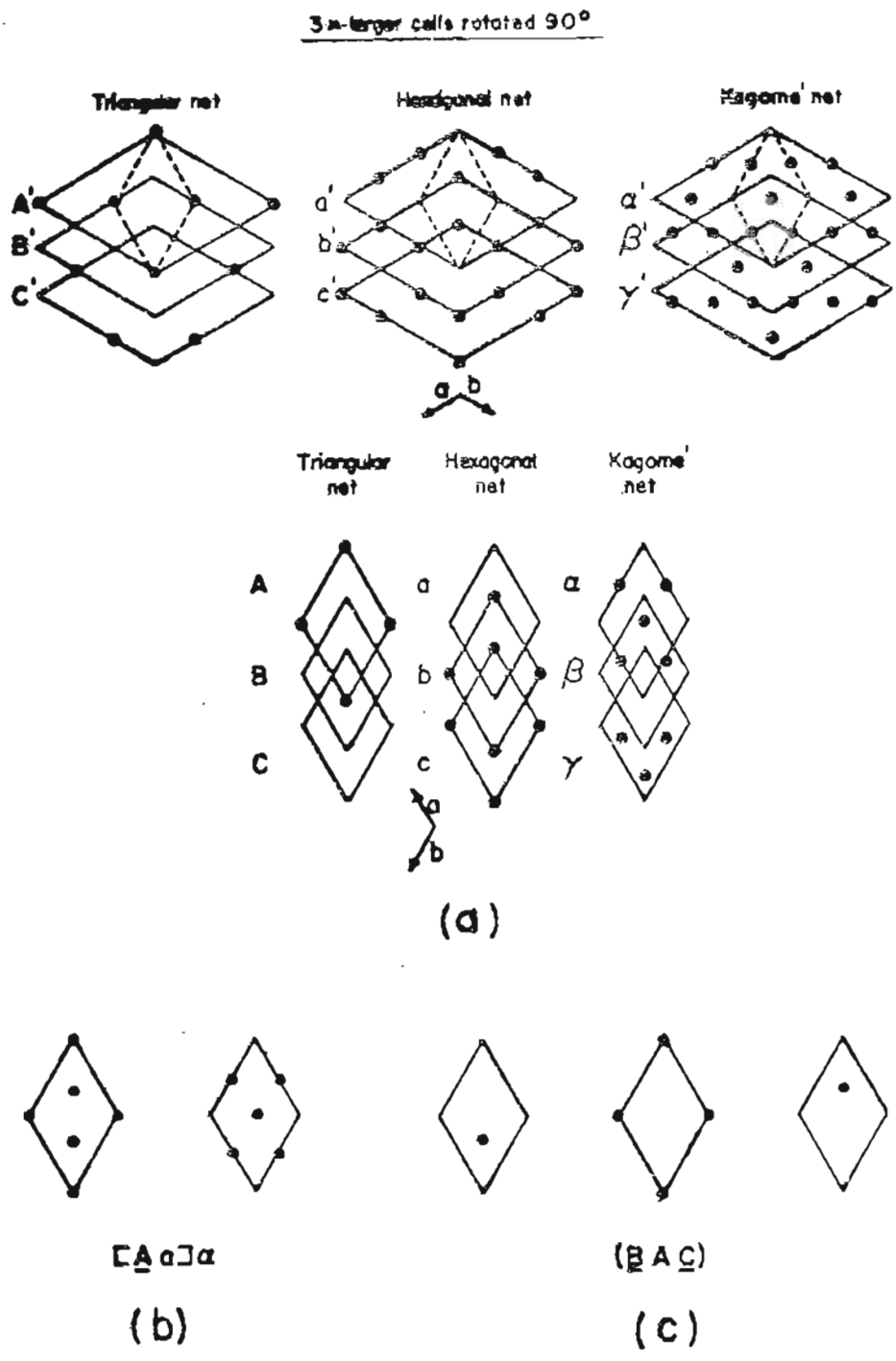

Figure 3. Layer nets (a) triangular, hexagonal and Kagome' nets (taken from Pearson[25]).
(b) Sequence of nets, [Aa]α, describing the $CaCu_5$ structure.
(c) Sequence of nets describing the basic (BAC) stacking.

average interlayer distances observed throughout the structure. Figure 3c shows the Laves phase sequence (BAC) as such a case.

The three site coordination polyhedra, interatomic distances and coordination numbers (CN) for $CaCu_5$ are shown in Table I, where the large atom sites are also underlined. The site positions and letterings (set as upper case letters in this work) are taken directly from the "International Tables for X-ray Crystallography."[30] Each of these polyhedra are shown in Figure 4 along with their CN. These polyhedra limit the filling capabilities of the structure according to e.c., electronegativity, atomic size and metallic bonding.

The CN 20 A site polyhedron is first surrounded by a coplanar hexagonal distribution of C sites, then by 2 coplanar hexagons each of 6 G sites at $+ c_o/2$. The first order polyhedron is then closed by 2 A sites at $\pm c_o$ (Figure 4a). The small atom sites are both CN 12 polyhedra. The C site (Figure 4b) system begins with a coplanar hexagon of alternating A and C site atoms. This polyhedron is then closed at $\pm c_o/2$ by a coplanar triangular array of G site atoms. The G site (Figure 4c) polyhedron begins with four coplanar G site atoms in a rectangular array and truncates with two rhombic arrays of alternating A and C sites.

A $CaCu_5$ nearest-neighbor diagram (n.n.d.) has been constructed by the author and is shown in Figure 5. A full description of this type of diagram is given by Pearson.[25] He considers the binary alloys R_xT_y to be compressed until R-R, R-T and T-T contacts are

TABLE I

Interatomic Distances of Respective A, C and G Sites of $CaCu_5$

Lattice Parameters: a_o = 5.092 Å, c_o = 4.086 Å

Number of Sites	Distance Å	Site Types	Coplanar Configuration	c_o Fraction
		A Site: c_o Fraction = 0		
6	2.940	C	Hexagonal	0
12	3.264	G	Hexagonal	±.5
2	4.086	A	Singles	+1
CN = 20				
		C Site: c_o Fraction = 0		
6	2.517	C	Triangular	±.5
6	2.939	(3)C, (3)A	Hexagonal	0
CN = 12				
		G Site: c_o Fraction = .5		
4	2.517	C	Singles	0,1
4	2.546	G	Rectangular	.5
4	3.264	A	Singles	0,1
CN = 12				

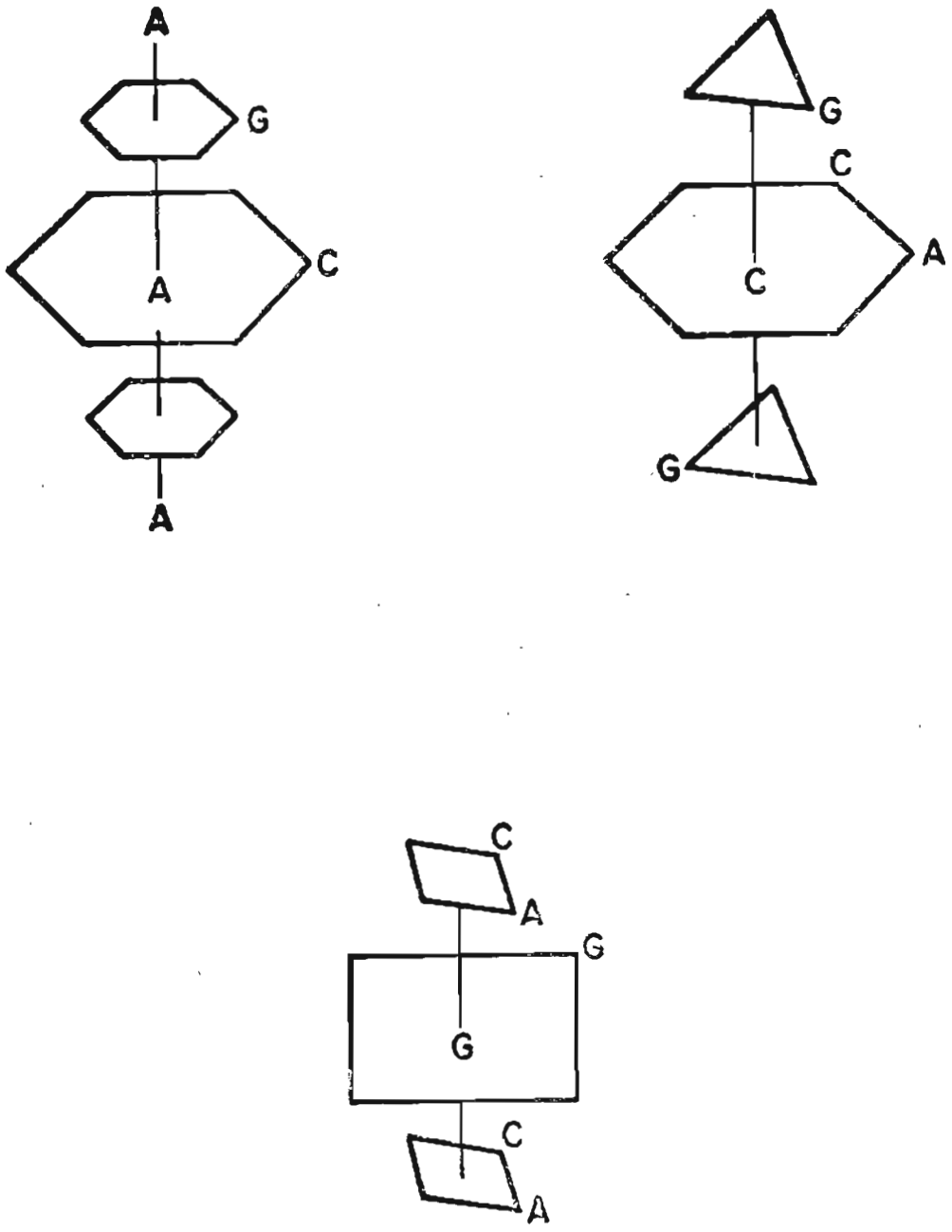

Figure 4. Coordination polyhedra of the $CaCu_5$ (a) A site with a CN of 20, (b) C site with a CN of 12 and (c) G site with a CN of 12.

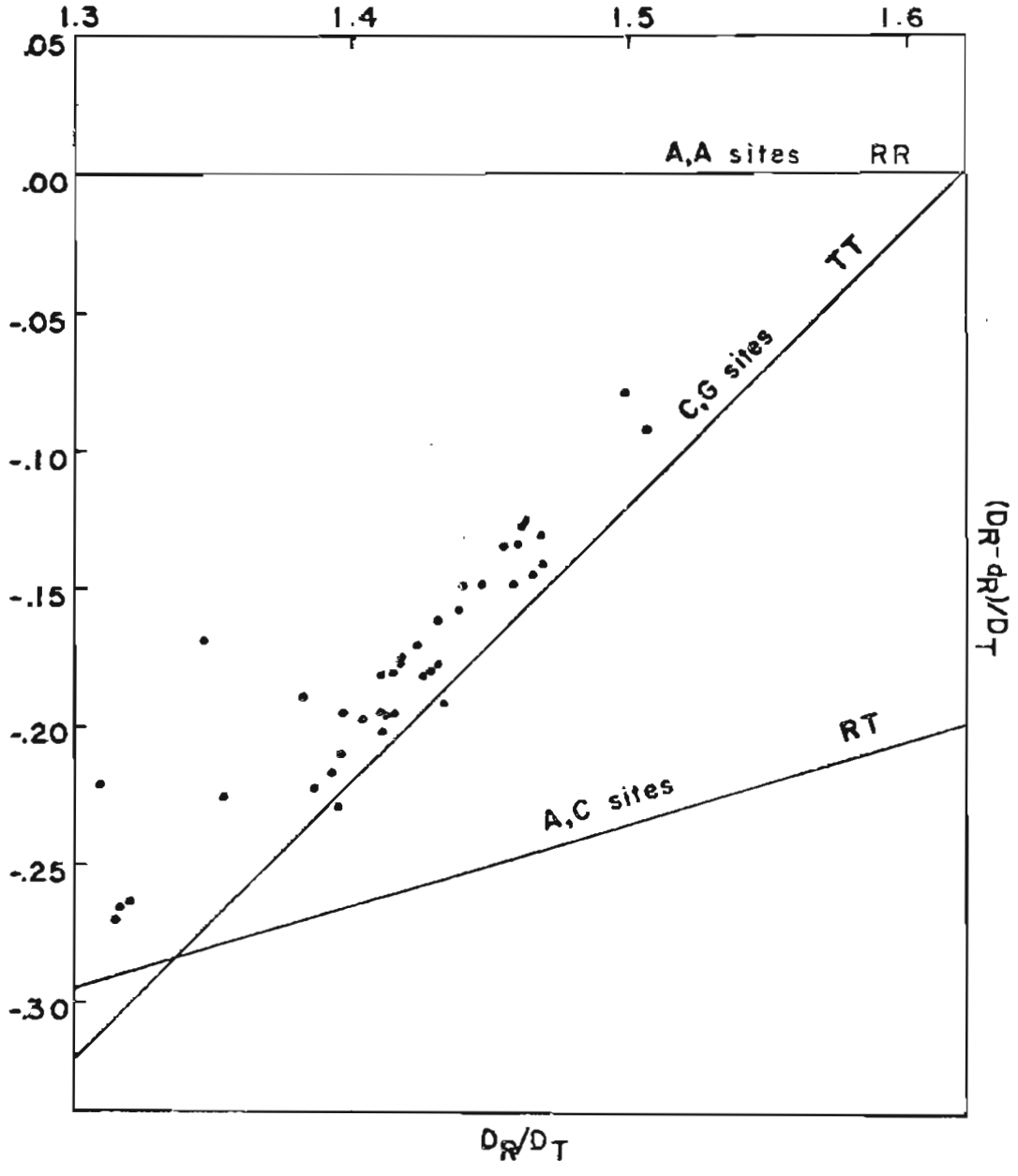

Figure 5. $CaCu_5$ binary near-neighbor diagram.

established as determined on the basis of the radii of the elements with CN 12 (after Pauling[31]). The ordinate of such graphs are a measure of the strain parameter $(D_R-d_R)/D_T$, where D_R and D_T are the R and T elemental diameters according to Pauling[31] and d_R is the R sites shortest interatomic distance in the given lattice (e.g. A to A site distance in RT_5 structures) according to the structural geometry (i.e. point positions and lattice parameters). The abscissa is the ratio of the R and T elemental diameters, D_R/D_T.

Of particular interest in the $CaCu_5$ n.n.d. is the observation that the large atom sites experience no compression by each other due to the T atom surrounding the R atoms, while their interaction with the small atoms produces a rather large compression. This is seen in Figure 5 as the RT contact line lies below the TT contact line, around which the binaries group themselves. It will be shown that the ternaries fill, and somewhat parallel, the RT contact lines. (This will be discussed further in Chapter 3.)

On the basis of these observations, one understands why certain structures like $SmFe_5$ will not stabilize. The R-R contacts are unimportant while the compression associated with the R-T contacts is a controlling factor in determining the stability of the RT_5 compounds. For instance, it has been noted that the RCo_5 compounds decompose between room temperature and 700°C into R_2Co_7 and R_2Co_{17}.[32-34] This decomposition coupled with the multiphasic formation of $SmFe_5$ exemplifies the instability of the RT_5 compounds.

This instability is probably related to the compressibility mentioned above and the bonding properties of Co and Fe. Since the electronegativity and atomic radii are virtually the same for these two elements, it appears as though the differences in the electronic structures (especially the 3d bands) are the determining factor in the formation of the RT_5 compounds.

The other basic structure is the Laves phase $MgCu_2$. Looking at planes perpendicular to the [111] direction, one obtains a sequence of triangular and Kagomé nets. These are stacked as $\underline{A})\alpha(\underline{AC}\underline{B})\beta(\underline{BA}\underline{C})\gamma(\underline{C}B$ with the large atom sites underlined according to Pearson.[25] Since extensive coverage has been given to these compounds in the literature, and hence, no further discussion will be presented here.

The hexagonal structures begin to increase in complexity at the 1:3 stoichiometry. $CeNi_3$, like $CaCu_5$, is hexagonal primitive with, however, four times as many atoms per unit cell (hP24) with a_o = 4.98 Å and c_o = 16.54 Å. Its stacking sequence is a mixture of $CaCu_5$ $[\underline{Aa}]\alpha$ and $MgCu_2\beta(\underline{BA}\underline{C})$ sequences giving $\underline{AB})\beta[\underline{Bb}]\beta(\underline{BA}\underline{C})\gamma[\underline{Cc}]\gamma(\underline{C}$, where again the large atom site layers are underlined.[25] Buschow[27] has described this structure in terms of a stacking variation of the double $CaCu_5$ base structure. Khan[29] has also presented a mathematical model associated with a stacking sequence of $CaCu_5$ sub-cells which produces the $CeNi_3$ structure. This is, however, comparable to that presented by Buschow.[27] Although these are interesting and

informative ways to view these structures they are, in principle, little different from Pearson's presentation.

The interatomic distances of the six nearest-neighbor polyhedra and their CN are presented in Table II. The R site (C and F) polyhedra have CNs of 20 and 16, respectively. The former is similar to the $CaCu_5$'s A site polyhedron (Figure 4a), while the latter has a coplanar hexagonal array of small atoms above, three triangular arrays below, the last being the only large atoms of these three arrays, and finally a single large atom above. The small atom sites all have a CN of 12 similar in form to the two $CaCu_5$ sites.

Since there are few alloys isostructural with $CeNi_3$ and since it is a substructure of $PuNi_3$, the 1:3 n.n.d. will be discussed in terms of $PuNi_3$. The $PuNi_3$ structure has a c_o axis one-third longer than $CeNi_3$. Its structure is rhombohedral with 12 atoms per unit cell (hR12). Its stacking sequence is also a sequence of $CaCu_5$ [Aa]α and Laves β(BAC) types to give [Aa]α(ABC) γ[Cc]γ(CAB)β(Bb]β(BAC)α where the large atom sites are underlined.[25] By use of this notation one can easily see the $CeNi_3$ structure in this sequence; it begins with the first γ and ends just before the α at the end of the structure. Khan discussed the $PuNi_3$ structure half-cell as a stacking of B,C,A and D type subcells.[29] The C and D units are of Laves $MgCu_2$ type which are shifted by one-third in the x-direction and by two-thirds in the y direction of the basal

TABLE II

Interatomic Distances of Respective A,B,C,D,F and K Sites of $CeNi_3$

Lattice Parameters: a_o = 4.93 Å, c_o = 16.54 Å

Number of Sites	Distance Å	Site Types	Coplanar Configuration	c_o Fraction
		A Site:	c_o Fraction = 0	
6	2.548	K	Triangular	±.127
6	2.957	F	Triangular	±.042
CN = 12				
		B Site:	c_o Fraction = .250	
6	2.488	K	Triangular	.127, .373
6	2.875	(3)C, (3)D	Hexagonal	.250
CN = 12				
		C Site:	c_o Fraction = .250	
6	2.875	(3)B, (3)D	Hexagonal	.250
12	3.213	K	Hexagonal	.127, .373
2	3.440	F	Singles	.042, .458
CN = 20				
		D Site:	c_o Fraction = .250	
6	2.488	K	Triangular	.127, .373
6	2.875	(3)B, (3)C	Hexagonal	.250
CN = 12				

TABLE II (continued)

Interatomic Distances of Respective A,B,C,D,F and K Sites of $CeNi_3$

Lattice Parameters: $a_o = 4.98$ Å, $c_o = 16.54$ Å

Number of Sites	Distance Å	Site Types	Coplanar Configuration	c_o Fraction
		F Site: c_o Fraction = .042		
6	2.863	K	Hexagonal	.127
3	2.957	A	Triangular	0
3	3.143	K	Triangular	-.127
3	3.190	F	Triangular	-.042
1	3.444	C	Single	.250
CN = 16				
		K Site: c_o Fraction = .127		
6	2.488	(2)B, (4)K	Line Connected, Rectangular	.25, .127
1	2.548	A	Single	0
2	2.863	F	Line Connected	.042
1	3.143	F	Single	-.042
2	3.213	B	Line Connected	.250
CN = 12				

plane. The B block is of the $CaCu_5$ type and A is the same as the B block except shifted by two-thirds in the x-direction and by one-third in the y-direction of the basal plane. Buschow on the other hand, presents this structure as a sequence of a double $CaCu_5$ type structure stacked three blocks high and each shifted by one-third in the basal plane.[27]

The interatomic distances of the five sites and their CN are given in Table III. The point positions for this calculation were taken from published data.[30] This calculation was done by the author. These sites closely resemble the $CeNi_3$ sites in size and shape of the surrounding polyhedron.

The binary n.n.d. of $PuNi_3$ was constructed by the author and is shown in Figure 6. Similar to the $CaCu_5$ n.n.d. the binary compounds follow the TT contact lines, and the RT contacts are compressed, though not as much as in the 1:5 structure. There is, however, a very striking difference here in that the RR contacts now are greatly compressed while in the 1:5 systems there was no compression. Thus, the nature of the R atoms has more of an influence on stability within the RT_3 isotypes.

The last two isotypes are of the R_2T_{17} stoichiometry. The structure with the smallest hexagonal cell is the Th_2Ni_{17} isotype with a_o and c_o of approximately equal length. This structure is hexagonally primitive with 38 atoms per unit cell (hP38). In

TABLE III

Interatomic Distances of Respective A,B,C_1,C_2 and H Sites of $PuNi_3$

Lattice Parameters: a_o = 5.00 Å, c_o = 24.35 Å

Number of Sites	Distance Å	Site Types	Coplanar Configuration	c_o Fraction
		A Site: c_o Fraction = 0		
6	2.886	C_1	Hexagonal	0
12	3.213	H	Hexagonal	±.083
2	3.443	C_2	Singles	±.141
CN = 20				
		B Site: c_o Fraction = .500		
6	2.499	H	Triangular	.416, .584
6	2.951	C_2	Triangular	.475, .525
CN = 12				
		C_1 Site: c_o Fraction = .333		
6	2.481	H	Triangular	.251, .416
6	2.886	(3)A, (3)C_1	Hexagonal	.333
CN = 12				
		C_2 Site: c_o Fraction = .141		
6	2.877	H	Hexagonal	.083
3	2.952	B	Triangular	.167
3	3.021	H	Triangular	.250
3	3.138	C_2	Triangular	.192
1	3.443	A	Single	0
CN = 16				

TABLE III (continued)

Interatomic Distances of Respective A, B, C_1, C_2 and H Sites of $PuNi_3$

Lattice Parameters: a_o = 5.00 Å, c_o = 24.35 Å

Number of Sites	Distance Å	Site Types	Coplanar Configuration	c_o Fraction
		H Site: c_o Fraction = .083		
2	2.481	C_1	Line Connected	0
5	2.500	(4)H, (1)B	Rectangular, Single	.083, .167
2	2.877	$\underline{C}_2$	Line Connected	.141
1	3.021	$\underline{C}_2$	Single	.192
2	3.213	$\underline{A}$	Line Connected	0

CN = 12

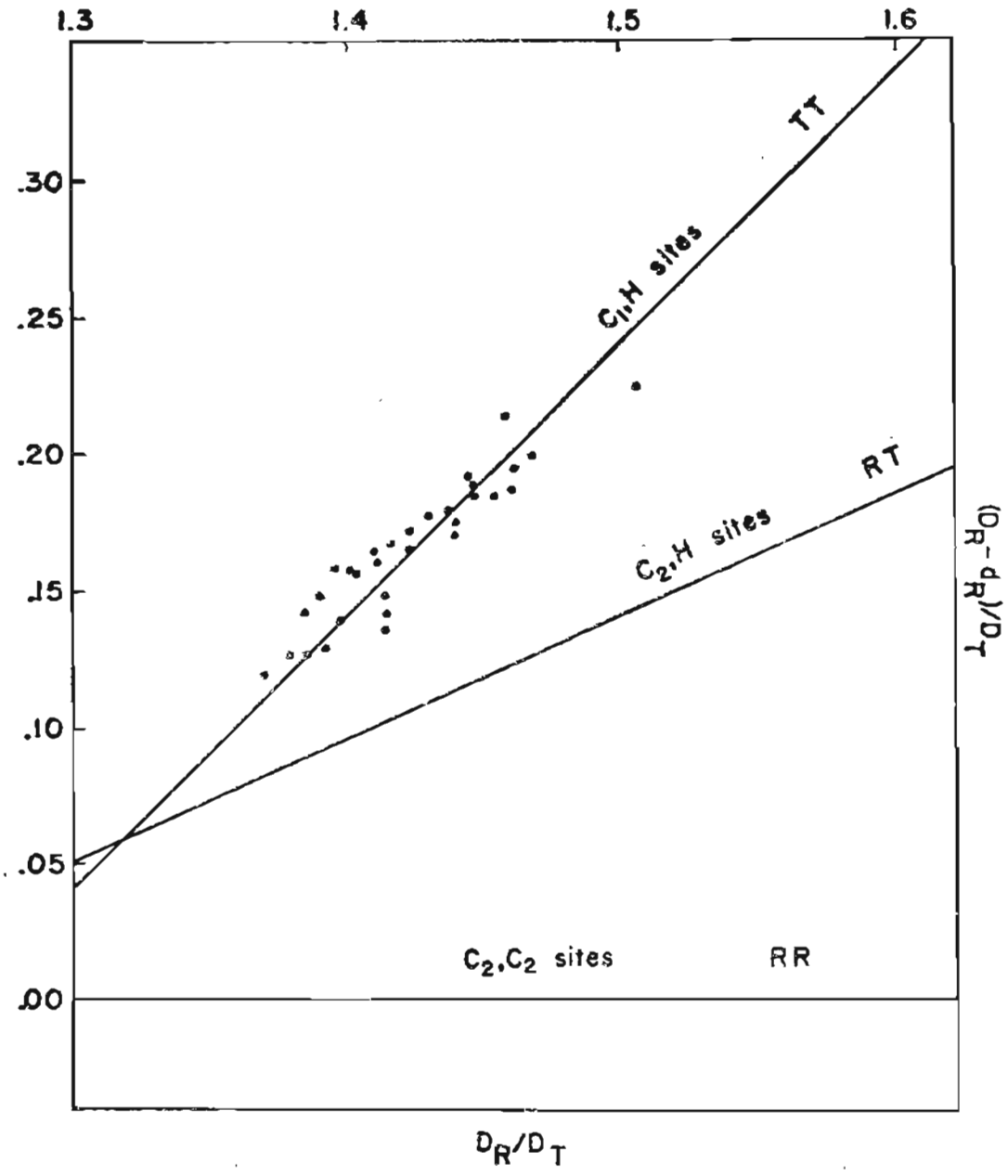

Figure 6. $PuNi_3$ binary near-neighbor diagram

Pearson's notation the layered structure is α'B[a'b]Bα'C[a'c]C.[25] Buschow describes this structure as a stacking of three $CaCu_5$ unit cells in the c_o direction while expanding the basal plane size by $3a_o$ and then replacing one-third of all R atoms by pairs of T atoms. The basal plane replacements occur at the A sites and the adjacent plane above containing R atoms have their C sites replaced. The final R atom replacement by T pairs occurs again at the A sites.

Table IV contains the interatomic distances of the nearest neighbor atoms and their CN. These were calculated by the author using available data.[30] The B and D site coordination polyhedra have CN 20 and are similar to the A site of $CaCu_5$ shown in Figure 4a. The D site, however, has no large atoms surrounding it. The small atom sites have CN 14 for F and J, while C and K have CN 12.

The binary n.n.d. is shown in Figure 7 as constructed by the author. This diagram is similar to that of $CaCu_5$ with the T-T atoms slightly compressed and the RT contacts under even more compression. The R's never make contact with one another. Thus, the RT contacts are the most influential in the stability of this structure.

The last hexagonal isotype considered is Th_2Zn_{17}. This structure is rhombohedral with 19 atoms per unit cell (hR19). The hexagonal unit cell has the same a_o basal plane dimension as Th_2Ni_{17} but c_o is 1.5 times as long. In Pearson's notation the layered structure is a' B)A(αβγ)C(Ba' A)C(γαβ)B(Aa' C)B(βγα)A(C where the large atom configurations are underlined. Buschow describes this structure

TABLE IV

Interatomic Distances of Respective B, D, F, G, J and K Sites of Th_2Ni_{17}

Lattice Parameters: a_o = 8.37 Å, c_o = 8.14 Å

Number of Sites	Distance Å	Site Types	Coplanar Configuration	c_o Fraction
		B Site: c_o Fraction = .25		
6	2.790	J	Hexagonal	.25
12	3.159	K	Hexagonal	0, .50
2	4.070	B	Singles	-.25, .75
CN = 20				
		D Site: c_o Fraction = .25		
6	2.790	J	Hexagonal	.25
2	2.930	F	Singles	-.11, .61
12	3.158	K	Hexagonal	0, .50
CN = 20				
		F Site: c_o Fraction = .11		
1	2.279	F	Single	.39
6	2.577	G	Hexagonal	0
1	2.930	B	Single	-.25
6	3.014	J	Hexagonal	.25
CN = 14				

TABLE IV (continued)

Interatomic Distances of Respective B, D, F, G, J and K Sites of Th_2Ni_{17}

Lattice Parameters: a_o = 8.37 Å, c_o = 8.14 Å

Number of Sites	Distance Å	Site Types	Coplanar Configuration	c_o Fraction
		G Site: c_o Fraction = 0		
4	2.416	K	Rectangular	0
4	2.467	J	Line Connected	±.25
2	2.576	F	Singles	±.11
2	3.159	D	Singles	±.25
CN = 12				
		J Site: c_o Fraction = .25		
6	2.467	(2)G, (4)K	Line Connected, Rectangular	0, .50
6	2.790	(4)J, (1)B, (1)D	Hexagonal	.25
2	3.013	F	Singles	.11, .39
CN = 14				
		K Site: c_o Fraction = 0		
4	2.416	(2)G, (2)K	Rectangular	0
4	2.467	J	Line Connected	±.25
1	2.577	F	Single	.11
3	3.159	(2)B, (1)D	Line Connected, Single	±.25
CN = 12				

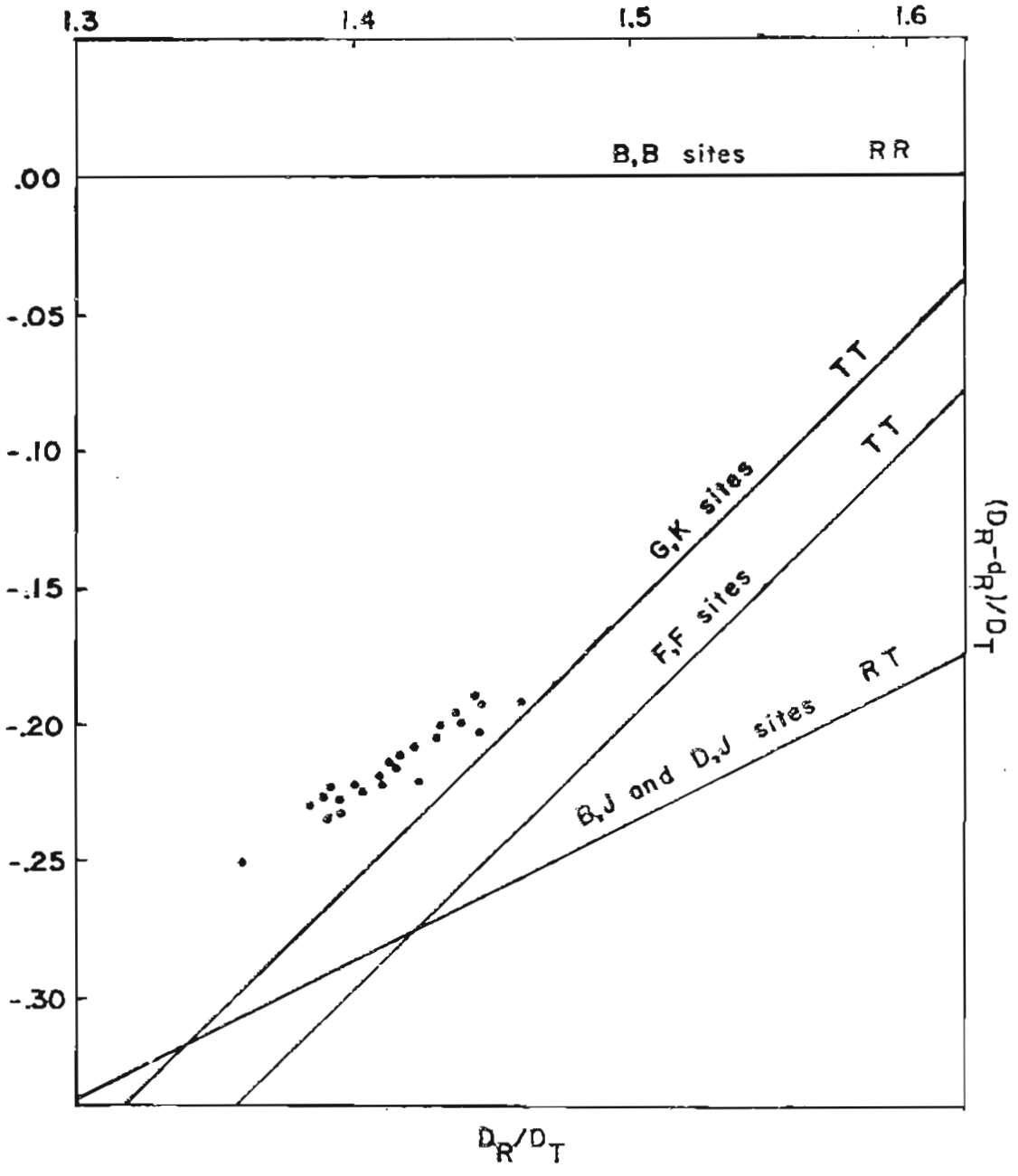

Figure 7. Th_2Ni_{17} binary near-neighbor diagram

as being the same as for the Th_2Ni_{17} isotypes with one exception, the last layer replacement of A sites by two transition metal atoms occurs instead of the F site in the Th_2Ni_{17} structure.[27]

Table V gives the interatomic distances of the 5 different Th_2Zn_{17} site nearest-neighbors and their CN. This table was developed by the author. Reference 30 was used to locate the point positions and the lettering of those positions. The R site is again similar to the $CaCu_5$ A site with CN 20. The remaining four sites vary from CN 12 to CN 14.

The binary n.n.d. was constructed by the author and is shown in Figure 8. This diagram is similar to that of $CaCu_5$ and Th_2Ni_{17} where the R atoms never make contact and the RT and TT contacts are the important ones.

The final structure to be considered is the Th_6Mn_{23} isotype. This structure is face centered cubic with 116 atoms per unit cell (cF 116). It is a structure of large size, packed with several icosahedra. Due to the size of this structure no information beyond the above will be considered except in Chapter 3 under $Dy_{.207}Fe_{.793-x}Al_x$.

In a consideration of magnetic hardness, the most important question is concerned with the magnetocrystalline anisotropy, i.e., the dependence of the internal energy on the direction of spontaneous magnetization. The hexagonal systems considered in this investigation usually exhibit (i) uniaxial anisotropy (moments aligning along the

TABLE V

Interatomic Distances of Respective C_1,C_2,D,F and H Sites of Th_2Zn_{17}

Lattice Parameters: a_o = 9.03 Å, c_o = 13.20 Å

Number of Sites	Distance Å	Site Types	Coplanar Configuration	c_o Fraction
		C_1 Site:	c_o Fraction = .333	
6	3.010	F	Hexagonal	.333
1	3.119	D	Single	.097
12	3.412	(9)H, (3)D	Hexagonal	.167, .500
1	4.401	C_1	Single	.667
CN = 20				
		C_2 Site:	c_o Fraction = -.097	
1	2.561	C_2	Single	-.097
6	2.765	(3)H, (3)D	Hexagonal	.167
1	3.119	D_1	Single	.333
6	3.271	F	Hexagonal	0
CN = 14				
		D Site:	c_o Fraction = .500	
4	2.606	H	Rectangular	.500
4	2.666	F	Line Connected	.333, .667
2	2.765	C_2	Singles	.430, .570
2	3.412	C_1	Singles	.333, .667
CN = 12				

TABLE V (continued)

Interatomic Distances of Respective $\underline{C}_1$,C_2,D,F and H Sites of Th_2Zn_{17}

Lattice Parameters: a_o = 9.03 Å, c_o = 13.20 Å

Number of Sites	Distance Å	Site Type	Coplanar Configuration	c_o Fraction
		F Site:	c_o Fraction = 0	
6	2.666	D	Triangular	±.167
5	3.010	F	Hexagonally Distorted	0
2	3.271	C_2	Hexagonally Distorted	±.097
CN = 13				
		H Site:	c_o Fraction = .167	
4	2.606	D	Rectangular	.167
4	2.665	F	Line Connected	0, .333
1	2.763	C_2	Single	.236
3	3.412	$\underline{C}_1$	Line Connected, Single	0, .333
CN = 12				

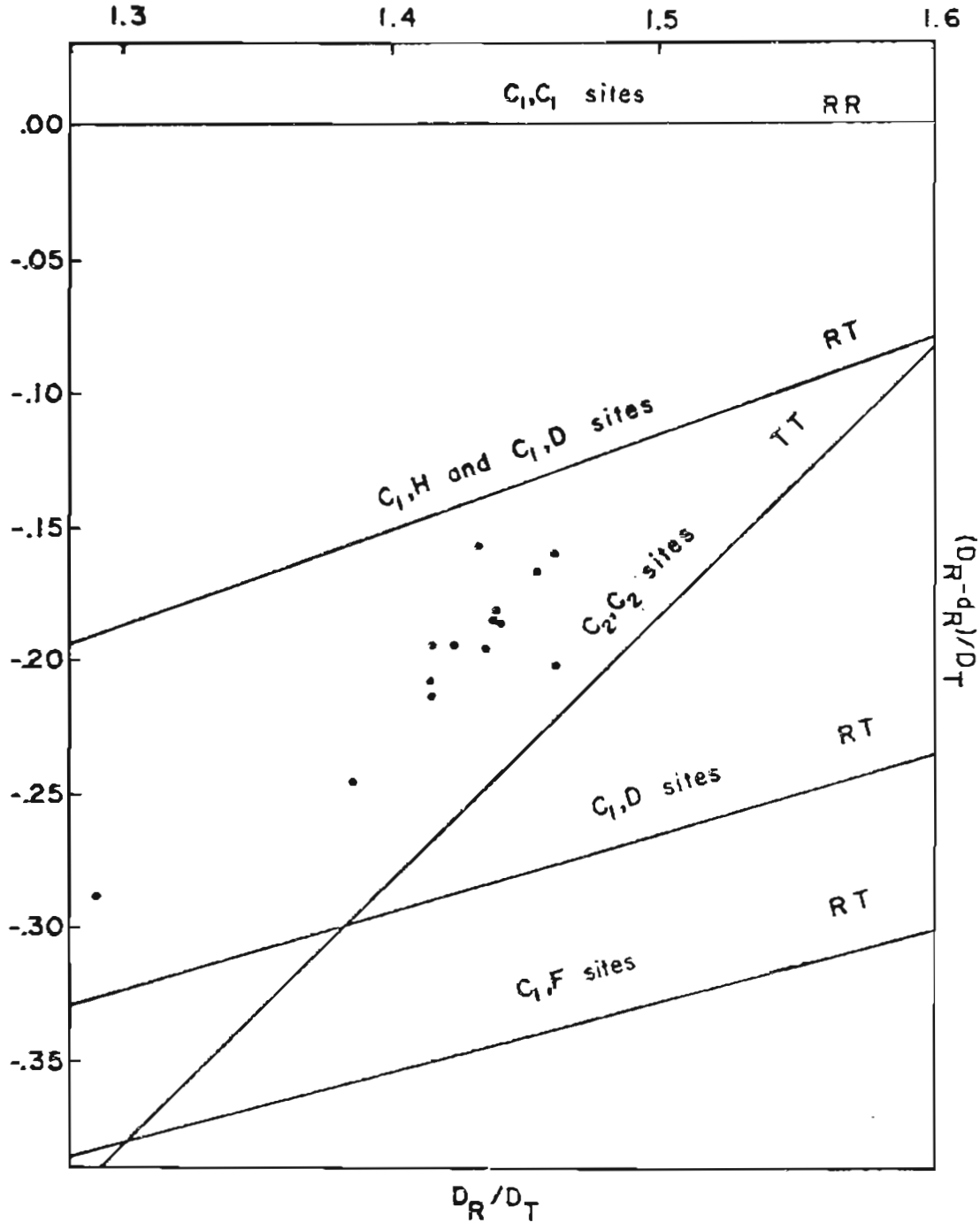

Figure 8. Th_2Zn_{17} binary near-neighbor diagram

c-axis of the structure) or (ii) coplanar anisotropy (moments oriented in the basal plane of the structure). The latter type is not desirable because its anisotropy is usually weaker. For the former case, the energy is expressed in a general expansion of the angle, ϕ, which the magnetic moment alignment makes with the co axis:

$$Ea = K_{u1}\sin 2\phi + K_{u2}\sin 4\phi + \ldots,$$

where the K_{ui} are the various material dependent anisotropy coefficients.[35]

There are two basic models describing magnetocrystalline anisotropy, the pair-ion model and the single-ion model.[35] The single-ion model considers only the spin-orbit interactions and the effects of the crystalline electric field (c.e.f.) on a single ion's spin and orbital angular momenta. This model is valid for the R-R and R-T atomic interactions and the anisotropy associated with these interactions. This is due to little or no wave function overlap associated with the unfilled 3d and 4f bands. The pair-ion model, however, deals with both the spin orbit and direct exchange interactions and the anisotropy due to the c.e.f. effect on both types of interactions. This model is of value where the T-T atomic interactions are considered important, since in such systems of atoms a direct interaction can predominate.

There are two experimental methods used to determine the anisotropy field, H_a. One of these involves the use of single crystals. Such crystals can be aligned parallel to an applied

magnetic field and then saturated to determine the magnetic saturation, M_s. The field is then applied perpendicular to the easy axis of the crystal. At zero field, M = 0. Then, as the applied field is increased, M should increase linearly until $M = M_s$ at which time M should remain constant. Since fields equivalent to H_a are often impossible to achieve in the laboratory, the value of H_a is often found by extrapolating the M curve to the point of intersection with M_s. Where single crystals are not available, a second method is to orient a powder of presumed single micro-crystals in a field and freeze them into position with a binder. Treating this specimen as a single crystal the subsequent procedures are the same as those for a single crystal.

Hoffer and Strnat[36] have measured the anisotropy constants K_1 and K_2 for a single crystal of YCo_5 and from their curve of H versus M one can extrapolate an H_a of ~ 184 kOe. Strnat et. al.[37] have used the powder method to obtain an anisotropy field of 129 kOe for YCo_5. In their powder method experiment, the hard axis curve is not totally a straight line but rather begins to increase rapidly at low fields and showing a slight shoulder in the curve. This is due to an imperfect alignment of moments within the powder. This shoulder is removed from the extrapolation calculation for H_a. The powder method indicates a lower H_a (in the YCo_5 case lower by 54 kOe). This is probably due to the rotation of the micro-crystals by the applied field.

As mentioned in Chapter 2, H_c is usually less than H_a due to domain wall effects. Whenever a magnetic field reverses one or more spins in a material, nucleation of a domain wall takes place. These spins are kept in alignment by the anisotropy field and the effective fields due to any exchange interactions with neighboring spins. In perfect crystals the exchange fields are noted to be very high (several million Oersteds) even at the surface of these crystals.[38] Such exchange fields far exceed H_c and in such materials $H_c = H_a$. Imperfections in crystals weaken the exchange coupling and nucleation of domain walls takes place even at low fields.

Various authors have considered the domain wall problem in detail. For instance Zijlstra has discussed the effects of critical particle fields, nucleation, and pinning as related to the domain wall problem.[38-40] He has pointed out through size arguments and known experimental evidence that critical fields rather than critical size govern the ability of a material to form domain walls. Such fields occur where a uniformly magnetized body becomes unstable and a wall is first nucleated and later unpinned. An example of this was shown in iron whiskers which were larger than the critical size.[41] These whiskers were perfect crystals, and the coercive field in them was equivalent to the anisotropy field.

The production of perfect crystals is difficult so that nucleation sites do exist in most materials. These fields are referred to as nucleation fields (H_n). Examples of such sites are

surface protrusions, impurities, stacking faults, inclusions and other inhomogeneities.

Having nucleated, a wall proceeds to grow in size across the crystal or within grains of the material. During this growth and often after its completion, the wall can become pinned at the same types of defects which gave rise to the initial nucleation. The release of a wall occurs at another field called the pinning field (H_p).

To further clarify the effects of H_n and H_p consider the processes occurring in a small imperfect crystal as shown in Figure 9. This figure shows two different ways to conceptually approach the process of nucleation and pinning. Beginning at point A on this curve and decreasing the external field, a point is reached where nucleation of a domain wall occurs. This wall continues to grow in size across the particle until the field reaches H_{p_1} and the wall is unpinned and moved to a point where it is pinned again. On further reduction of the external field H_{p_2} is reached where the wall is again unpinned and driven from the particle. The return loop is similar except that at the nucleation field the wall rapidly moves on to be pinned elsewhere in the crystal rather than remaining pinned around the nucleation site. The wall is again unpinned at H_p, and saturation is again reached.

Nucleation and pinning were observed in small particles of $SmCo_5$ by Zijlstra.[40] In large polycrystalline powders and bulk

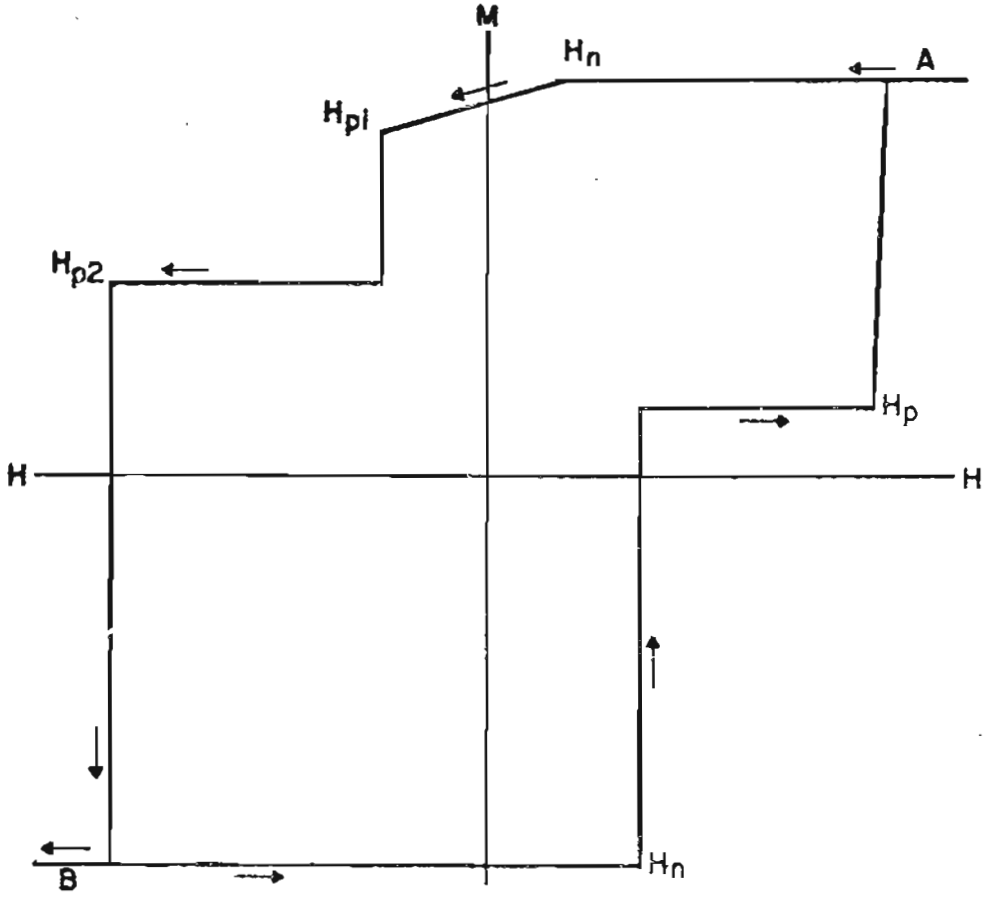

Figure 9. Conceptual hysteresis loop showing pinning (H_p) and nucleation (H_n) fields of domain walls.

materials, the effect of combined pinning and nucleation taking place simultaneously results in the usual imperfect hysteresis loops observed.

Materials which are highly anisotropic also have very thin domain walls as was pointed out by Trammell.[42] Wall thicknesses have been known to attain a size of a few Angstroms, comparable to lattice dimensions. In homogeneous materials these walls often become pinned at the lattice of materials possessing an electron rich nonmagnetic element. This phenomenon was pointed out by Oesterreicher in a study of $Sm_{.167}Co_{.833-x}Al_x$.[43] He attributed the high coercivity in these materials to pinning, possibly at the Al in the lattice, rather than to a nucleation effect. This is especially evident since $SmCo_5$ domain wall nucleation is avoided by mechanically breaking down the material, for example by powdering $SmCo_5$ to a size of ~ 100 microns. Since the high coercive fields are observed in bulk materials of $Sm_{.167}Co_{.633}Al_{.200}$, the pinning effect is introduced through the addition of Al to the lattice.

As noted earlier, exchange interactions and crystal field effects play an important role in magnetic hardness. These effects will not be considered in greater detail.

The T-T exchange has been previously considered in detail on the basis of both localized and itinerant electron models, however, it is still little understood.[44] The approach to understanding this interaction is to look at the T elements and their moments:[31]

$$M_{Fe} = 2.2\ \mu_B$$

$$M_{Co} = 1.7\ \mu_B$$

$$M_{Ni} = .6\ \mu_B$$

In addition, the T moments in alloys with the nonmagnetic elements Y, La and Lu can be considered and extrapolations can be made to the magnetic rare earth systems. As mentioned in Chapter 1, the R-T and R-R exchange interactions appear to be of the RKKY type.

An RKKY interaction takes place between the spins of the localized core electrons, $\overline{S}$, and the spin of the conduction electrons, $\overline{s}$. The Hamiltonian of the system is given by:

$$H = -\Gamma\overline{S}.\overline{s},$$

where Γ is the effective exchange integral. Bleaney and Stevens[45-47] have calculated this effect through second order perturbation theory and found the spin density, ρ, versus spatial extent, r, from the ion cores to be:

$$\rho = -[9\pi Z^2 S/4E_F]F(2k_F r),$$

where Z is the number of conduction electrons per atom and $E_F = k_F h/2m$ is the free electron Fermi energy. The RKKY damped oscillatory function is given by:

$$F(2k_F r) = (2k_F r)^{-4}\ [2k_F r\cos(2k_F r) - \sin(2k_F r)],$$

where k_F is the radius of the Fermi sphere.

This expression is of great utility in assessing the magnetic moment alignment in solids possessing conduction electrons, such as the metallic solids considered in this investigation. The two most important features of this equation are that it is a damped oscillatory

function in r extending from the magnetic ion and that, since $k \propto 1/r$, lattice parameter changes in a given structure have no effect on the function while the electron concentration does.

Figure 10, taken from Wallace,[48] shows the pairwise coupling of the light and heavy R elements with the T elements in this scheme. This scheme is the basis of the ferromagnetic versus ferrimagnetic coupling discussed earlier. As shown, the heavy R elements with Hund spin and orbital coupling, $\overline{L}$-$\overline{S}$, align ferrimagnetically while the light R elements with $\overline{L}$+$\overline{S}$ coupling, align ferromagnetically. Also, it is evident that the only possible way to change this coupling for the heavy R elements would be to change the e.c.

As first noted by Kasuya,[8] the polarized electrons in these systems contribute to the overall saturation magnetic moments. This was observed by experiments which showed that Gd^{3+} has a saturation of 7.55 μ_B exceeding by 0.55 μ_B the free ion value of 7.00 μ_B.[8]

In a consideration of the moment alignment, the question arises as to just what is the localized moment of each atom in the solid? The free ion values are given by:

$$\overline{M} = g\overline{J},$$

where $\overline{J}$ is the resultant of a coupling of orbital and spin moments, $\overline{L}\pm\overline{S}$, according to Hund's rules. This is on the basis that the internal and applied fields are sufficiently low that uncoupling of $\overline{L}$ and $\overline{S}$ does not occur.

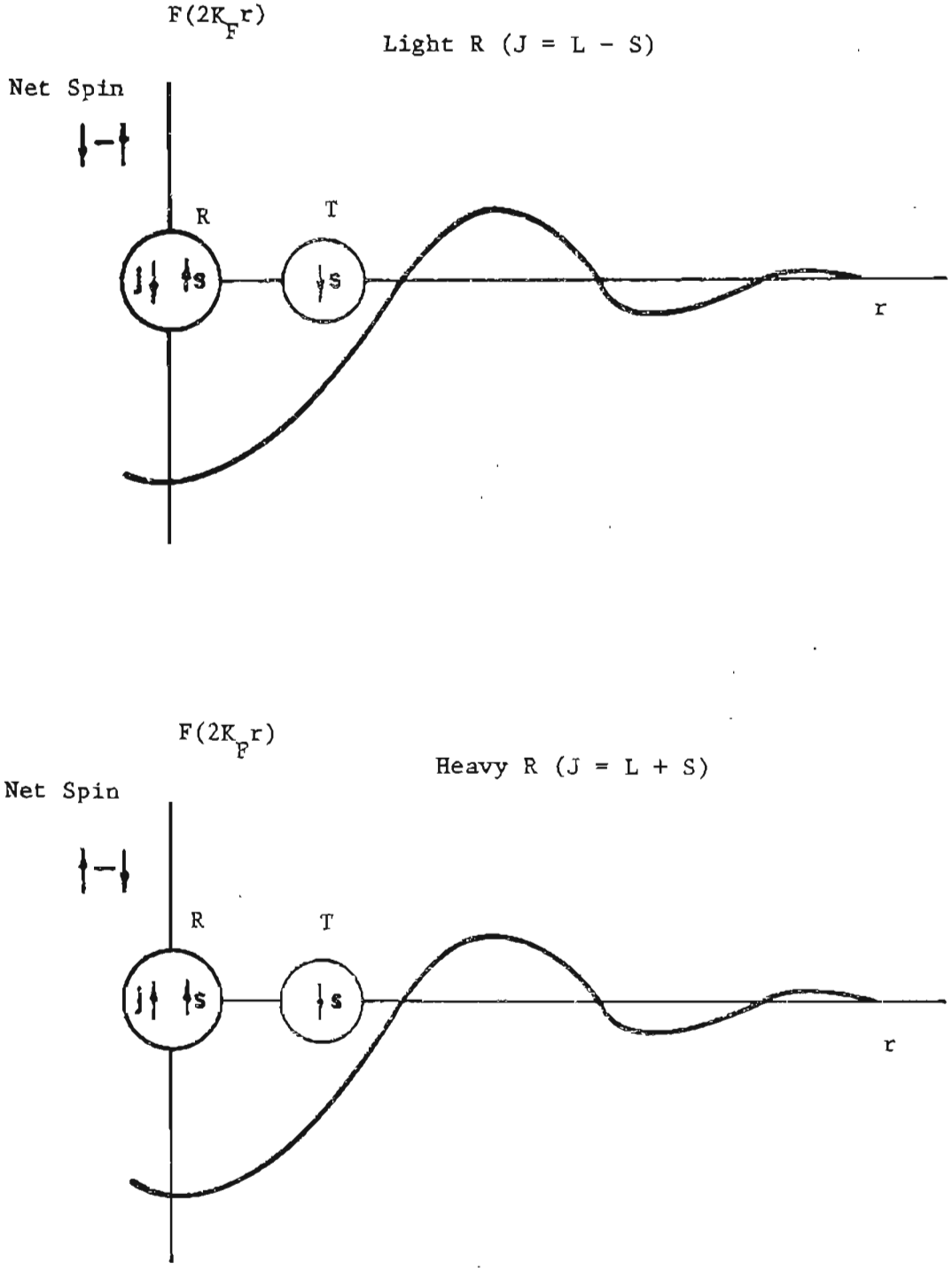

Figure 10. The pairwise coupling of the light and heavy R elements with the T elements in the RKKY coupling scheme

In solids, as pointed out by Kittel,[49] the orbital contribution to the magnetic moment is often quenched by the crystalline electric field. This interaction changes the effective moments on varying sites within solids. The cubic compounds, RT_2 were investigated by Penny and Schlapp[50] and Lea et. al.[51] in this respect. Hexagonal compounds were investigated by Segal and Wallace.[52-55]

The terms in the Hamiltonian of electron-electron and spin-orbit couplings, as discussed earlier, are related to the c.e.f. Fortunately, the symmetry relations reduce the wave function calculations to a reasonable size which can be handled through the equivalent operator method and computer calculations. In this way the ground and excited state eigenvalues of the crystal field states can be calculated.

To a first approximation, Y^{3+}, Eu^{2+}, Gd^{3+} and Lu^{3+} have spherically symmetric charge distributions. Thus, their crystal field states are little affected by neighboring ions in a lattice. The crystal field states in the balance of the R elements, however, are affected to varying degrees. The degree of influence on the affected R elements in compounds can be determined through correlations of the affected with the unaffected R elements in similar compounds.

One of the weaknesses of this crystal field model is that it is based on a point charge concept which is too naive an approach. Also, there is work yet to be done in considering the array of

surrounding neighbor atoms as being of a different species such as T-Al mixtures. A future model would be necessary to explain many of the systems in this work.

Thus, to best understand the magnitude of magnetic moments and their alignments with respect to one another it is currently necessary to rely on existing experimental evidence. Such evidence is fairly well characterized in the literature as seen in Appendix III.

The basic experimental evidence is gathered by three rather powerful methods. These are (1) magnetometer measurements, (2) neutron diffraction measurements, and (3) Mossbauer studies. These measurements are usually performed on randomly oriented powders, but occasionally single crystal measurements are made. The paucity of single crystal data is due to the difficulty in growing single crystals in systems since twinning often takes place.[56]

The most straightforward measurements are made by use of magnetometers. They indicate the total saturation moments and, therefore, do not separate the various effects discussed earlier. Here it is especially necessary to identify effects among varying species which can shed light on the moment alignments and their magnitudes.

Since the neutron possesses a magnetic moment due to its intrinsic spin and also since it has no electrostatic charge, it lends itself well to characterization of the effects in the conduction band solids such as metallic alloys. Measurements of this

type are sparse since the cost of gathering information is high. This method of characterizing effects in alloys can in many cases distinguish between important properties, such as site moments, their alignment relationships, and the magnetically oriented axes.

Mossbauer measurements make use of low energy, recoilless γ-ray emissions from nuclei which interact with the surrounding solid. Such interactions result in a characteristic hyperfine splitting at the various nuclear sites of the atoms within the material under investigation. Various moments and c.e.f. states in such materials can often be characterized with this method. One of the weaknesses of Mossbauer spectroscopy is the difficulty in resolving the different spectra which are superimposed on one another. For selected cases resolution of the data is possible and useful information can be gathered.

CHAPTER III

EXPERIMENTAL RESULTS AND DISCUSSIONS

This chapter is organized according to structural composition and under each section all the earlier topics discussed will be related to each structural type. The order of coverage is RT_5, RT_3, R_6T_{23}, and finally R_2T_{17}. Structural considerations include discussion about stability. Magnetic considerations include discussion of saturation moments, Curie temperatures and coercive fields. Some discussion is included on domain wall effects, such as pinning, nucleation and temperature dependence of wall motion. The specific experimental procedures and error analyses are presented in Appendix V.

RT_5

Oesterreicher[57] has found that, in general, Al substituted in binary alloys for a transition metal usually fills the various sites of the lattice statistically. This is also the case in many of the RT_5 compounds as illustrated by the intensity calculation for $Tb_{.167}Co_{.685}Al_{.150}$ shown in Table VI. Since the $CaCu_5$ structure has two sites open for Al substitution (the 2C and 3G sites), three calculations were carried out. The first was based on a totally statistical model, the second regarded the Al as partially replacing the Co on the 3G site, and the third considered replacement of Co on the 2C site. The observed intensities support the concept of statistical site substitutions.

TABLE VI

Powder X-ray Diffraction Data of $Tb_{.167}Co_{.683}Al_{.15}$

Material: Induction melted and annealed for 200 h at 800°C

Radiation: CoK_{α}

Structural Data: $CaCU_5$ type, hexagonal a = 4.9902 Å, c = 4.0200 Å

Atomic Positions

1a	0,0,0
2c	2/3,1/3,0; 1/3,2/3,0
3g	0,1/2,1/2; 1/2,0,1/2; 1/2,1/2,1/2

Calculated Ordering Schemes:*

Ordering 1 (Statistical)	Ordering 2	Ordering 3
1a Tb	1a Tb	1a Tb
2c Co 82% Al 18%	2c Co	2c Co 55% Al 45%
3g Co 82% Al 18%	3g Co 70% Al 30%	3g Co

*Computed with the aid of Cromer's x-ray scattering factor equation.[58]

TABLE VI (continued)

Powder X-ray Diffraction Data of $Tb_{.167}Co_{.583}Al_{.15}$

hkl	θ calc.	θ obs.	d calc	Relative Intensity			
				I obs.	I calc.		
					Ord. 1	Ord. 2	Ord. 3
100	11.95	11.98	4.322	1.0	0.6	0.5	0.7
001	12.87	12.89	4.020	2.0	0.9	1.4	0.4
101	17.70	17.73	2.943	6.5	6.1	5.0	8.0
110	21.02	21.02	2.495	3.5	3.5	3.9	3.0
200	24.47	24.50	2.161	4.0	3.7	3.0	4.8
111	24.98	25.01	2.120	10.0	10.0	10.0	10.0
002	26.44	26.46	2.010	2.5	2.5	2.4	2.7
201	28.05	28.11	1.903	1.0	0.2	0.2	0.4
102	29.41	29.43	1.823	0.1	0.1	0.1	0.2
210	33.23	33.25	1.633	0.1	0.1	0.1	0.1
112	34.88	34.91	1.565	2.0	1.6	1.8	1.4
211	36.26	36.30	1.513	2.0	1.6	1.4	2.1
202	37.46	37.46	1.472	2.5	2.1	1.7	2.7
300	38.42	38.46	1.441	1.0	0.6	0.7	0.5
301	41.30	41.34	1.356	2.5	2.3	2.3	2.3
003	41.91	-	1.340	-	0.0	0.0	0.0
103	44.38	44.40	1.280	0.9	0.5	0.4	0.7
212	44.91	44.92	1.268	0.1	0.0	0.0	0.1
220	45.85	45.90	1.248	2.0	1.7	1.6	1.8
310	48.30	-	1.199	-	0.0	0.0	0.1

TABLE VI (continued)

Powder X-ray Diffraction Data of $Tb_{.167}Co_{.683}Al_{.15}$

hkl	θ calc.	θ obs.	d calc	Relative Intensity			
				I obs.	I calc.		
					Ord. 1	Ord. 2	Ord. 3
221	48.69	48.70	1.191	0.2	0.2	0.1	0.1
113	49.31	49.29	1.181	2.0	1.7	1.7	1.7
302	49.86	49.88	1.171	1.0	0.8	0.8	0.7
311	51.19	51.21	1.149	1.0	0.9	0.7	1.1
203	51.80	-	1.139	-	0.0	0.0	0.0
400	55.94	44.98	1.080	0.5	0.4	0.5	0.8

The ternary n.n.d. for the $CaCu_5$ isotypes was constructed considering statistical ordering and is shown in Figure 11. The diameters of the T type atoms were calculated as average diameters of the constituent atoms. For instance in $Tb_{.167}Co_{.683}Al_{.15}$ the diameter of T is given by:

$$D_T = (.683/.833)\ D_{Co} + (.150/.833)\ D_{AL}$$

In this diagram the compounds which stabilize as a single phase follow a slope between the slope of TT and RT contact lines. The TT contacts are slightly compressed, while the RT contacts are greatly compressed in these compounds. Al substitution follows this trend in both $Sm(Co, Al)_5$ and $Ce(Co, Al)_5$ as does Zr substitution in $Sm_{.167-x}Zr_xCo_{.833}$. Contrary to this, Al substitution in $Tb(Co, Al)_5$ has a tendency to destabilize the structure which is shown in Figure 11 as a move away from the RT and TT contact lines. After an initial compression of the RT and TT contacts, $Tb_{.167}Co_{.633}Al_{.200}$ breaks into two phases. One of these phases is again of the $CaCu_5$ type which moves back in line on the n.n.d. A similar situation occurs for the Zr-rich region of the $Sm_{.167-x}Zr_xCo_{.833}$ curve. The $Sm_{.167}Co_{.833-x}Si_x$ curve shows the same trends towards destabilization. The compression between the R and T atoms was discussed in Chapter 2 with respect to the $SmFe_5$ compound and its instability. In the ternary compounds one sees a similar situation where an electron rich third constituent is added to the lattice and destabilization takes place. As will be pointed out later, the addition of an electron rich third substituent to the binary

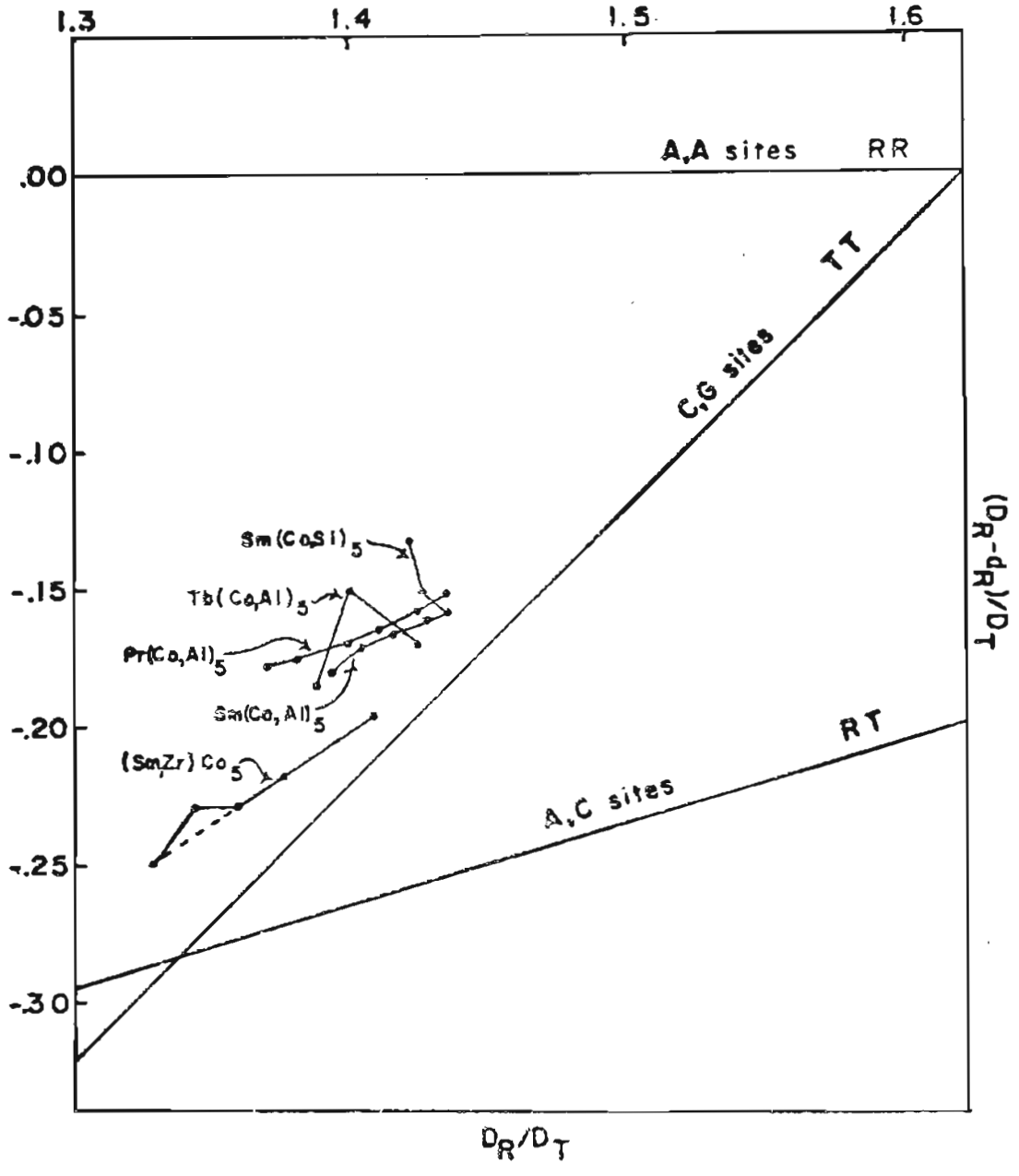

Figure 11. $CaCu_5$ ternary near-neighbor diagram

RCo_5 compounds has little effect on the d-band of Co. Thus the e.c. (electrons/atom in the conduction band) is being increased in the $R(Co, E)_5$ compounds. This change in e.c. is apparently the reason for the lack of stability as more of the electron rich substituent is added to the RCo_5 lattice.

Further substitutions of the form $Sm_{.167}Co_{.833-x}Ex$ at x = .150 show the same e.c. effects on structural stability. For instance, E = Cu or Ni form stable compounds and fit on the n.n.d. in Figure 11. Since their size and electronegativities are similar to Co and since they contribute fewer electrons to the conduction bands, stability is to be expected. E = Ag also fits the geometrical factors above and it likewise maintains the $CaCu_5$ type structure on substitution. E = Pt, Au, In or Sn form multiphase compounds on substitution. Magnetic data on the RT_5 compounds, including the results of the present study, are shown in Appendix IV. Unfortunately, there is no neutron diffraction data available on $SmCo_5$ to explain the coupling scheme in this material. However, neutron diffraction experiments on YCo_5,[36] $TbCo_5$ and $NdCo_5$[59] were performed. These experiments can reveal the Co moments in compounds of these types. For the Tb compounds at 4.2°K the Co sites have moments of CoI (2C sites) M = 1.55 ± .20 μ_B and CoII (3G sites) M = 1.70 ± .10 μ_B. The two sites give an average moment for Co in this structure of 1.64 ± .14 μ_B. Assigning a moment of 0.7 μ_B to Sm in $SmCo_5$, the total moment for this compound with ferromagnetic coupling would be M_s = 8.9 ± 0.7 μ_B per formula unit.

With ferrimagnetic coupling M_s would be 7.5 ± 0.7 μ_B per formula unit. M_s for $SmCo_5$ has been observed to be 7.8 μ_B.[60-62] This value seems to support ferrimagnetic coupling of the R and T sublattices contrary to the RKKY coupling scheme. This experimental evidence is not as conclusive as that which would be provided by a neutron diffraction study on $SmCo_5$; hence, the exact form of coupling in this compound will remain obscure until such evidence is available. $NdCo_5$ however, couples ferromagnetically and $TbCo_5$ couples ferrimagnetically as demonstrated by Lemaire et. al.[59] by means of neutron diffraction measurements.

Upon substitution of a nonmagnetic element, such as Ag, for Co in the Co sublattice one would expect M_s = 6.27 μ_B per formula unit for $Sm_{.167}Co_{.683}Ag_{.150}$ assuming ferrimagnetic coupling. In the present study, M_s for the $Ag_{.150}$ compound was found to be 5.9 μ_B per formulat unit. $Sm_{.167}Co_{.683}Si_{.150}$ should also show an M_s = 6.27 μ_B per formula unit. The results of the present study show M_s = 3.3 μ_B per formula unit. The difference between the theoretical ferrimagnetic value of M_s and the experimental value is probably due to insufficiently high fields attainable with the laboratory apparatus to saturate the material.

Figures 12 and 13 show the hysteresis loops of $Sm_{.167}Co_{.633}Si_{.200}$ for bulk and powdered materials respectively at 4.2°K. This material shows the principal mechanism of domain wall pinning. Apparently, these walls are extremely thin and become pinned at the aluminum in

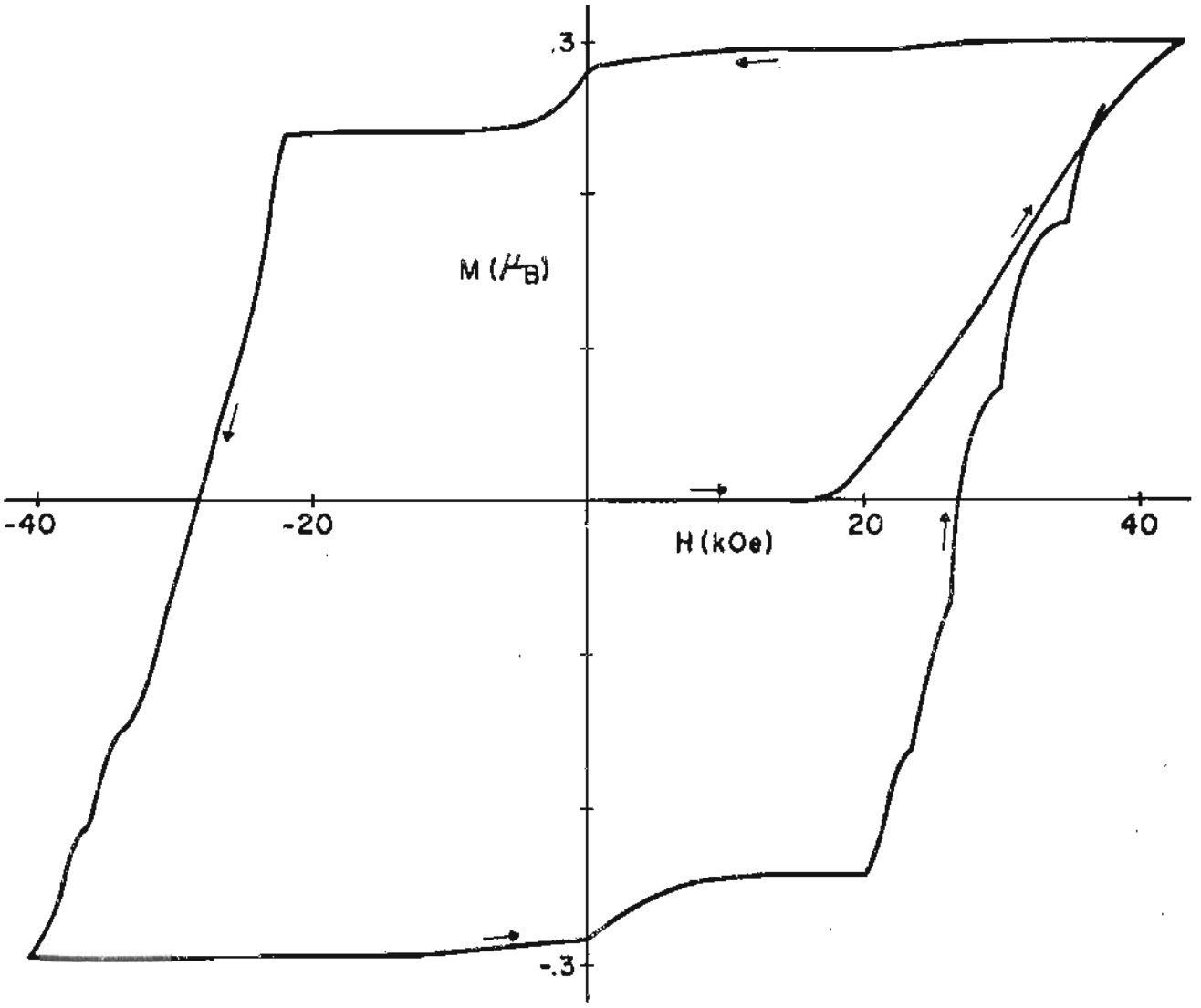

Figure 12. Hysteresis loop of the bulk alloy $Sm_{.167}Co_{.633}Si_{.20}$

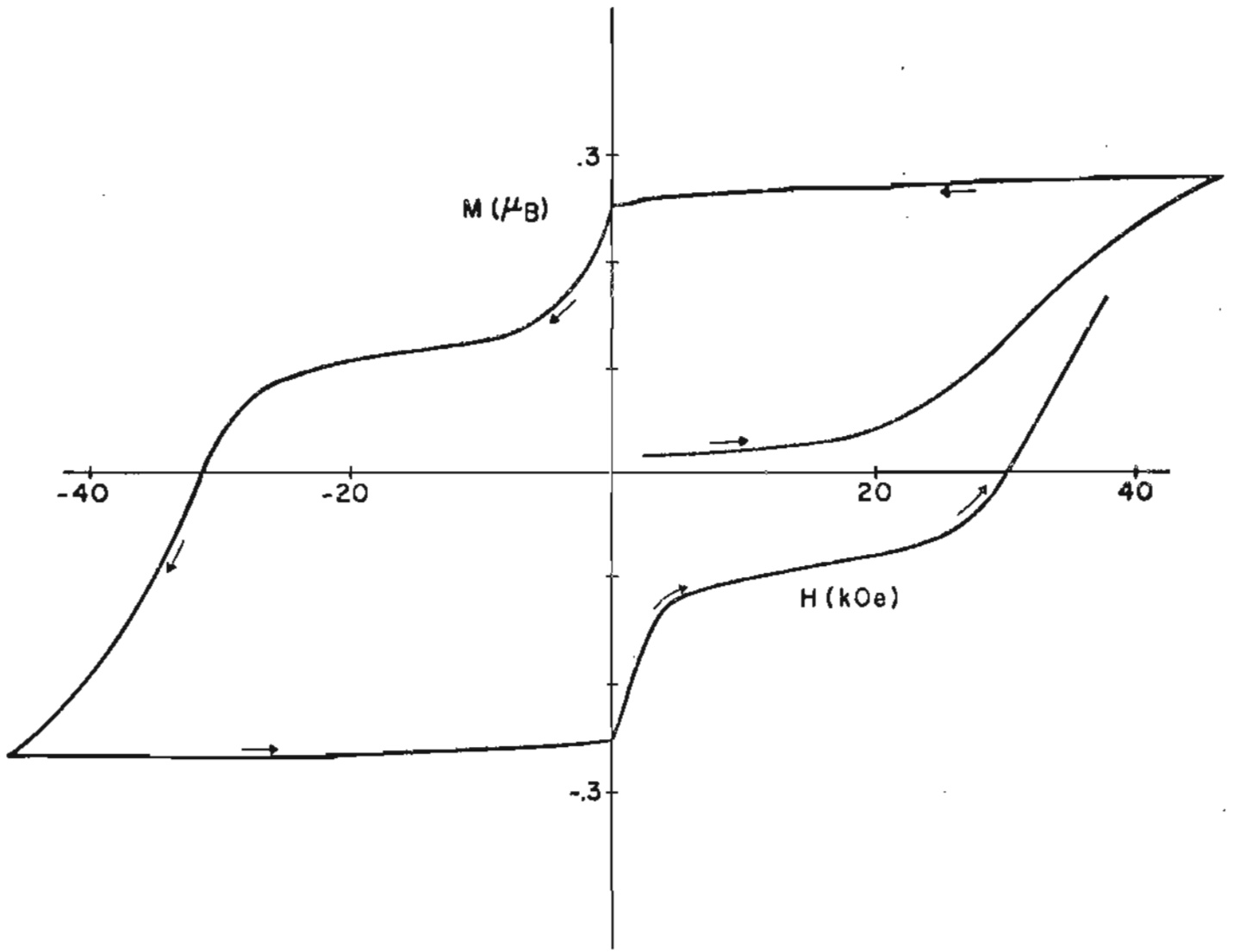

Figure 13. Hysteresis loop of powdered alloy $Sm_{.167}Co_{.633}Si_{.20}$

the lattice. The presence of several pinning fields is very evident in the scallop-shaped curves in Figure 12. Upon pulverizing the bulk material there is an increase in nucleation effects, as seen by the continuous decrease of M_s upon reversal of the applied field. This is probably due to the mechanical stresses experienced by the material during preparation.

The coercive fields of the other $Sm_{.167}Co_{.683}E_{.150}$ compounds are rather low. For instance, Zr substitution for Sm shows a reduction in H_c and H_a as shown in Appendix IV. The same is true when the Sm is totally replaced by Tb and Ce. Of these two compounds the one with Tb reaches a peak value of H_c = 6.0 kOe. Cu and Ni substitutions for Co, however, do show fair H_c values (12.5 kOe and 7.5 kOe, respectively).

The addition of Zr points out that H_a is reduced as Sm is depleted from the lattice. This is most likely due to the c.e.f. between Sm and Co. The Tb compound does apparently maintain a reasonably high H_a due to the c.e.f. while Ce shows a substantial decrease in coupling with Co. One can, therefore, assume that the origin of magnetic hardness in these alloys is connected with high domain wall energies and strong crystal field coupling.

RT_3

The RT_3 compounds considered in the present study are the pseudobinary $Dy_{.25}Fe_{.75-x}Al_x$ with x = 0.0 to 0.3. Plots of the lattice parameter versus composition are shown in Figure 14. The break in

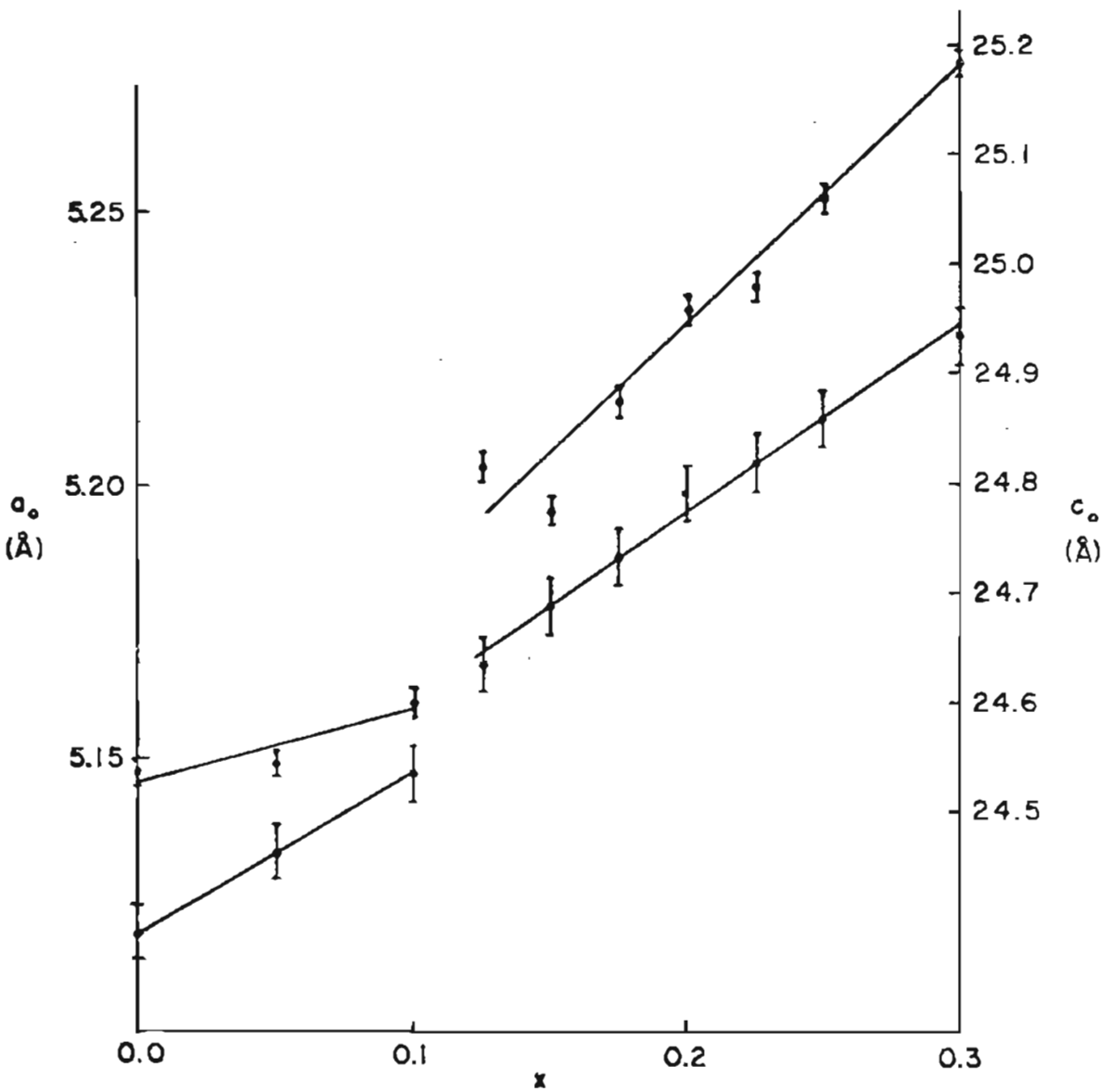

Figure 14. Plot of lattice parameters versus composition of $Dy_{.25}Fe_{.75-x}Al_x$

these curves at x = 0.10 indicates that the $PuNi_3$ structure is stable to that point, and within a short range of composition, a mixture of $PuNi_3$ and $CeNi_3$ structural types occurs. Above x = 0.15 the $CeNi_3$ structural type stabilizes.

The n.n.d. for these alloys is constructed on the basis of the $PuNi_3$ isotypes since only a few $CeNi_3$ isotypes are currently known. Similar to the $CaCu_5$ ternary n.n.d., the radii of the constituent atoms which share sites were calculated on a statistical basis. Figure 15 shows this n.n.d. Also shown on this diagram are the two pseudobinaries $Dy_{.25}Fe_{.75-x}Ni_x$ and $Dy_{.25}Fe_{.75-x}Al_x$. The substitution of Ni for Fe shows a tendency to relieve the compressed RR and TT contacts. This is due to the Ni taking up electrons in its d-band. The analogous material rich in Al, on the other hand, closely follows the RT contact as it replaces Fe in the lattice and as the smaller unit cell of the $CeNi_3$ isotype evolves.

The $CeNi_3$ and $PuNi_3$ structures are closely related. The evolution of the $CeNi_3$ structure via the addition of Al in $Dy_{.25}Fe_{.75-x}Al_x$ is either related to the change in directional bonding of the Fe in the lattice or the more subtle interaction between the Fermi surface and Brillouin zone planes resulting from the change in e.c. in this material. Since the substitution of Ni for Fe in $DyFe_3$ does not involve the $CeNi_3$ structural type, the Fermi surface and Brillouin zone interactions are probably more important.

Table VII shows two calculations for the intensities of an x-ray diagram of $Dy_{.25}Fe_{.50}Al_{.25}$. The possibility of this being an ordered

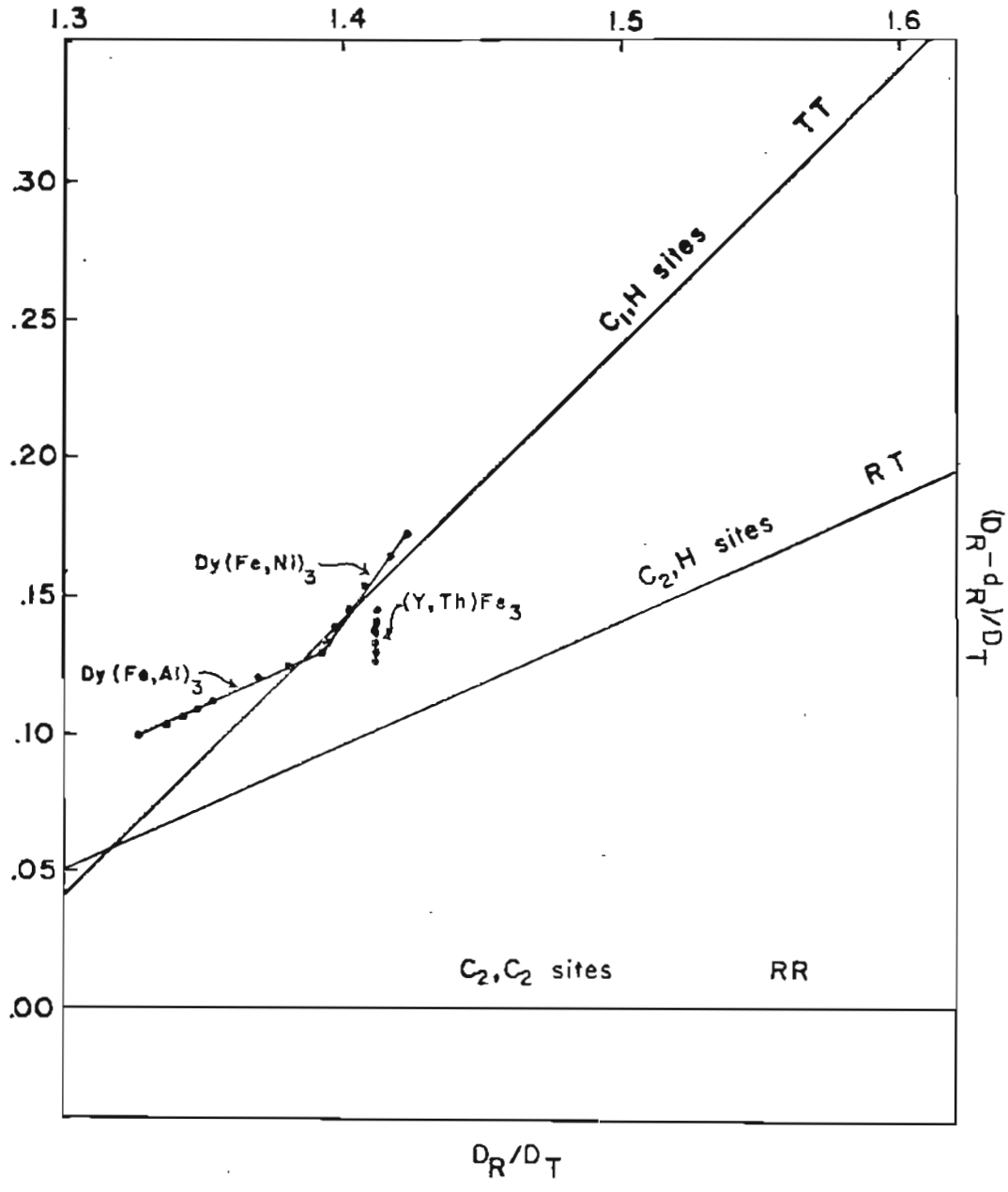

Figure 15. $PuNi_3$ ternary near-neighbor diagram

TABLE VII

Powder X-ray Diffraction Data of $Dy_{0.25}Fe_{0.50}Al_{0.25}$

Material: Induction melted

Radiation: CrK_{α}

Structural Data: $CeNi_3$ type, hexagonal a = 5.212 Å, c = 16.690

Atomic Positions

2c	1/3,2/3,1/4
4f	1/3,2/3,z (z = .0418)
2a	0,0,0
2b	0,0,1/4
2d	1/3,2/3,3/4
12k	2,2x,z (x = .8334; z = .1272)

Calculated Ordering Schemes:

Ordering 1		Ordering 2	
2c	Dy	2c	Dy
4f	Dy	4f	Dy
2a	Al	2a	Fe
2b	Al	2b	Fe
2d	Al	2d	Fe
12k	Fe	12k	50% Fe; 50% Al

TABLE VII (continued)

Powder X-ray Diffraction Data of $Dy_{0.25}Fe_{0.50}Al_{0.25}$

hkl	θ calc.	θ obs.	d calc.	Relative Intensity		
				I obs.	I calc.	
					Ord. 1	Ord. 2
100	14.70	14.77	4.514	1.0	1.6	1.0
101	15.24	15.32	4.358	1.6	1.9	1.9
004	15.93	15.97	4.173	1.2	0.1	1.4
102	16.77	-	3.970	-	0.3	0.1
103	19.08	-	3.505	-	0.0	0.4
104	21.96	22.01	3.064	1.4	2.1	1.0
006	24.32	24.22	2.781	0.4	0.2	0.4
105	25.27	25.31	2.684	8.0	9.9	9.0
110	26.08	26.11	2.606	7.2	4.4	7.8
112	27.40	27.43	2.488	0.2	0.3	0.2
106	28.93	28.95	2.368	0.4	0.3	0.5
200	30.50	30.52	2.257	1.1	1.9	1.3
201	30.81	30.83	2.237	2.4	4.4	3.2
114	31.22	31.24	2.210	10.0	7.3	10.0
107	32.91	32.93	2.108	1.1	1.1	1.3
203	33.21	33.27	2.091	2.3	1.9	1.7
008	33.31		2.086		0.7	0.8
204	35.24	35.30	1.985	0.1	0.1	0.1
116	37.04	37.02	1.902	0.6	0.7	1.0

TABLE VII (continued)

Powder X-ray Diffraction Data of $Dy_{0.25}Fe_{0.50}Al_{0.25}$

hkl	θ calc.	θ obs.	d calc.	Relative Intensity		
				I obs.	I calc.	
					Ord. 1	Ord. 2
108	37.22	37.25	1.894	0.2	0.2	0.3
205	37.79	37.75	1.870	0.5	0.4	0.6
206	40.81	-	1.753	-	0.1	0.1
109	41.89	41.85	1.715	0.8	0.7	0.7
210	42.18	42.20	1.706	0.2	0.2	0.2
211	42.45	42.41	1.697	0.4	0.3	0.3
0010	43.34	43.34	1.669	0.8	0.5	0.6
213	44.61	44.65	1.631	0.2	0.0	0.1
118	44.70		1.629		0.0	0.1
214	46.50	46.50	1.579	0.1	0.6	0.3
1010	47.03	46.99	1.565	0.4	0.5	0.7
208	48.39	48.35	1.532	0.4	0.1	0.0
215	48.95	48.95	1.519	3.3	4.1	3.9
300	49.58	49.62	1.505	2.0	1.0	1.8
302	50.68	-	1.481	-	0.1	0.0
216	51.97	52.00	1.454	0.2	0.2	0.3
1011	52.30	-	1.438	1.0	0.1	0.0
209	53.08	53.05	1.433	2.5	2.8	2.3
304	54.03	54.04	1.415	3.5	2.6	3.5
1110	54.59	54.56	1.405	2.3	3.0	2.5

TABLE VII (continued)

Powder X-ray Diffraction Data of $Dy_{0.25}Fe_{0.50}Al_{0.25}$

hkl	θ calc.	θ obs.	d calc.	Relative Intensity		
				I obs.	I calc.	
					Ord. 1	Ord. 2
0012	55.45	-	1.391	-	0.3	0.1
217	55.65	55.61	1.387	1.3	0.9	1.1
2010	58.60	58.59	1.342	0.2	0.7	0.8
1012	59.52	59.46	1.329	0.2	0.1	0.2
306	59.95	59.97	1.323	0.2	0.4	0.6
218	60.15	60.11	1.321	0.3	0.2	0.4
220	61.53	61.53	1.303	6.0	4.4	4.9
222	62.85	-	1.259	-	0.1	0.0
2011	65.47	65.75	1.259	1.8	0.2	0.2
219	65.83		1.256		1.4	1.5
310	66.20	66.30	1.252	0.1	0.3	0.2
311	66.57	66.44	1.248	0.3	0.4	0.4
224	67.07	67.05	1.244	0.3	0.1	0.8
312	67.70	-	1.238	-	0.1	0.0
1013	68.06	68.01	1.235	0.5	0.2	0.1
1112	68.99	-	1.227	-	0.0	0.1
313	69.70	-	1.220	-	0.0	0.1
308	69.83	-	1.221	-	0.0	0.1
314	72.80	72.84	1.199	0.3	1.0	0.6
2110	73.76	79.77	1.193	2.0	1.9	2.4

TABLE VII (continued)

Powder X-ray Diffraction Data of $Dy_{0.25}Fe_{0.50}Al_{0.25}$

hkl	θ calc.	θ obs.	d calc.	Relative Intensity		
				I obs.	I calc.	
					Ord. 1	Ord. 2
0014	73.91	74.05	1.192	0.8	0.5	0.7
2012	75.33	75.27	1.184	1.2	1.6	1.8
226	76.11	76.10	1.180	0.5	0.6	0.9
315_1	77.60	77.63	1.172	8.6	10.0	9.6
315_2	78.05	78.04				

structure with the Al on the 2a, 2b and 2d sites was considered. This showed poor agreement with the observed intensities. The other possibility considered was that of the Fe and Al sharing the 12K sites. This is in better agreement with the observed intensities.

M_s values for these RT_3 compounds are plotted versus composition at 4.2°K in Figure 16. The line drawn on this figure represents ferrimagnetic coupling between the Dy and Fe, respectively. On Al substitution in $Dy_{.25}Fe_{.75-x}Al_x$ this coupling is maintained until x = 0.30 where the saturation moment increases 0.5 μ_B above the antiferromagnetic coupling curve. This is interpreted as a possible trend towards ferromagnetic coupling through the change in e.c. and its effect on the RKKY coupling of the Dy and Fe sublattices. Since the $Dy_{.25}Fe_{.75-x}Al_x$ compound is multiphasic beyond x = 0.30, this change in coupling cannot be demonstrated conclusively.

As in the RCo_5 compounds with Si and Al substitution, the $Dy_{.25}Fe_{.75-x}Al_x$ compounds show little difference in coercivity at 4.2°K between the bulk and powdered materials. The hysteresis loops of bulk and powdered $Dy_{.25}Fe_{.525}Al_{.225}$ are shown in Figures 17 and 18, respectively. Similar to the $Sm_{.167}Co_{.833-x}Si_x$ alloys, there is a marked difference between the shape of curves corresponding to bulk and powdered materials. The bulk material shows a smooth change in M with increasing negative field. The powdered material, however, shows at least one pinning field on the curve; in fact, in one case pinning did not take place until M had passed through the M = 0 point,

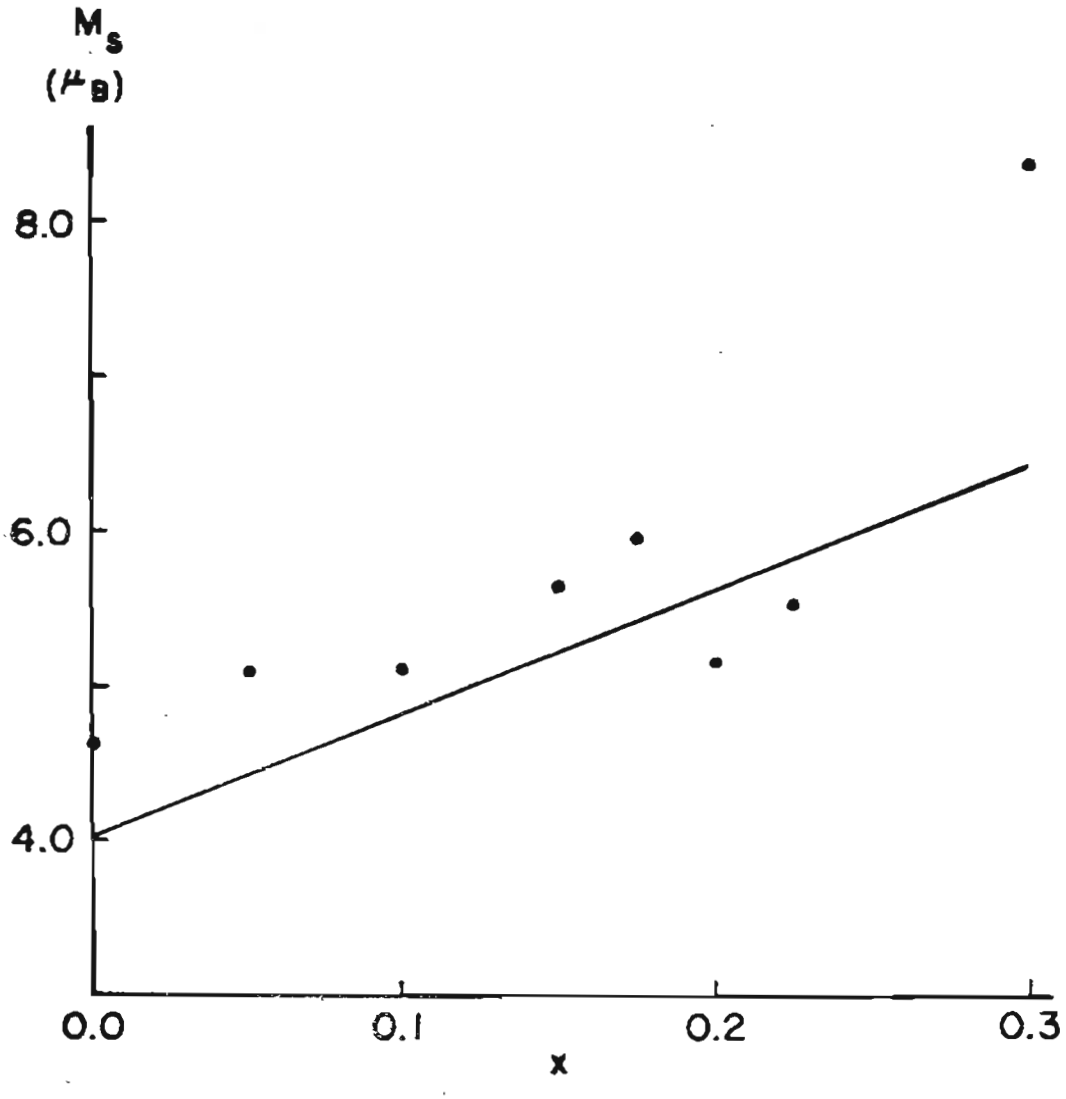

Figure 16. Plot of M_s @ 4.2°K versus composition of $Dy_{.25}Fe_{.75-x}Al_x$.

(The line represents theoretical ferrimagnetic coupling between Fe (2.0 μ_B) and Dy (10.0 μ_B).)

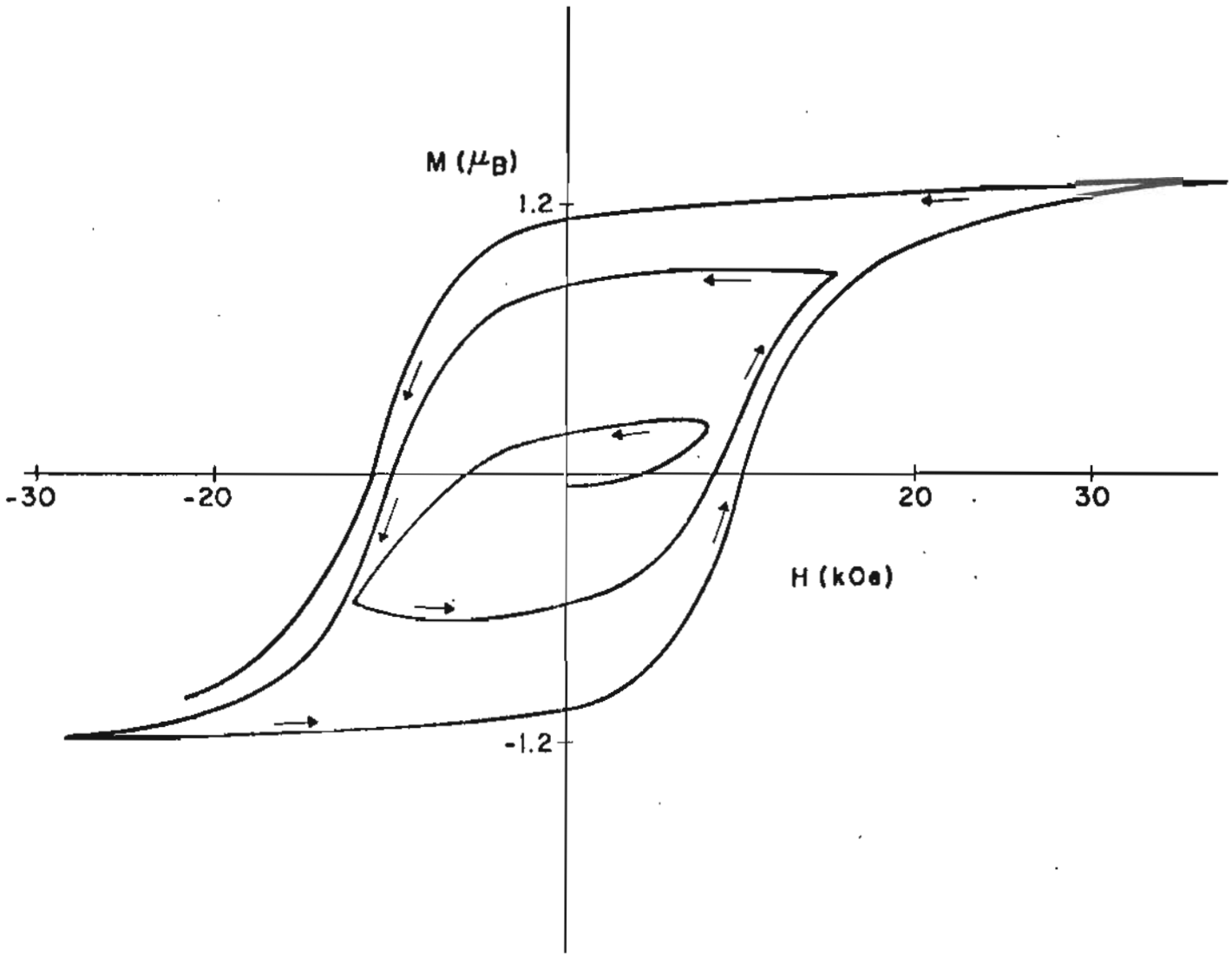

Figure 17. Hysteresis loops of the bulk alloy $Dy_{.25}Fe_{.525}Al_{.225}$

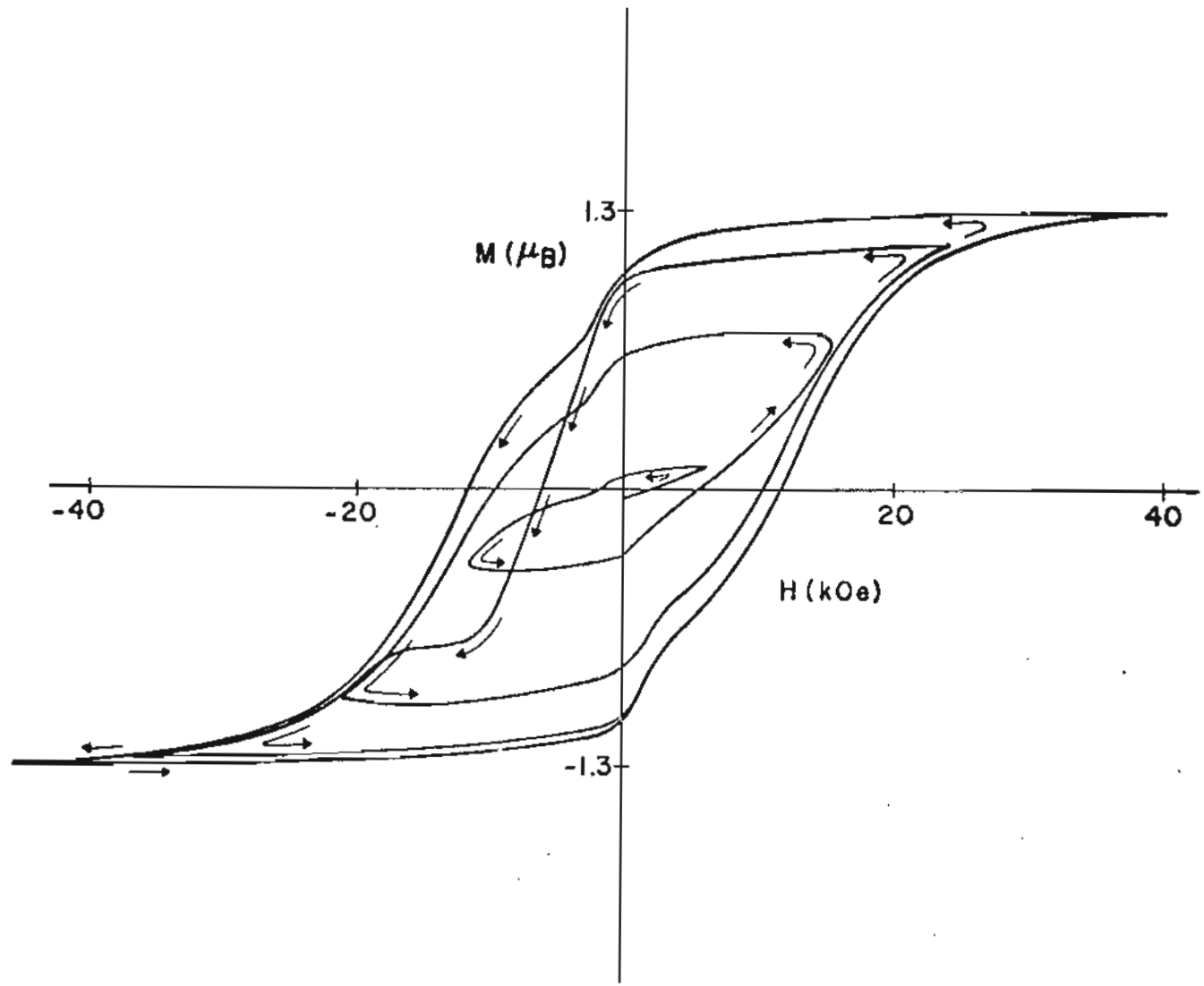

Figure 18. Hysteresis loops of the powdered alloy $Dy_{.25}Fe_{.525}Al_{.225}$

and thus exhibited a lower H_c value. The H_c value for the powdered material was 2 kOe less than that of the bulk material. These differences are thought to be due to the shape of the small crystallites produced on powdering or to a mechanical reorientation of the powders in their sample holders.

The temperature dependence of magnetic hardness was studied in the bulk material $Dy_{.25}Fe_{.75-x}Al_x$ from x = 0.05 to 0.225. It was found that values of H_c decrease with increasing temperature. A Curie-type temperature dependence is observed in the region from 4.2 to 200°K when $1/H_c$ is plotted versus temperature. This is presented in Figure 19. The negative intercepts on the temperature axis as well as the slope vary somewhat with composition but no clear trends can be discerned as shown in Table VIII.

R_6T_{23}

The cubic Th_6Mn_{23} isotypes $Dy_{.207}Fe_{.793-x}Al_x$ are close to a 1:4 stoichiometry. In order to stabilize these compounds from their melts, they were annealed at 1000°C for 100 hours. Al is soluble in these pseudobinary compounds up to a concentration of 20% as shown in Figure 20.

The saturation moments of these materials is shown in Figure 21. The initial Al substitution shows a possible change in the coupling scheme from ferrimagnetic coupling, and as the Al concentration nears 20%, the theoretical ferrimagnetic curve is again approached. H_c

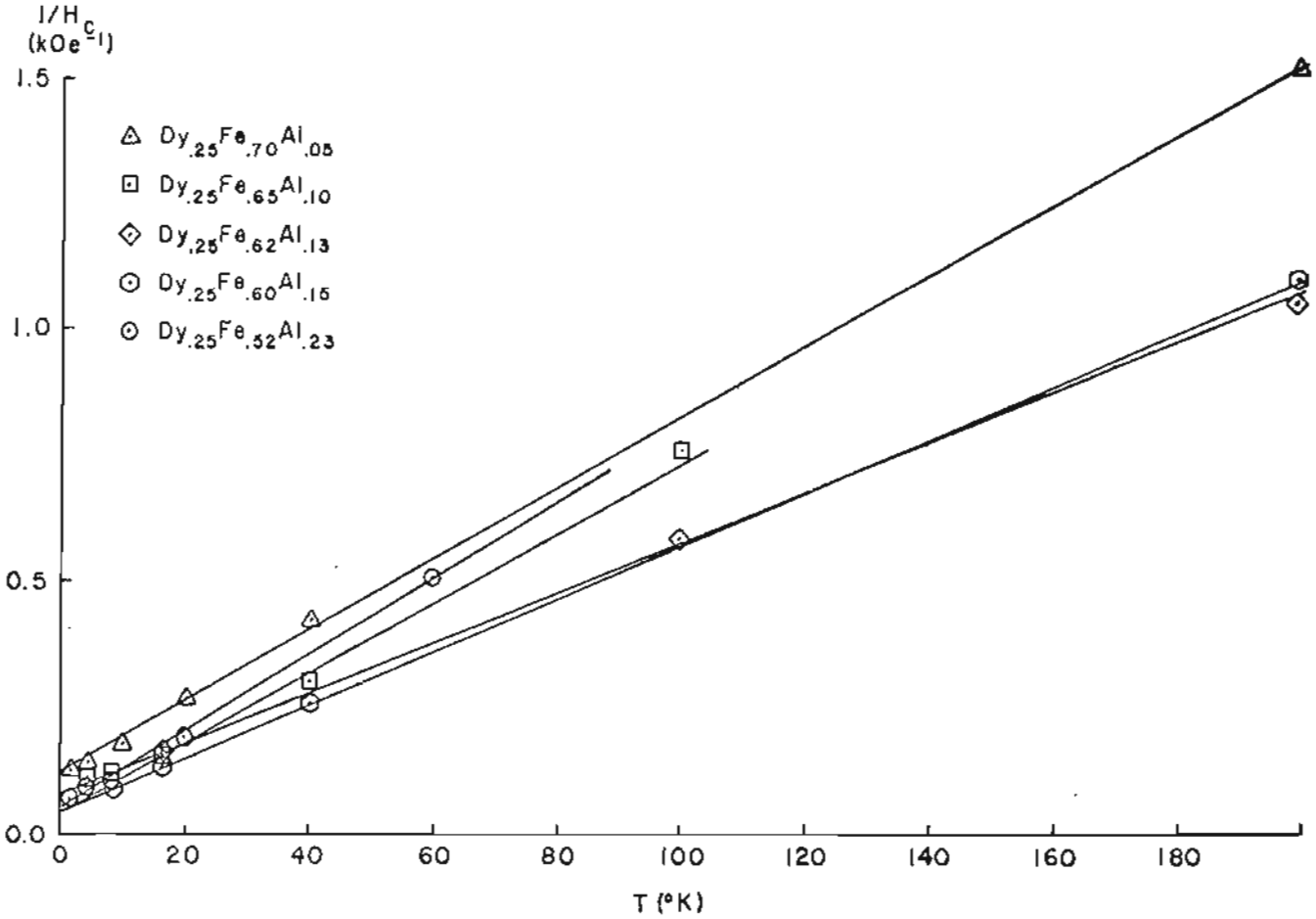

Figure 19. Plots of $1/H_c$ versus T for the noted compositions of $Dy(Fe, Al)_3$

TABLE VIII

Intercepts and slopes of $1/H_c$ versus temperature plots shown in Figure 16 for varying compositions of $Dy(FeAl)_3$ compounds

$Dy_{.25}$ $Fe_{.75-x}$ Al_x	Intercept (°K)	Slope: $1/H_c$ per 100°K (H_c in kOe)
x = .05	-20	.69
.10	-5	.71
.125	-10	.51
.15	-15	.51
.225	-6	.75

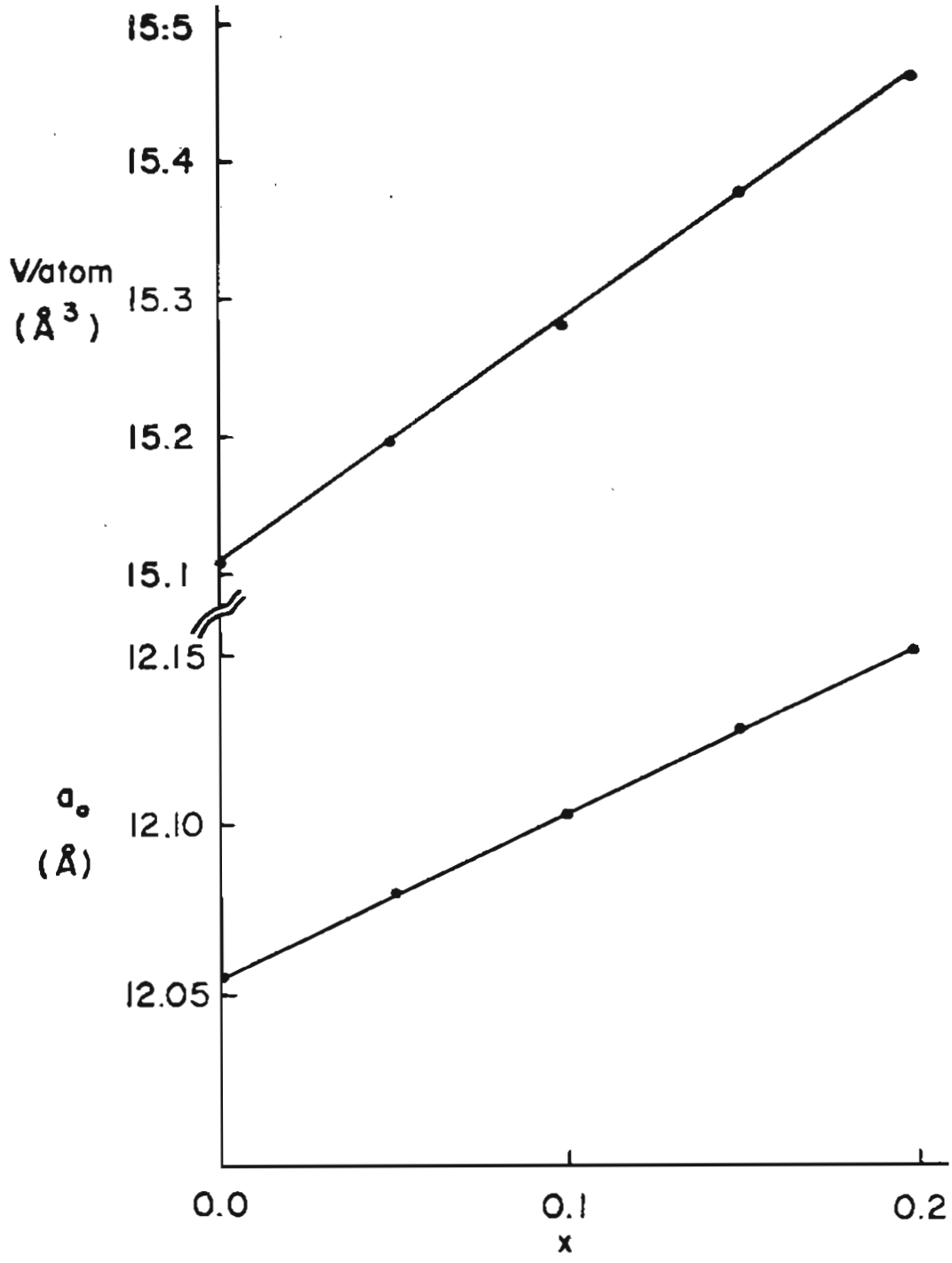

Figure 20. Plot of volume/atom and lattice parameter versus composition of $Dy_{.207}Fe_{.793-x}Al_x$

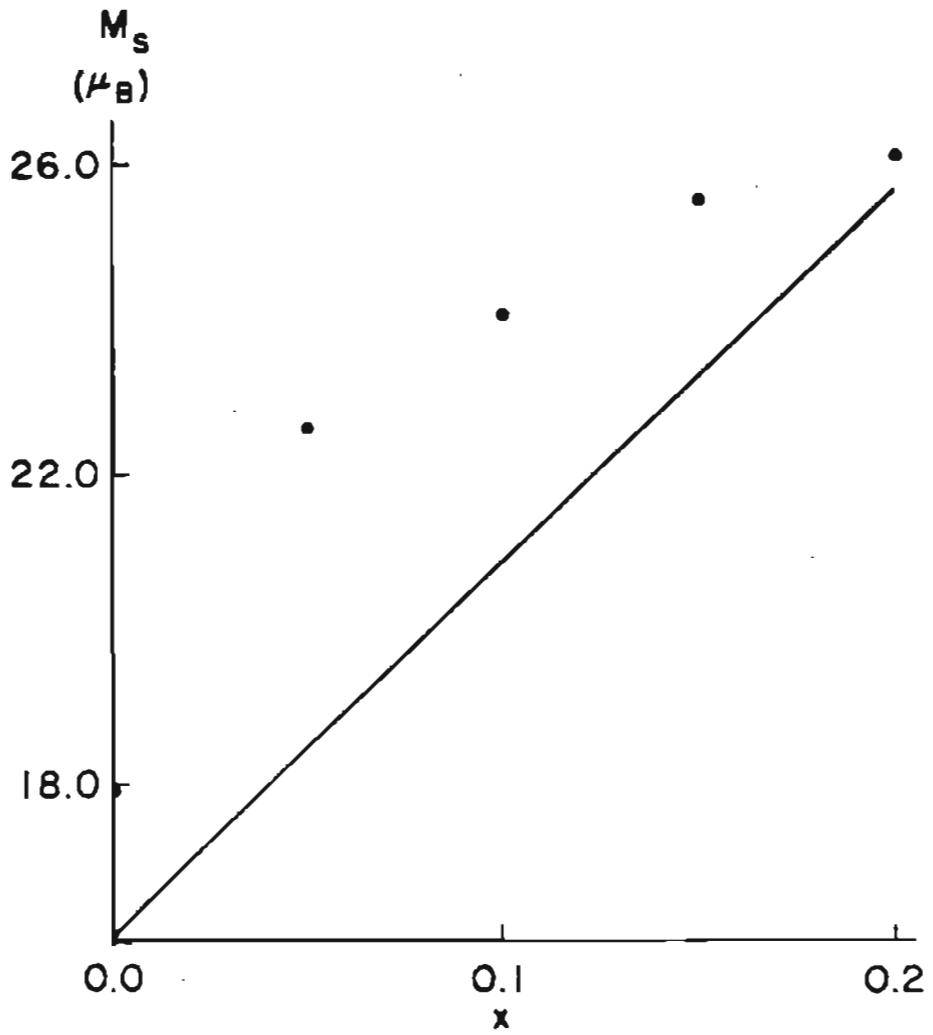

Figure 21. Plot of M_s @ 4.2°K versus composition of $Dy_{.207}Fe_{.793-x}Al_x$. (The line represents theoretical ferrimagnetic coupling between Fe (2.0 μ_B) and Dy (10.0 μ_B).)

increases for these alloys from 2 kOe for Dy_6Fe_{23} to 5.4 kOe for $Dy_{.207}Fe_{.593}Al_{.200}$ at 4.2°K. These compounds show a reasonable degree of magnetic hardness indicating a trend towards developing thin energetic domain walls.

R_2T_{17}

The three pseudobinary cuts, $Sm_{.105}Fe_{.895-x}Al_x$, $Sm_{.105-x}Zr_x$ $Co_{.895}$ and $Dy_{.105}Fe_{.895-x}Al_x$ were investigated. $Sm_{.105}Fe_{.895-x}Al_x$ alloys in the Fe rich composition region of the cut are principally of the Th_2Zn_{17} type with some Fe present. The $Dy_{.105}Fe_{.895-x}Al_x$ alloys are also principally of this Th_2Zn_{17} type; however, between 20 and 25% Al concentrations the Th_2Ni_{17} phase exists. The $Sm_{.105-x}Zr_xCo_{.895}$ was also of the Th_2Zn_{17} type and remained single phase up to 6 atomic percent Zr.

The ternary n.n.d. of these materials is shown in Figure 22 where, as before, a statistical radius is assumed. Since there are a small number of the Th_2Ni_{17} phases, they are also included on this diagram. The $Sm_{.105}Fe_{.895-x}Al_x$ and $Dy_{.105}Fe_{.895-x}Al_x$ phases parallel the RT contact lines with the RT, as well as the TT, contacts under compression. As in the $CaCu_5$ structure, the RR contacts are not under compression. The $Sm_{.105-x}Zr_xCo_{.895}$, as well as several of the other Co compounds of R_2T_{17} variety, parallel the TT contacts and further compress the RT contacts.

The lattice parameters of the $Sm_{.105}Fe_{.895-x}Al_x$ are shown in Figure 23. The basal plane of these compounds expands continuously

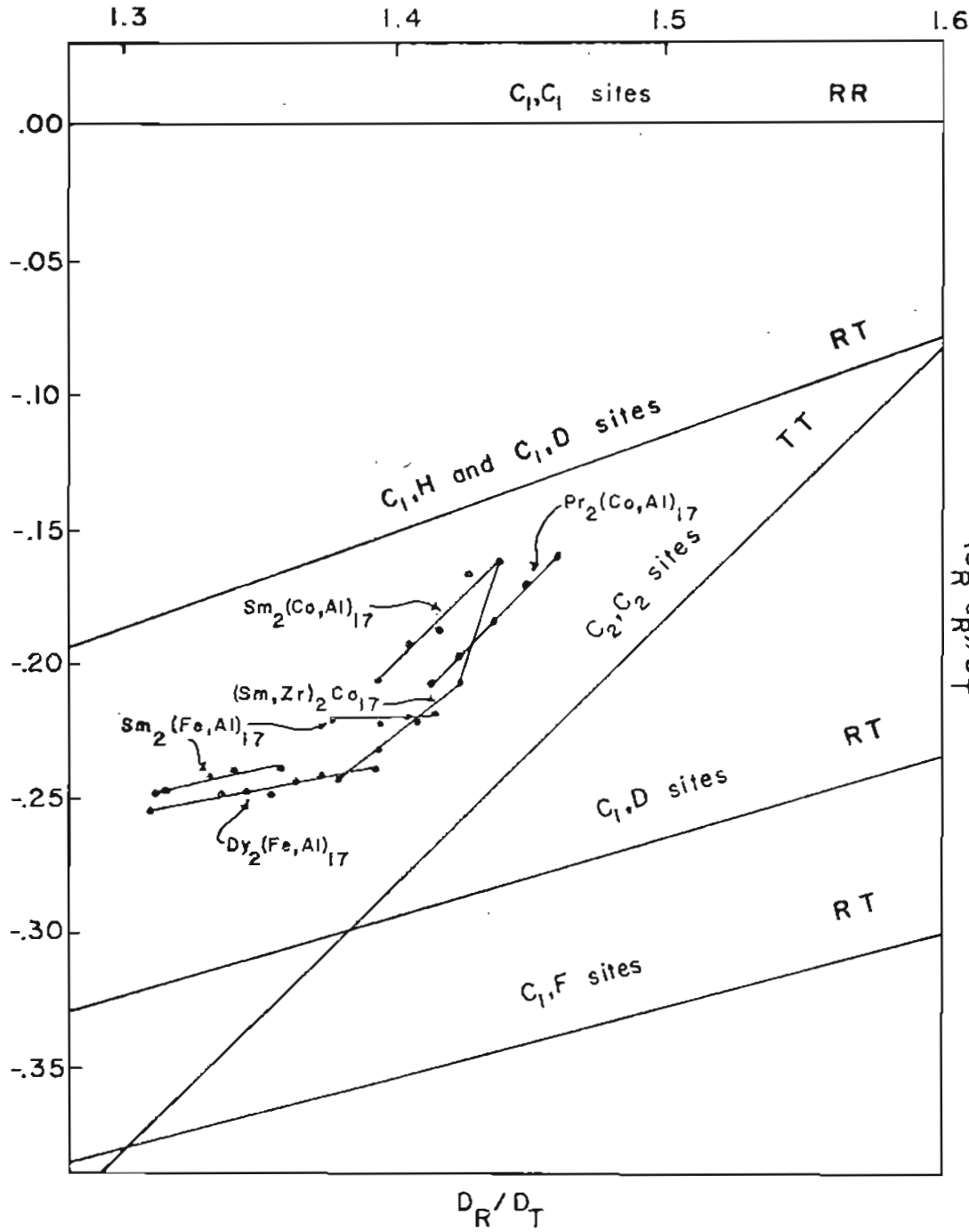

Figure 22. Th_2Zn_{17} ternary near-neighbor diagram

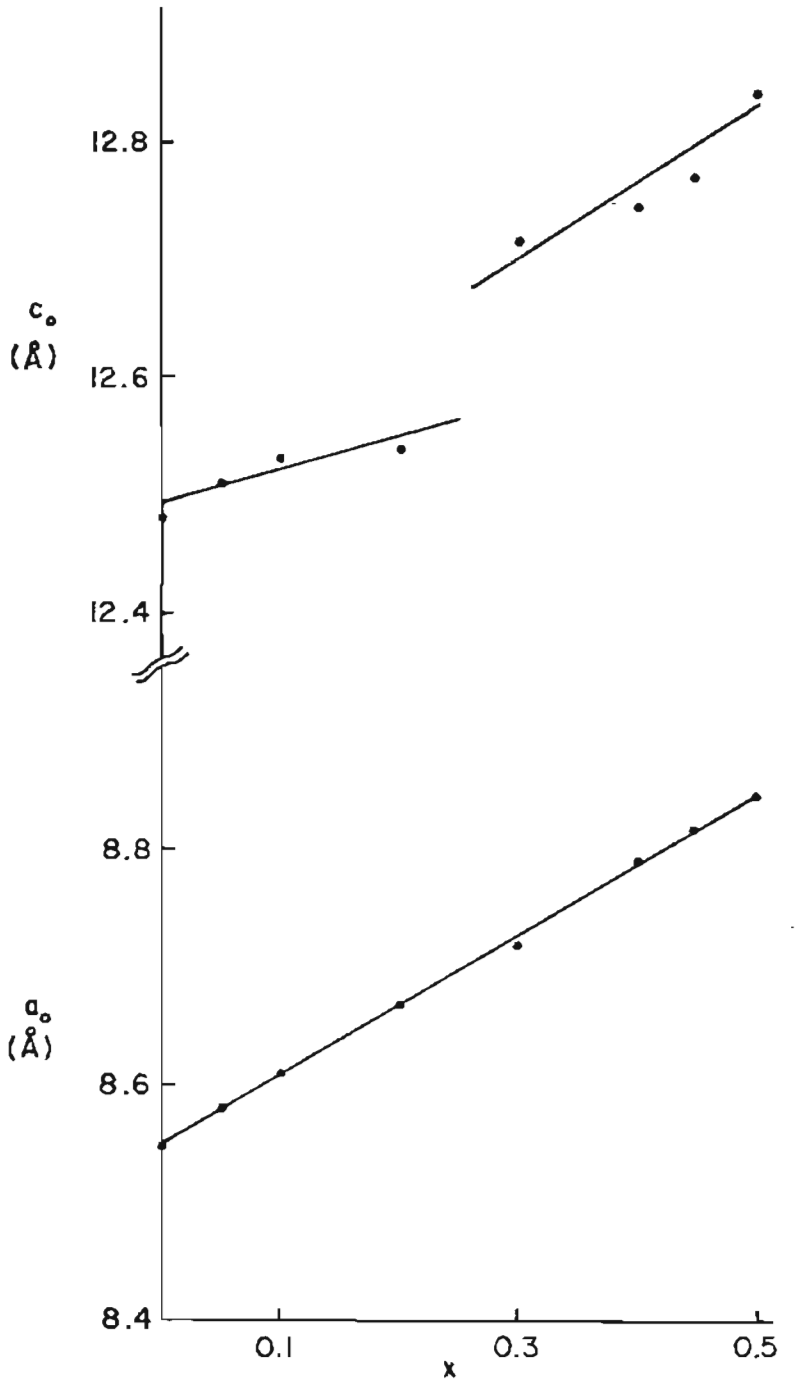

Figure 23. Plot of lattice parameters of $Sm_{.105}Fe_{.895-x}Al_x$

with no apparent indication of a phase change as seen on the a_o axis plot. The c_o axis, however, shows a discontinuity at 30% Al substitution. This is where the total solubility of the Fe related phase is reached and the Th_2Zn_{17} phase is stabilized.

The lattice parameter related plots of the $Dy_{.105}Fe_{.895-x}Al_x$ alloys are shown in Figure 24. The region of the Th_2Ni_{17} structure is plotted with the Th_2Zn_{17}-type lattice parameter. Interestingly, there is only a change in slope related to the a_o axis transformation while the c_o axis shows a discontinuity in growth.

An intensity calculation for the Debye-Scherrer diagram was carried out on the compound $Sm_{.105}Fe_{.385}Al_{.500}$. Five different ordering schemes were considered. From Table IX the best fit to the observed intensities occurs in the 2nd ordering scheme where the Fe and Al share the small atom sites statistically. This appears consistent with the general trend in Al substitutions as seen in all the intensity calculations carried out in this study.

The saturation moments of the $Sm_{.105}Fe_{.895-x}Al_x$ alloys are shown in Figure 25 where they appear to follow the ferrimagnetic coupling line in which Fe is assumed to have a constant moment of 2.0 μ_B and Sm a constant moment of 1.7 μ_B.

The saturation moments of the $Dy_{.105}Fe_{.895-x}Al_x$ compounds in Figure 26. The change from ferri- to ferromagnetic coupling that could take place according to the RKKY theory of the $Dy_{.25}Fe_{.75-x}Al_x$ compounds apparently fails to occur in these materials.

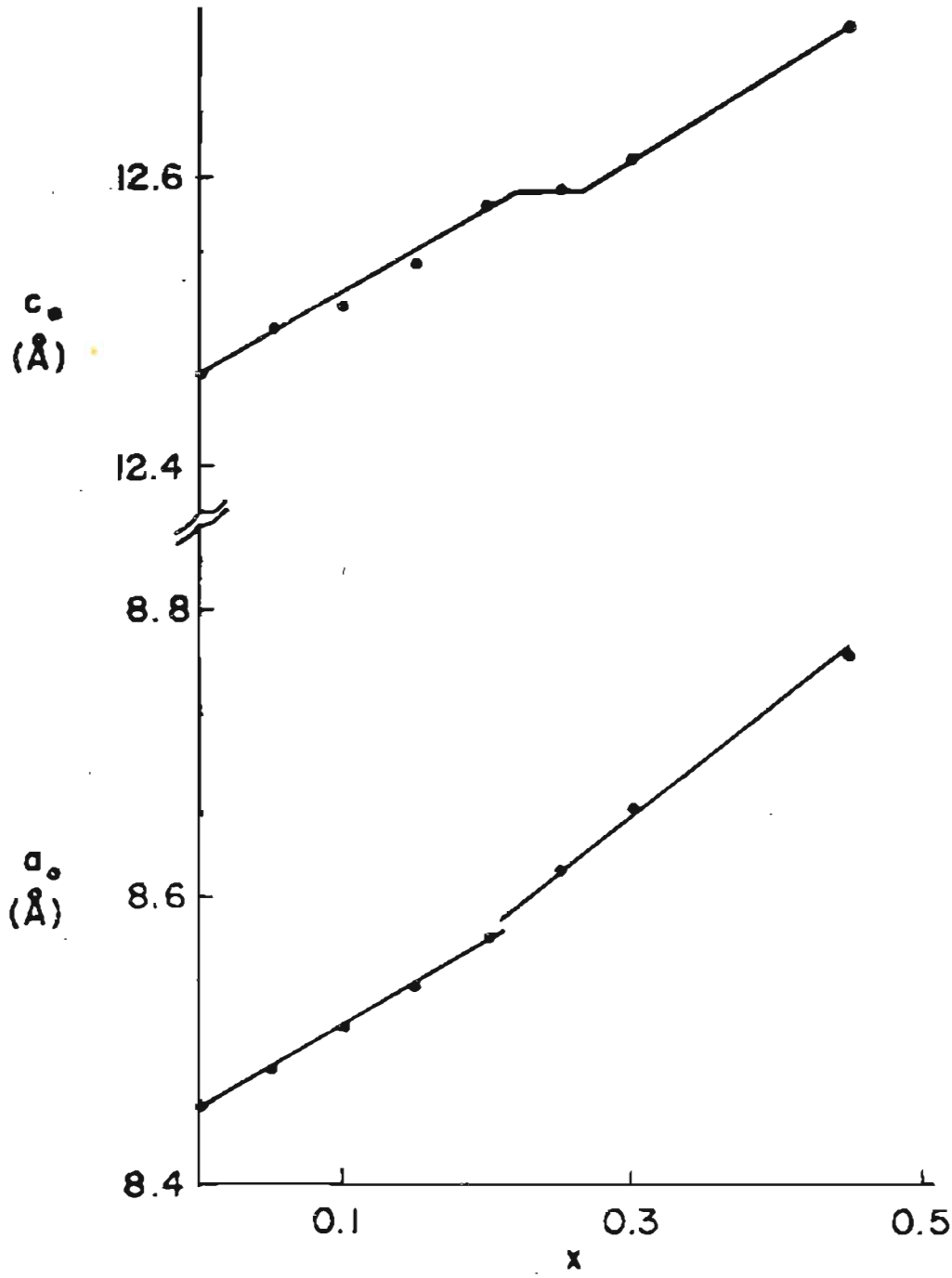

Figure 24. Plot of lattice parameters versus composition of $Dy_{.105}Fe_{.895-x}Al_x$

TABLE IX

Powder X-ray Diffraction Data of $Sm_{.105}Fe_{.395}Al_{.50}$

Material: Induction melted

Radiation: CrKα

Structural Data: Th_2Zn_{17} type Rhombohedral (hex. a = 8.846 Å, c = 12.841 Å)

Atomic Positions:

$6c_1$	0,0,Z; etc.	Z = 1/3
$6c_2$	0,0,Z; etc.	Z = .097
9d	1/2,1/2,1/2; etc.	
18f	X,0,0; etc.	X = 1/3
18h	X,2X,Z; etc.	X = 1/2; Z = 1/6

Calculated Ordering Schemes

Ordering 1		Ordering 2 (Statistical)		Ordering 3	
$6c_1$	Sm	$6c_1$	Sm 100%	$6c_1$	Sm 100%
$6c_2$	Al	$6c_2$	Fe 44% Al 56%	$6c_2$	Al 25% Fe 75%
9d	Fe	9d	Fe 44% Al 56%	9d	Al 100%
18f	Al	18f	Fe 44% Al 56%	18f	Al 100%
18h	Fe	18h	Fe 44% Al 56%	18h	Fe 100%

TABLE IX (continued)

Powder X-ray Diffraction Data of $Sm_{.105}Fe_{.395}Al_{.50}$

Ordering 4		Ordering 5	
$6c_1$	Sm 100%	$6c_1$	Sm 100%
$6c_2$	Al 100%	$6c_2$	Vacant
9d	Al 50% Fe 50%	9d	Fe 100%
18f	Al 100%	18f	Al 100%
18h	Fe 100%	18h	Fe 50% Al 50%

TABLE IX (continued)

Powder X-ray Diffraction Data of $Sm_{.105}Fe_{.395}Al_{.50}$

hkl	θ calc.	θ obs.	Iobs.	1	2	3	4	5
101	10.03	10.03	1.2	2.3	1.8	2.3	3.4	4.4
012	13.46	13.48	0.9	2.0	2.0	0.9	1.6	3.5
110	15.01	15.01	1.2	0.7	2.1	3.1	1.1	0.4
003	15.52	-	-	0.2	0.8	0.0	0.0	0.0
021	18.18	18.20	2.6	0.6	0.5	0.1	0.2	2.4
202	20.38	-	-	0.7	0.7	2.2	1.5	0.5
113	21.86	21.90	6.5	10	6.1	9.2	9.9	9.9
104	22.76	22.79	2.0	1.1	1.5	1.4	1.0	0.9
211	23.92	23.95	1.5	0.6	0.5	0.6	0.9	1.1
122	25.72	25.75	0.7	0.8	0.8	0.3	0.6	1.3
300	26.65	26.68	3.5	2.3	5.2	4.2	2.8	2.2
024	27.75	27.78	2.4	0.6	0.8	2.2	1.1	0.2
015	28.06	-	-	0.7	1.0	1.7	0.9	0.3
220	31.20	31.19	5	8.1	4.9	8.6	7.8	5.8
303	31.49	31.53	10	9.7	10	10	10	10
214	32.19	32.20	3.0	0.9	1.1	1.1	0.8	0.7
006	32.36	32.38	3.0	3.4	2.5	3.0	3.3	3.3
205	32.48	-	-	0.5	0.6	0.3	0.3	0.5
131	33.12	-	-	0.2	0.2	0.2	0.3	0.4
312	34.60	-	-	0.3	0.4	0.2	0.3	0.6
223	35.66	35.69	2.4	1.7	0.3	1.1	1.3	0.8
116	36.48	-	-	0.0	0.0	0.0	0.0	0.1

TABLE IX (continued)

Powder X-ray Diffraction Data of $Sm_{.105}Fe_{.395}Al_{.50}$

hkl	θ calc.	θ obs.	Iobs.	1	2	3	4	5
125	36.60	35.59	0.4	0.7	0.9	1.5	0.9	0.3
401	37.21	-	-	0.1	0.1	0.0	0.0	0.4
042	38.62	-	-	0.1	0.1	0.3	0.3	0.1
107	39.95	39.99	0.6	0.2	0.2	0.4	0.3	0.1
134	40.2	40.29	1.1	0.5	0.6	0.7	0.4	0.4
321	41.13	41.14	0.6	0.1	0.1	0.1	0.2	0.3
232	42.51	42.53	0.8	0.2	0.2	0.1	0.2	0.4
410	43.25	43.25	0.5	0.1	0.4	0.4	0.2	0.1
027	43.82	43.84	0.6	0.2	0.2	0.1	0.1	0.3
404	44.17	-	-	0.2	0.3	0.7	0.4	0.1
306	44.29	44.34	1.1	0.7	1.5	0.8	0.8	1.3
315	44.40							
018	46.81	-	-	0.1	0.1	0.1	0.1	0.2
143	47.36	47.35	2.5	2.9	1.9	2.8	2.9	2.9
217	47.66	47.68	0.9	0.3	0.4	0.6	0.4	0.2
324	47.99	47.99	1.5	0.4	0.5	0.4	0.3	0.3
226	48.14	48.12	3.5	4.7	2.2	3.6	4.3	4.3
045	48.25	-	-	0.2	0.3	0.1	0.1	0.2
051	48.84	-	-	0.1	0.1	0.1	0.1	0.1
502	50.23	-	-	0.1	0.1	0.0	0.1	0.2
208	50.69	50.68	0.2	0.1	0.1	0.3	0.2	0.1
330	50.98	51.00	1.0	0.6	1.2	1.0	0.7	0.6

TABLE IX (continued)

Power X-ray Diffraction Data of $Sm_{.105}Fe_{.395}Al_{.50}$

hkl	θ calc.	θ obs.	Iobs.	1	2	3	4	5
235	52.16	52.22	0.3	0.4	0.5	0.9	0.5	0.2
241	52.77	52.83	0.5	0.1	0.1	0.0	0.0	0.4
009	53.40	-	-	0.0	0.1	0.0	0.0	0.0
422	54.20	-	-	0.2	0.2	0.4	0.4	0.1
128	54.68	-	-	0.2	0.2	0.1	0.2	0.3
333	55.26	55.23	2.5	3.7	3.6	3.9	3.8	3.8
137	55.58	-	-	0.3	0.4	0.6	0.4	0.2
054	55.93	56.00	0.9	0.2	0.2	0.2	0.2	0.2
511	56.85	56.85	0.9	0.1	0.1	0.1	0.2	0.2
119	57.52	57.49	1.5	1.8	1.4	2.2	1.8	1.4
152	58.36	58.37	0.5	0.2	0.2	0.1	0.1	0.3
407	59.84	-	-	0.2	0.2	0.1	0.1	0.2
244	60.22	60.18	1.6	0.4	0.5	1.2	0.7	0.1
416	60.40	-	-	0.0	0.1	0.0	0.0	0.2
505	60.52	-	-	0.2	0.3	0.4	0.3	0.1
318	63.43	-	-	0.2	0.3	0.1	0.2	0.4
600	63.78	63.79	5.0	6.1	4.7	6.6	5.9	4.7
327	64.50	64.53	1.6	0.4	0.4	0.6	0.5	0.2
1010	64.75	-	-	0.1	0.1	0.0	0.0	0.2
514	64.92	64.94	1.6	0.5	0.6	0.6	0.4	0.4
425	65.26	65.24	1.6	0.5	0.7	0.3	0.3	0.6
431	66.05	-	-	0.2	0.1	0.2	0.2	0.3

TABLE IX (continued)

Powder X-ray Diffraction Data of $Sm_{.105}Fe_{.395}Al_{.50}$

hkl	θ calc.	θ obs.	Iobs.	1	2	3	4	5
309	66.87	66.88	6.5	5.5	5.7	6.6	5.7	4.8
342	67.95	-	-	0.2	0.2	0.1	0.2	0.4
048	68.61	68.58	0.9	0.1	0.1	0.3	0.2	0.1
520	69.03	-	-	0.1	0.4	0.4	0.2	0.1
603	69.42	-	-	0.0	0.4	0.0	0.0	0.1
0210	70.19	70.12	0.9	0.0	0.0	0.1	0.1	0.1
336	70.64	70.63	1.0	0.6	1.3	0.7	0.7	1.1
155	70.81	-	-	0.4	0.5	0.9	0.5	0.2
229	72.83	72.74	0.9	0.4	0.0	0.1	0.3	0.2
238	75.12	-	-	0.1	0.2	0.1	0.1	0.2
523	76.25	76.17	4.5	1.8	1.2	1.8	1.8	1.8
057	76.92	-	-	0.1	0.1	0.2	0.1	0.1
2110	77.37	77.29	1.0	0.1	0.1	0.0	0.0	0.2

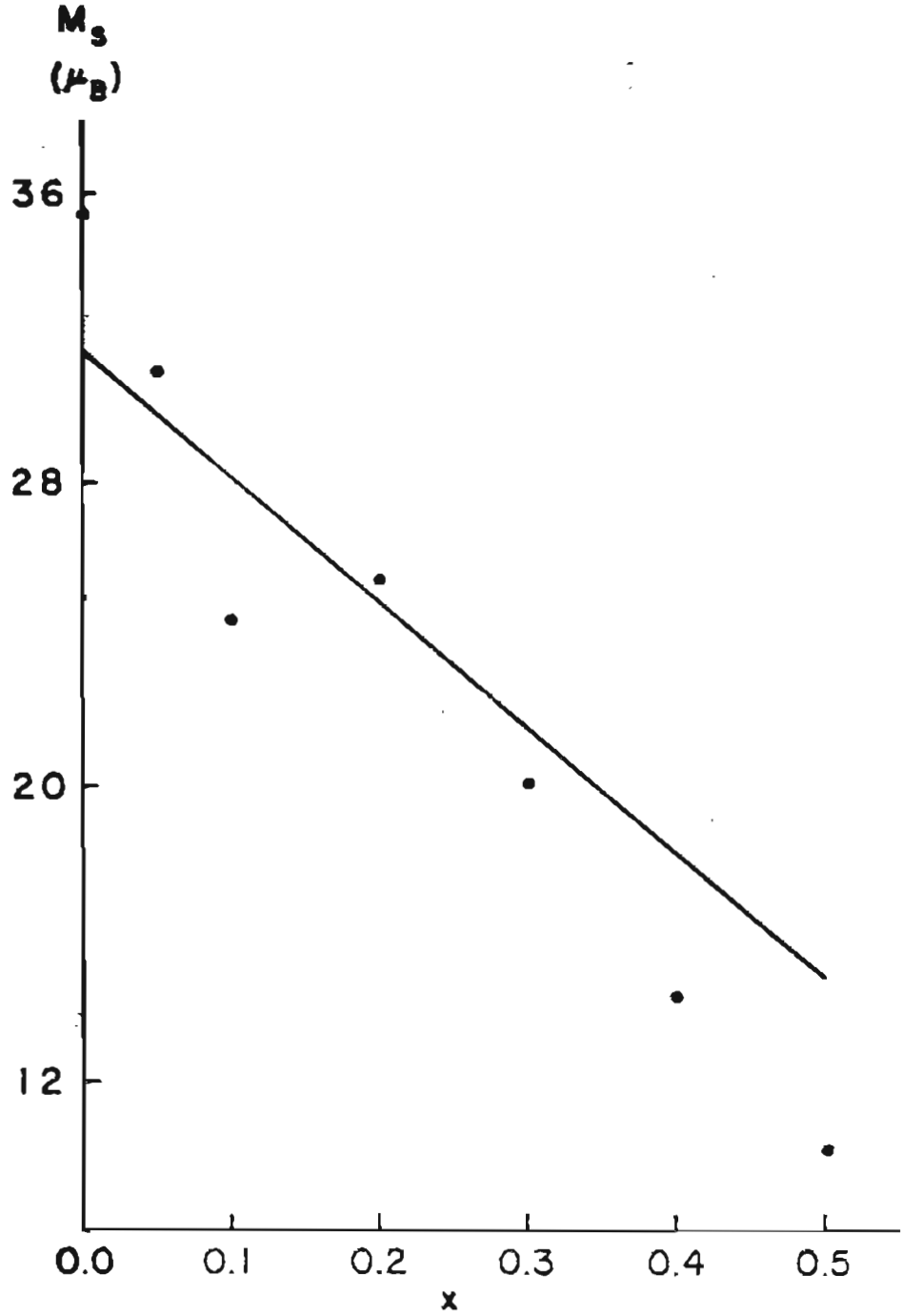

Figure 25. Plot of M_s @ 4.2°K versus composition of $Sm_{.105}Fe_{.895-x}Al_x$
(The line represents theoretical ferromagnetic coupling of Fe (2.0 μ_β) and Sm (0.7 μ_β)).

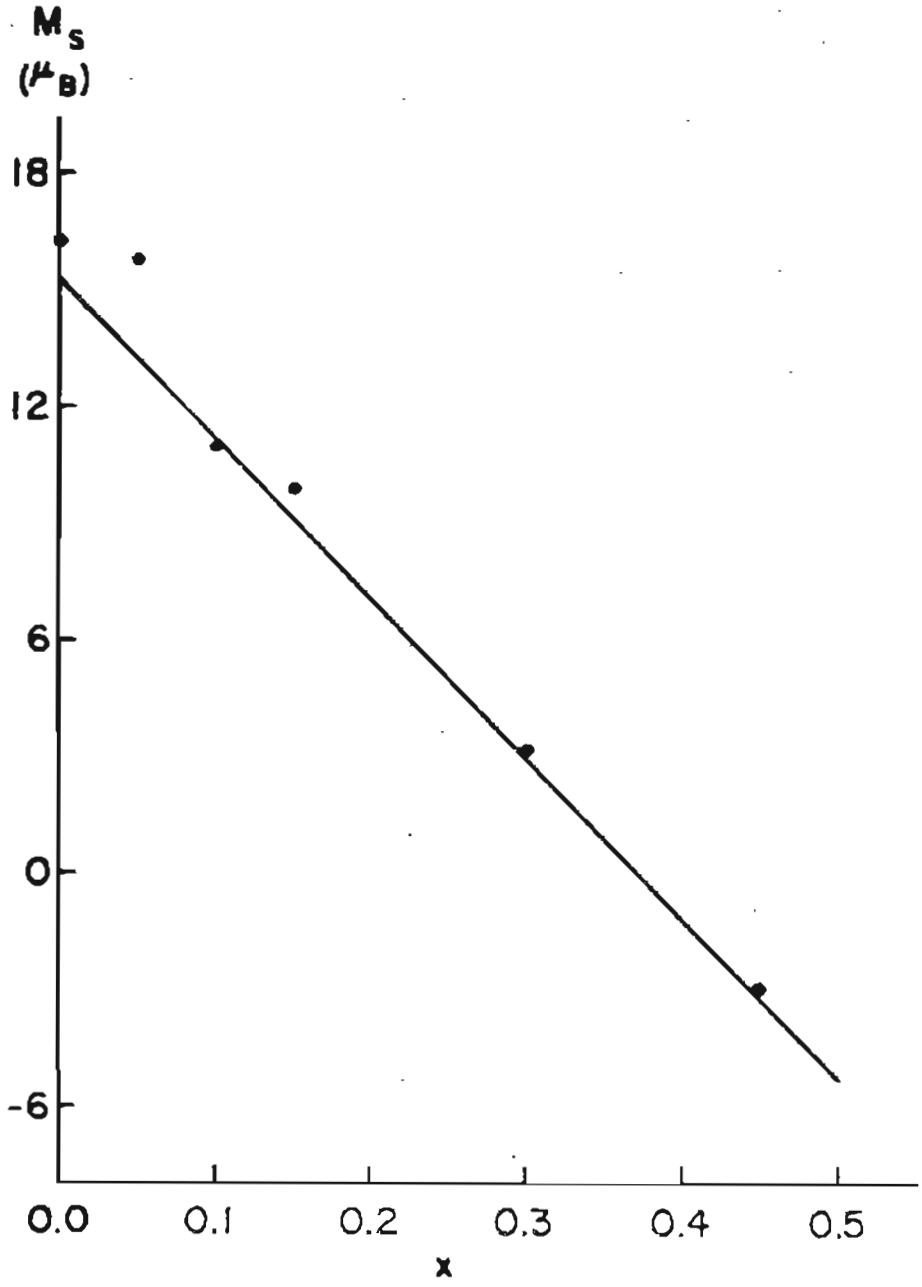

Figure 26. Plot of M_s @ 4.2°K versus composition of $Dy_{.105}Fe_{.895-x}Al_x$
(The line represents theoretical ferrimagnetic coupling of Fe (2.0 μ_β) and Dy (9.4 μ_β))

Hysteresis loops of $Sm_{.105}Fe_{.395}Al_{.500}$ are shown in Figures 27 and 28. In a fashion similar to the previously discussed compounds on the basis of Si and Al substitutions, this material predominantly shows a pinning effect in the bulk materials and nucleation in the powdered samples.

The coercive fields of these materials remains low up to 30% Al; the coercive fields then increase with further substitution of Al and finally peak at 15.0 kOe for the 50% Al samples. Sm was successfully replaced by Gd and Y in the lattice. As seen on the n.n.d., the RR contacts are of little significance. These substituted materials, however, had rather low coercive fields.

Hysteresis loops at 4.2°K and 10°K of $Dy_{.1050}Fe_{.4475}Al_{.4475}$ are shown in Figure 29. The laboratory fields available were insufficient to approach Ms at 4.2°K in this material. Saturation was still difficult at 10°K. In order to determine H_c at 4.2°K in this material, it was necessary to measure H_c at various temperatures to T = 100°K. A plot of $1/H_c$ versus T is shown in Figure 30. H_c in this material was found to show a Curie law dependence similar to the $Dy_{.25}Fe_{.75-x}Al_x$ compounds. From the $1/H_c$ versus T plot where $1/H_c$ intersects with T = 4.2°K, it was possible to obtain an extrapolated value for H_c on the order of 60 kOe at 4.2°K.

The Curie temperature dependence on Al substitution in the $Sm_{.105}Fe_{.895-x}Al_x$ pseudobinary alloys is seen in Figure 31. As discussed in the previous chapter it was hoped that the electron rich Al

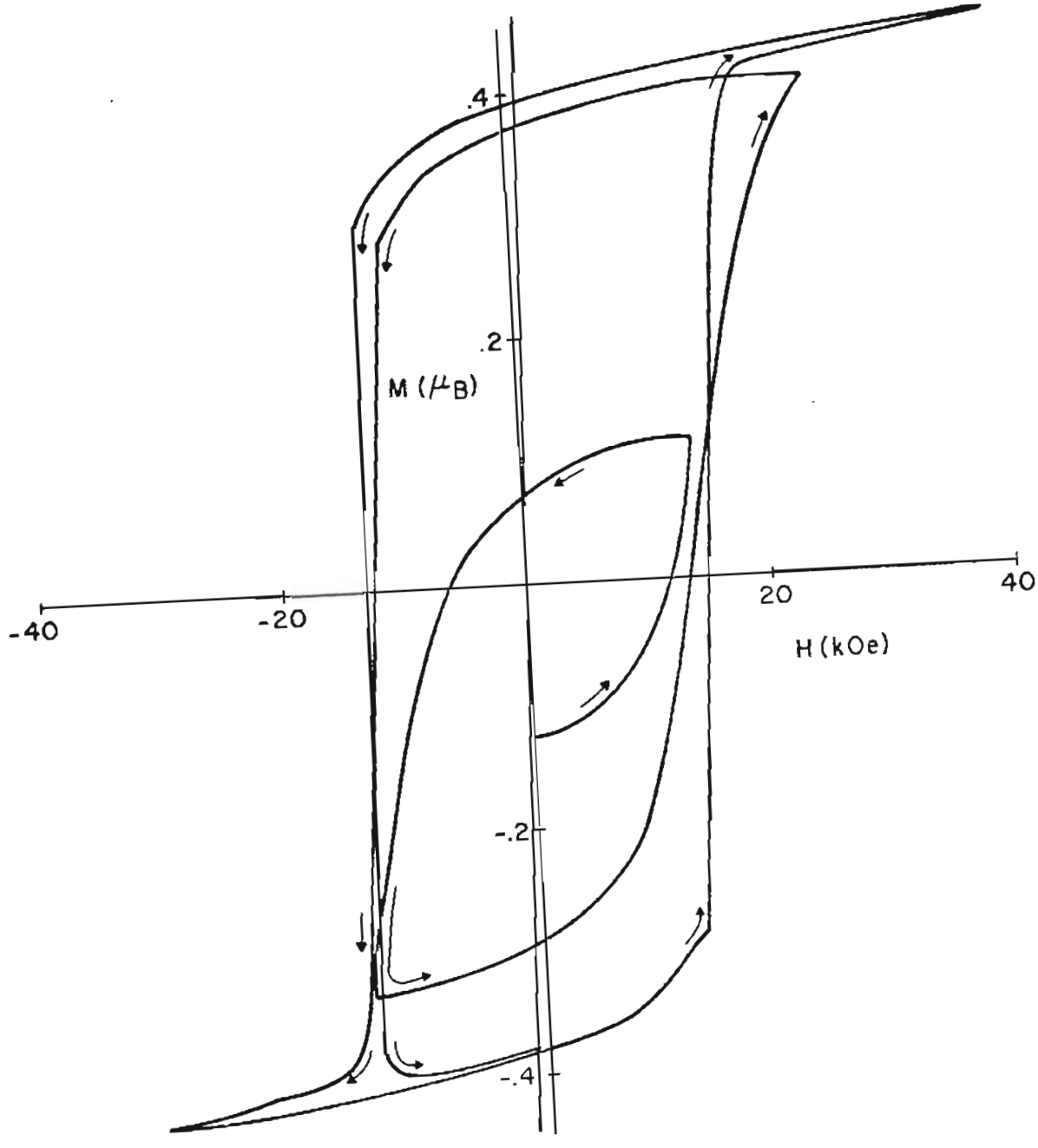

Figure 27. Hysteresis loops of the bulk alloy $Sm_{.105}Fe_{.395}Al_{.500}$

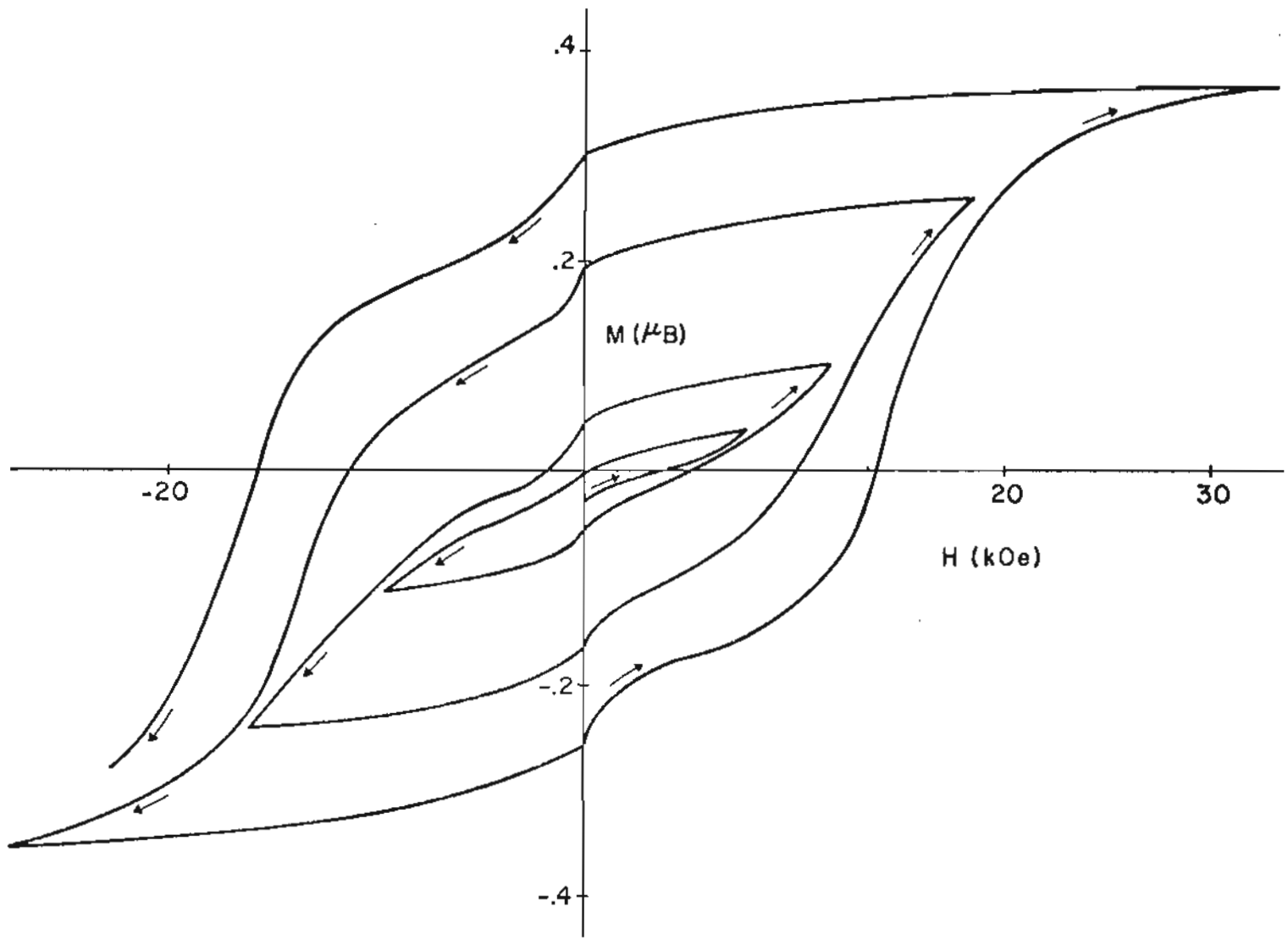

Figure 28. Hysteresis loops of the powdered alloy $Sm_{.105}Fe_{.395}Al_{.500}$

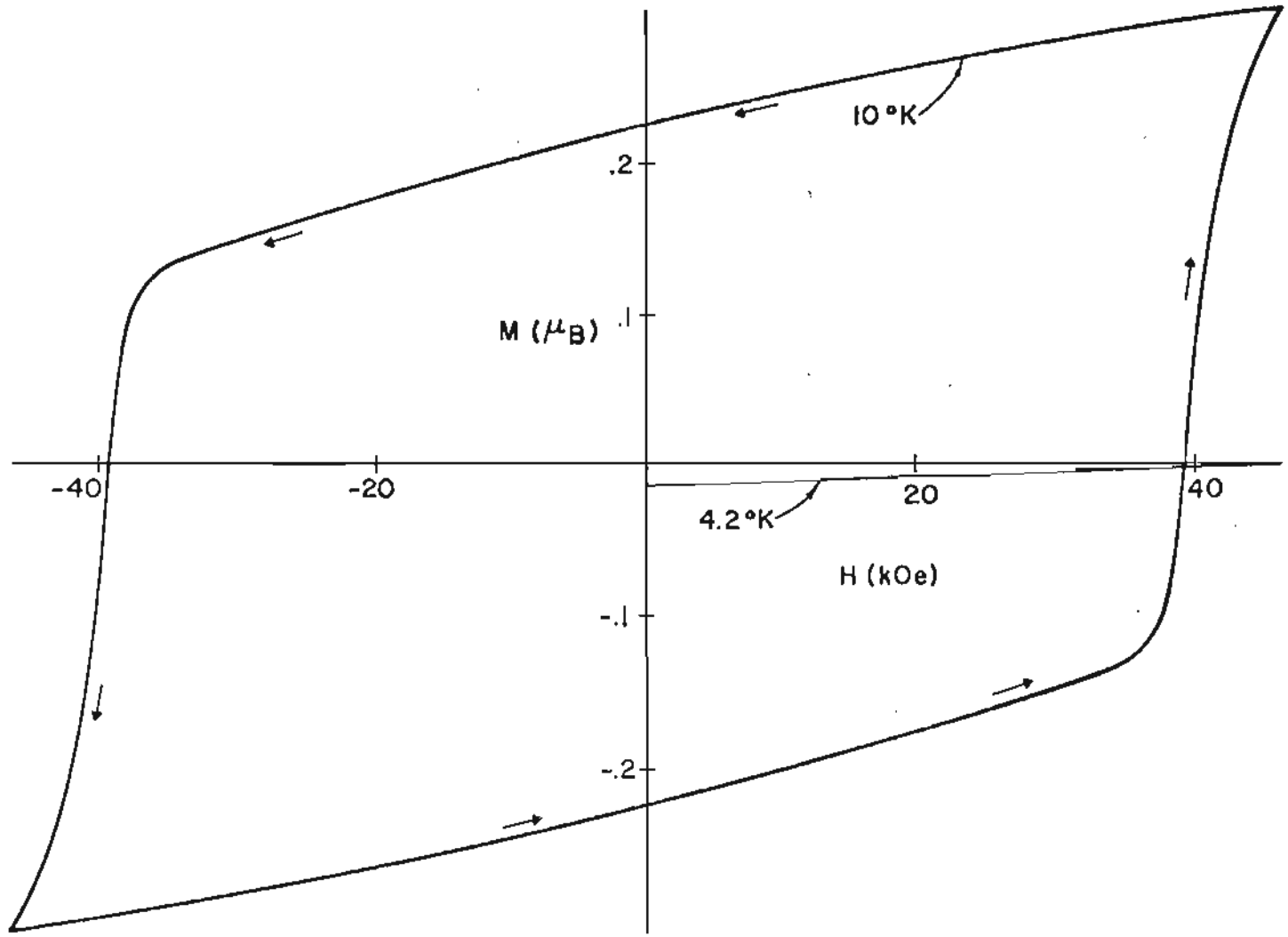

Figure 23. Hysteresis loops of $Dy_{.1050}Fe_{.4475}Al_{.4475}$ at 4.2 and 10°K

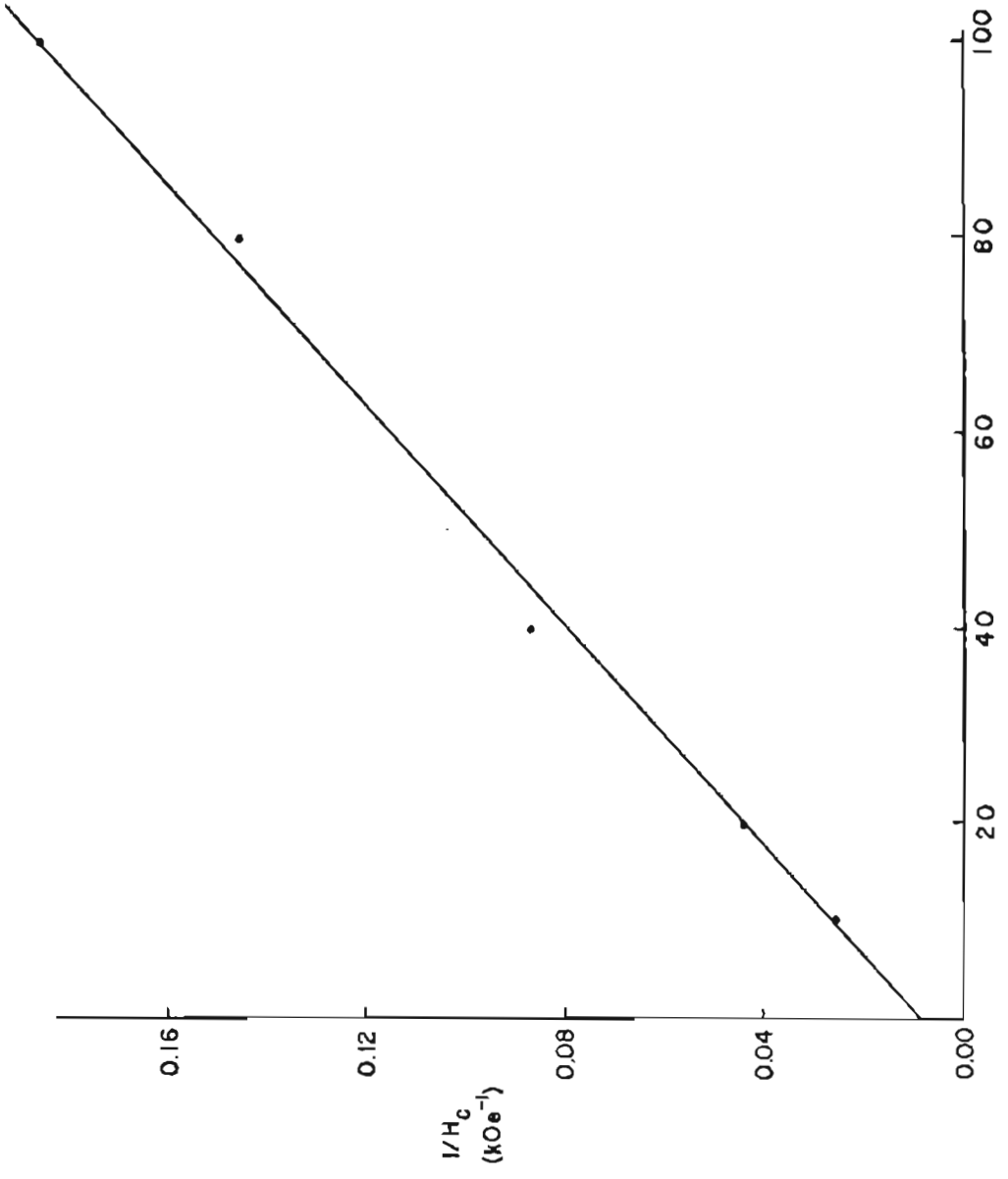

Figure 30. $1/H_c$ versus T for $Dy_{.1050}Fe_{.4475}Al_{.4475}$

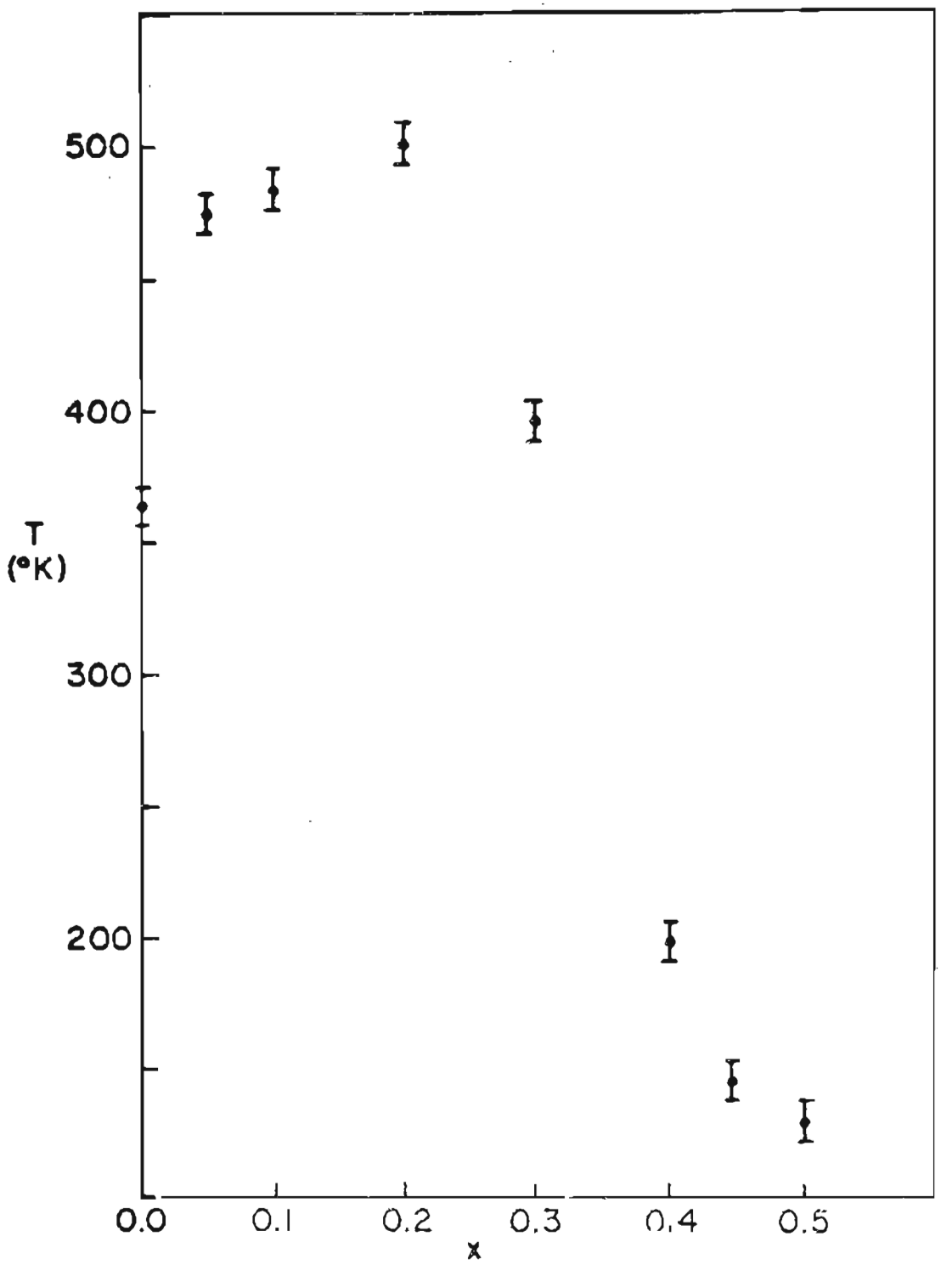

Figure 31. Curie temperature versus composition of $Sm_{.105}Fe_{.895-x}Al_x$

substitution in such materials would alter the RKKY coupling scheme sufficiently to raise the Curie temperature. On initial substitution of Al this was indeed the case. However, as the Al concentration reaches 30%, the Curie temperature is again diminished, and further substitution of Al reduces Tc even further.

CHAPTER IV

SUMMARY

Selected rare earth transitional metal intermetallics were studied with respect to their structural and magnetic properties. These intermetallics were based on stable binary compounds in which a third constituent was added as a partial replacement for the transition metal or rare earth element. Structural stability was considered on the basis of space filling by nonrigid, deformable spheres. Magnetic properties such as saturation magnetization (M_s) and Curie temperature (T_c), were discussed in terms of the Rudermann, Kittel, Kasuya, and Yosida indirect exchange interaction (RKKY). Variations in coercive fields (H_c) were examined with respect to nucleation and pinning of domain walls.

The near neighbor diagram (n.n.d.) of the structural types studied revealed two distinguishing trends in these compounds: (i) the $CaCu_5$, Th_2Ni_{17}, and Th_2Zn_{17} structural types all exhibit a high degree of compression between the rare earth and transition metal atoms as shown in Figures 11 and 22, while (ii) the $PuNi_3$ and $CeNi_3$ structural types exhibit compression principally between the rare earth atoms as shown in Figure 15.

The saturation magnetization is believed to be related to coupling of the rare earth sublattice with the transition metal sublattice via polarization of the conduction band electrons as

described in the RKKY formalism. If this mechanism were to predominate, the heavy rare earth elements could be coupled ferromagnetically with the transition metal sublattice through the addition of an electron rich atom to the binary alloy. This effect may have been predominant in the $Dy(Fe, Al)_3$ compounds of this study; however, since the coupling change was indicated only by the compound $Dy_{.25}Fe_{.45}Al_{.30}$, and since the solubility of Al in the lattice ends at 30 atomic percent, the coupling change could not be demonstrated conclusively. There is a need for further study here. For example, neutron diffraction studies of this compound would provide a better indication of the moments of the rare earth and transition metal atoms in this compound and, hence, reveal their modes of coupling. Also further study, concentrated on the $R(T,Al)_3$ compounds, should attempt to demonstrate whether this coupling change takes place in other compounds. Since the $Dy_2(Fe,Al)_{17}$ compounds of this study did not show a change in coupling similar to the $Dy(Fe,Al)_3$ compounds, it is believed that direct exchange interaction of the transition metal predominates in the former compounds.

Curie temperature measurements on the $Sm_2(Fe,Al)_{17}$ alloys revealed an initial trend towards increasing T_c with increasing Al concentration; however, very highly Al substituted materials showed a decrease in T_c. Since the curie temperature is related to both the indirect and direct exchange interactions, the exact interrelation of these interactions in the $Sm_2(Fe,Al)_{17}$ alloys is poorly

understood. Additional study of this type would be of value for both $Dy(Fe,Al)_3$ and $Dy_2(Fe,Al)_{17}$ compounds in order to better understand the effects of the addition of an electron rich element on T_c.

The addition of an electron rich element to the rare earth transition metal lattice indicated increases in the coercive fields of the alloys studied. The addition of Si to $SmCo_5$ showed a trend towards moderately thin and energetic domain walls. The compounds $Dy(Fe,Al)_3$ and $Dy_6(Fe,Al)_{23}$ showed increases in H_c as Al was substituted for Fe. The compound $Dy_2(Fe,Al)_{17}$ at 44.75 atomic percent Al had the highest coercive field of any material known at the time the measurement was performed in the laboratory. Extrapolation of a plot of $1/H_c$ versus temperature indicates a coercive field for this alloy in excess of 60 kOe at 4.2°K. Additional studies centered around this alloy could be of value, for example, changing the rare earth and/or transition metal elements in this compound could result in materials with yet higher values of H_c.

REFERENCES

1. E. A. Nesbitt, J. H. Wernick and E. Corenzwit, J. Appl. Phys. 38, 365 (1959).

2. W. M. Hubbard, E. Adams and J. V. Gilfrich, J. Appl. Phys. 32, 3685 (1960).

3. G. Hoffer and K. Strnat, IEEE Trans. Mag. 2, 487 (1966).

4. H. Oesterreicher, Solid State Comm. 14, 571 (1974).

5. R. Pitts, Masters Thesis, Oregon Graduate Center (1972).

6. W. E. Wallace, "Rare Earth Intermetallics" (Academic Press, New York, 1973).

7. M. A. Ruderman and C. Kittel, Phys. Rev. 96, 99 (1954).

8. T. Kasuya, Prog. Theor. Phys. 16, 45 (1956).

9. K. Yosida, Phys. Rev. 106, 893 (1957).

10. K. Sekizawa and K. Yasukochi, J. Phys. Soc. Japan 21, 684 (1966).

11. W. M. Swift and W. E. Wallace, J. Solid State Chem. 3, 180 (1966).

12. A. J. Morrish, "The Physical Principles of Magnetism" (John Wiley and Sons, New York, 1965).

13. K. H. J. Buschow and A. S. Van Der Goot, J. Less-Common Metals 17, 249 (1969).

14. R. Lemaire, Cobalt 33, 201 (1966).

15. L. R. Salmans, G. I. Hoffer and K. Strnat, AFML-TR-68-159 (1968).

16. K. Strnat, G. Hoffer and A. E. Ray, IEEE Transactions on Magnetics 2, 489 (1966).

17. A. S. Van Der and K. H. J. Buschow, J. Less-Common Metals 21, 151 (1970).

18. R. J. Parker and R. J. Studders, "Permanent Magnets and Their Applications" (John Wiley and Sons, New York, 1962).

19. O. I. Vivchar, O. S. Zarechnyuk and V. R. Ryabov, Dopov. Akad. Nawk Ukr. RSR A35, 159 (1973).

20. M. Tinkham, "Group Theory and Quantum Mechanics" (McGraw-Hill, New York, 1964).

21. I. Prigogine and R. Defay, "Chemical Thermodynamics" (Jarrold and Sons, Norwich, 1954) p. 175.

22. E. Rudy and J. Throop, Monatsh. Chem. 104(5), 1164 (1973).

23. F. Laves, "Theory of Alloy Phases" (American Society of Metals, Cleveland, 1956).

24. E. Parthe, Z. Kristallogr. 115, 52 (1961).

25. W. B. Pearson, "The Crystal Chemistry and Physics of Metals and Alloys" (Wiley and Sons, New York, 1972).

26. Y. Khan, Acta Cryst. B30, 1533 (1974).

27. K. H. J. Buschow, Phys. Stat. Sol. A7, 199 (1971).

28. Y. Khan, Phys. Stat. Sol. A21, 69 (1974).

29. Y. Khan, Z. Melallkde. 65, No. 7, 489 (1974).

30. "International Tables for X-Ray Crystallography" (Kynoch Press, Birmingham, England, 1969).

31. L. Pauling, "The Nature of the Chemical Bond" 3rd ed. (Cornell University Press, Ithaca, New York, 1960).

32. K. H. J. Buschow, J. Less-Common Metals 35, 305 (1974).

33. A. Riley, J. Less-Common Metals 37, 305 (1974).

34. K. H. J. Buschow, J. Less-Common Metals 37, 91 (1974).

35. S. Chikazumi, "Physics of Magnetism" (John Wiley and Sons, New York, 1964).

36. G. Hoffer and K. Strnat, J. Appl. Phys. 38(3), 1377 (1967).

37. K. Strnat, G. Hoffer, J. Olson, W. Ostertag, and J. J. Becker, J. Appl. Phys. 38(3), 1001 (1967).

38. H. Zijlstra, IEEE Trans. Mag. 6, No. 2, 179 (1970).

39. H. Zijlstra, J. Appl. Phys. 41, No. 12, 4881 (1970).

40. H. Zijlstra, J. Appl. Phys. 42, No. 4, 1510 (1970).

41. R. W. Ed Blois and C. P. Bean, J. Appl. Phys. 30, 2258 (1959).

42. G. T. Trammell, Phys. Rev. 131, No. 3, 932 (1963).

43. Oesterreicher, Solid State Comm. 14, 571 (1974).

44. D. H. Martin, "Magnetism in Solids" (Iliffe Books, London, 1967).

45. B. Bleaney and K. W. Stevens, rep. Progr. Phys. 16, 108 (1953).

46. B. Bleaney, Proc. Roy. Soc. A276, 39 (1963).

47. K. W. H. Stevens, Proc. Phys. Soc., London, A65, 299 (1952).

48. Editor L. Eyring, "Progress in the Science and Technology of the Rare Earths" Vol. 3 (Pergamon Press, Great Britain, 1968).

49. C. Kittel, "Introduction to Solid State Physics" 3rd ed. (John Wiley and Sons, New York, 1966).

50. W. G. Penney and R. Schlapp, Phys. Rev. 41, 194 (1932).

51. K. R. Lea, M. J. M. Leask and W. P. Wolf, J. Phys. Chem. Solids 23, 1381 (1962).

52. E. Segal and W. E. Wallace, J. Solid State Chem. 2, 347 (1970).

53. E. Segal and W. E. Wallace, J. Solid State Chem. 6, 99 (1973).

54. E. Segal and W. E. Wallace, J. Solid State Chem. 11, 203 (1974).

55. E. Segal and W. E. Wallace, J. Solid State Chem. 13, 201 (1975).

56. M. Buerger, "The Precession Method" (John Wiley and Sons, New York, 1964).

57. H. Oesterreicher, J. Less-Common Metals 33, 25 (1973).

58. D. T. Cromer and J. B. Mann, Acta Cryst. A24, 321 (1968).

59. R. Lemaire and J. Schweizer, Le Journal De Physique 28, 216 (1967).

60. J. H. N. van Vucht, J. Less-Common Metals 10, 146 (1965).

61. J. F. Smith and D. A. Hansen, Acta Cryt. 19, 1019 (1965).

62. F. Givord and R. Lemaire, Solid State Comm. 9, 341 (1971).

63. J. Pelleg and O. N. Carlson, J. Less-Common Metals 9, 28 (1965).

64. E. Kreń, J. Schweizer and F. Tasset, Phys. Rev. 186, No.2, 479 (1969).

65. D. Paccard and R. Pauthenet, C. R. Acad. Sc. Paris 264B, 1056 (1967).

66. A. V. Virkar and A. Raman, J. Less-Common Metals 18, 59 (1969).

67. C. J. Kunesh, K. S. V. L. Narasimhar and R. A. Butera, J. Phys. Chem. Solids 34, 2003 (1973).

68. C. J. Kunesh, K. S. V. L. Narasimhar and R. A. Butera, J. Phys. Chem. Solids 34, 817 (1973).

69. K. H. J. Buschow, J. Less-Common Metals 25, 131 (1971).

70. K. H. J. Buschow and A. S. Van Der Goot, J. Less-Common Metals 14, 323 (1968).

71. F. Lihl, J. R. Ehold, H. R. Kirchmager and H. D. Wolf, Acto Physica Austria 30, 169 (1969).

72. A. E. Dwight, Acta Cryst. B24, 1395 (1968).

73. M. Simmons, J. M. Moreau, W. J. James, F. Givord and R. Lemaire, J. Less-Common Metals 30, 75 (1973).

74. M. R. Dariel and G. Erez, J. Less-Common Metals 22, 360 (1970).

75. S. C. Tsai, K. S. V. L. Narasimhan, C. J. Kunesh and R. A. Butera, J. Appl. Phys. 45, 3582 (1974).

76. T. J. O'Keefe, G. J. Roe and W. J. James, J. Less-Common Metals 15, 357 (1968).

77. K. H. J. Buschow and A. S. Van Der Goot, J. Less-Common Metals 19, 153 (1969).

78. E. G. Bertaut, R. Lemaire and J. Schweizer, C. R. Acad. Sc. Paris 260, 3595 (1965).

79. K. H. J. Buschow, Z. Melallkde. 57, 728 (1966).

80. K. H. J. Buschow, J. Less-Common Metals 16, 45 (1968).

81. K. H. J. Buschow, J. Less-Common Metals 26, 329 (1972).

82. W. Ostertag, Acta Cryst. 19, 150 (1965).

83. D. T. Cromer and C. E. Olsen, Acta Cryst. 12, 689 (1959).

84. F. W. Wang and J. R. Holder, Trans. Met. Soc. AIME 233, 731 (1965).

85. M. Morariu, E. Burzo and D. Barb, Phys. Stat. Sol. B62, K55 (1974).

86. H. Oesterreicher and R. Pitts, J. Less-Common Metals 29, 100 (1972).

87. W. B. Pearson, "Handbook of Lattice Spacings and Structures of Metals," Vol. 2 (Pergamon Press, New York, 1967).

88. R. Lemaire, Cobalt 32, 132 (1966).

89. W. A. J. J. Velze and K. H. J. Buschow, J. Appl. Phys. 39, 1717 (1968).

90. J. C. Barrick, M. Simmons, W. J. James, J. Laforest and J. S. Shah, J. Less-Common Metals 37, 379 (1974).

91. Yu. B. Kuzma, P. J. Krypyakevich and N. S. Bilonishko, Dopov Akad. Nauk Ukr. RSR. A10, 939 (1969).

92. K. N. R. Taylor and C. A. Poldy, J. Less-Common Metals 27, 255 (1972).

93. M. L. Green, J. Less-Common Metals 37, 169 (1974).

94. D. Givoid, R. Lemaire, W. J. James, J-M Moreau and J. S. Shah, IEEE Trans. Mag. 7, 657 (1971).

95. K. H. J. Buschow and W. A. J. J. Velze, J. Less-Common Metals 13, 11 (1967).

96. Y. Khan, J. Less-Common Metals 34, 191 (1974).

97. P. Rogl, Monats. Chem. 104, 1623 (1973).

98. H. Oesterreicher, J. Less-Common Metals 32, 385 (1973).

99. T. Shibata, T. Katayama and T. Mizuhara, Japan J. Appl. Phys. 10, 1479 (1971).

100. Y. Khan and B. Mueller, J. Less-Common Metals 32, 39 (1973).

101. K. H. J. Buschow and F. J. A. Den Broeder, J. Less-Common Metals 33, 191 (1973).

102. J. Shidlovsky and W. E. Wallace, J. Solid State Chem. 2, 193 (1970).

103. P. D. Carfagna and W. E. Wallace, J. Appl. Phys. 39, 5259 (1968).

104. J. Laforest, R. Lemaire, D. Paccard and R. Pauthenet, C. R. Acad. Sc. Paris B264, 676 (1967).

105. W. Steiner, H. R. Kirchmayr, and W. Springs, Zangew. Phys. 32, 146 (1971).

106. P. D. Carfagna, W. E. Wallace and R. S. Craig, J. Solid State Chem. 2, 1 (1970).

107. K. H. J. Buschow and J. S. van Wieringen, Phys. Stat. Sol. 42, 231 (1970).

108. W. Ostertag and K. J. Strnat, Acta Cryst. 21, 560 (1966).

109. G. Bouchet, J. Laforest, R. Lemaire and J. Schweizer, C. R. Acad. Sc. Paris B262, 1227 (1966).

110. A. Deryagin, A. Vlyanov, N. Kudrevatykj, E. Barabanova, Y. Bashkov, A. Andrew and E. Tarasov, Phys. Stat. Sol. A23, K15 (1974).

111. D. Givoid, R. Lemaire, J. M. Moreau and E. Roudaut, J. Less-Common Metals 29, 361 (1972).

112. Q. Johnson, G. S. Smith and D. H. Wood, Acta Cryst. B25, 464 (1969).

113. R. Lemaire, R. Pauthenet, J. Schweizer and I. S. Silvera, J. Phys. Chem. Solids 28, 247 (1967).

114. H. Bartholin, B. Van Laar, R. Lemaire and J. Schweizer, J. Phys. Chem. Solids 27, 1287 (1966).

115. J. Rossat-Mignod and J. Yakinthos, Phys. Stat. Sol. B47, 239 (1971).

116. K. S. V. L. Narasimhan, R. A. Butera and R. S. Craig, J. Appl. Phys. 44, 879 (1973).

117. J. Yakinthos, J. Rossat-Mignod and M. Belakhovsky, Phys. Stat. Sol. B47, 247 (1971).

118. J. Yakinthos and D. Paccard, Solid State Comm. 10, 989 (1972).

119. M. Brouha and K. H. J. Buschow, J. Appl. Phys. 44, 1813 (1973).

120. H. Kirchmayr, Ph.D. Thesis, Technische Hochschule, Vienna (1968).

121. K. R. Kirchmar, IEEE Trans. Mag. 2, 493 (1966).

122. A. Dworak, H. R. Kirchmayr and H. Rauch, Z. Angew. Phys. 24, 318 (1968).

123. B. F. DeSavage, R. M. Bozorth, F. E. Wang and E. R. Callen, J. Appl. Phys. 36, 992 (1965).

124. K. H. Buschow and A. S. Van Der Goot, Phys. Stat. Sol. 35, 515 (1969).

125. E. Tatsumoto, T. Okamoto, H. Fujii and C. Inoue, J. de Phys. 32, C1-550 (1970).

126. K. Bachmann and F. Hoffer, Z. Angew. Phys. 32, 41 (1971).

127. R. C. Sherwood, E. A. Nesbitt, G. Y. Chin and M. L. Green, Materials Research Bulletin 7, 489 (1972).

128. W. E. Wallace, T. V. Volkmann and H. P. Hopkins, Jr., J. Solid State Chem. 1, 39 (1969).

129. W. E. Wallace, H. P. Hopkins, Jr. and K. Lehman, J. Solid State Chem. 1, 39 (1969).

130. J. D. Livingston and M. D. McConnell, J. Appl. Phys. 43, 4756 (1972).

131. O. A. W. Strydon and L. Alberta, J. Less-Common Metals 22, 503 (1970).

132. T. Okamoto, H. Fujii, C. Inoue and E. Tatsumoto, J. Phys. Soc. Japan 34, 835 (1973).

133. E. Burzo and I. Ursu, Solid State Comm. 9, 2289 (1971).

134. E. Burzo and J. Laforest, C. R. Acad. Sc. Paris B274, 114 (1972).

135. W. E. Wallace and M. Aoyagi, Monats. Chem. 102, 1455 (1971).

136. H. Oesterreicher and R. Pitts, J. Appl. Phys. 44, 5570 (1973).

137. H. J. Schaller, R. S. Craig and W. E. Wallace, J. Appl. Phys. 43, 3161 (1972).

138. J. Yakinthos and J. Rossat-Mignod, Phys. State Spol. B50, 747 (1972).

139. A. E. Berkowitz and E. Kneller, "Magnetism and Metallurgy" (Academic Press, New York, 1969).

Appendix I Crystal Structure Data of Other Researchers

Legend and Abbreviations

1) am indicates arc melt
2) im indicates induction melt
3) lim indicates levitation induction melt
4) ann XX time @ XX°C indicates annealing followed by duration in minutes (m) or hours (h) or days (d) or weeks (w) and temperature in degrees Centigrade (°C).
5) Compositions are given as presented by authors and are all atomic percent or stoichiometric figures.
6) ~ indicates approximate value and taken from graphs
7) If the method of preparation column is left blank the previously referred to procedure holds also for this compound.
8) ns indicates not stated

STRUCTURAL TYPE - $PuNi_3$

Composition	Lattice Parameters a(Å)	c(Å)	c/a	Method of Preparation	Ref.
YFe_3	5.1330	24.600	4.79	am; ann 48 h @ 1000°C	60
YCo_3	5.0200	24.400	4.86	am; 31% Y	61
	5.0133	24.371	4.86	am; ann 48 h @ 1000°C	60
	5.0100	24.400	4.87	lim only	60
	5.0200	24.400	4.86	am 3 times	63
	5.0160	24.350	4.85	drawn single crystal	64
YNi_3	4.9730	24.370	4.90	lim; ann 800-1000°C	65
	4.9782	24.468	4.92	am; ann 48 h @ 1000°C	60
	4.9760	24.380	4.90	am only	66
	4.9779	24.449	4.91	am 31% Y	61
$Y_{1-x}Th_xFe_3$				im in Cu boat; ann 950°C time given in days	67
x = .1	5.1460	24.675	4.79	33	
.3	5.1610	24.777	4.80	33	
.35	5.1660	24.803	4.80	22	
.4	5.1700	24.826	4.80	22	
.45	5.1730	24.854	4.80	22	
.5	5.1800	24.884	4.80	33	
.7	5.1900	24.988	4.81	33	
.9	5.2010	25.084	4.82	34	
.9 @ 77°K	5.2040	24.995	4.80	34	68
1.0	5.2080	25.168	4.83	5	67

STRUCTURAL TYPE - $PuNi_3$ (continued)

Composition	Lattice Parameters a(Å)	c(Å)	c/a	Method of Preparation	Ref.
$LaNi_3$	5.0860	25.010	4.92	am; ann @ 600°C	66
$La_{.1}Th_{.9}Fe_3$	5.2240	25.315	4.85	im in Cu boat; ann 24 d @ 950°C	68
$CeCo_3$	4.9600	24.810	5.00	am; 7-14 d @ 900°C	26
$PrCo_3$	5.0800	24.630	4.85	am; homogenized 500-1150°C 1-3 w	
$PrNi_3$	5.0300	25.010	4.97	lim; ann 800-1000°C	65
$Pr_{.1}Th_{.9}Fe_3$	5.2160	25.257	4.84	lim in Cu boat; ann 24 d @ 950°C	68
$NdCo_3$	5.0600	24.820	4.91	am; homogenize 500-1150°C 1-3 w	26
$NdNi_3$	5.0150	24.670	4.92	am; ann @ 800°C	
	5.0240	24.710	4.92	lim; ann @ 800-1000°C	65
$SmFe_3$	4.1870	24.910	4.80	am only	69
$SmCo_3$	5.0500	24.590	4.87	am; ann 2 w @ 800°C	70
	5.0584	24.618	4.87	am only	29
	5.0610	24.610	4.86	im only	71
$SmNi_3$	5.0030	24.590	4.92	lim; ann 800-1000°C	65
$GdFe_3$	5.1480	24.620	4.78	am only	61
	5.1654	24.707	4.78	am; ann 3 d @ 1000°C	72
	5.1692	24.737	4.79	am; ann 48 h @ 1000°C	60
	5.1660	24.760	4.79	ns	27
$GdCo_3$	5.0530	24.555	4.860	im only	71
	5.0390	24.522	4.870	am only	13
	5.0400	24.552	4.870	am; ann 48 h @ 1000°C	60

STRUCTURAL TYPE - $PuNi_3$ (continued)

Composition	Lattice Parameters a(Å)	c(Å)	c/a	Method of Preparation	Ref.
$GdNi_3$	4.9900	24.539	4.920	lim; ann 800-1000°C	65
	4.9906	24.450	4.900	am; ann 48 h @ 1000°C	60
	4.9870	24.480	4.910	am; ann 900°C	66
$TbFe_3$	5.1100	24.420	4.780	induction heated in ZrO_2 boat	73
	5.1450	24.630	4.790		27
$TbCo_3$	5.0156	24.424	4.870	am; ann 5 d @ 500°C, powder 3 h @ 500°C	72
$TbNi_3$	4.9670	24.460	4.920	lim; ann 800-1000°C	65
$Tb_{.25}Fe_{.75-x}Al_x$					5
x = 0	5.1350	24.620	4.794	im only	
	5.1350	24.629	4.796	im; ann 200 h @ 1000°C	
.05	5.1600	24.781	4.803	im only	
	5.1590	24.771	4.801	im; ann 200 h @ 1000°C	
$DyFe_3$	5.1160	24.550	4.800	am several times	17
	5.1230	24.570	4.795	am; ann 200-700 h @ 900-1100°C	74
$DyNi_3$	4.9640	24.160	4.870	lim; ann 800-1000°C	65
$DyFe_{3-x}Ni_x$				im in Cu boat and where thermal magnetic analysis showed more phases they were ann 2 w @ 950°C	75
x = 0	5.1210	24.586	4.801		
.25	5.1100	24.597	4.814		
.5	5.089	24.598	4.834		
1	5.068	24.590	4.852		

STRUCTURAL TYPE - $PuNi_3$ (continued)

Composition	Lattice Parameters a(Å)	c(Å)	c/a	Method of Preparation	Ref.
1.5	5.033	24.584	4.880		75
2.0	5.036	24.566	4.879		
2.5	4.992	24.481	4.904		
2.75	4.993	24.470	4.901		
3.0	4.959	24.379	4.896		
$(Dy_{1-x}Thx)Fe_3$				im in water cooled Cu boat	68
x = 0	5.131	24.584	4.791	am; 18 days @ 750°C and 25 days @ 950°C	
.1	5.135	24.682	4.807	am; 18 days @ 750°C	
.2	5.193	24.771	4.816	18 days @ 750°C	
.3	5.159	24.812	4.809	33 days @ 950°C	
.4	5.161	24.885	4.822	18 days @ 750°C	
.5	5.173	24.923	4.818	33 days @ 950°C	
.6	5.190	25.073	4.831	18 days @ 750°C and 23 days @ 950°C	
.7	5.200	25.097	4.826	33 days @ 950°C	
.8	5.207	25.110	4.822	33 days @ 950°C	
.9	5.2080	25.144	4.828	33 days @ 950°C	
1.0	5.2080	25.168	4.833	5 d @ 950°C	
$HoFe_3$	5.1100	24.530	4.800	am; 3 times	73
	5.1000	24.500	4.800		27
	5.0840	24.450	4.810	im; ann 1 d to 4 w @ 1100°C to 1350°C	76
	5.1097	24.526	4.80	am; ann 19 h @ 900°C	72

STRUCTURAL TYPE - $PuNi_3$ (continued)

Composition	Lattice Parameters a(Å)	c(Å)	c/a	Method of Preparation	Ref.
$HoCo_3$	4.9810	24.290	4.88	am; 24 h @ 950°C	77
	4.9900	24.250	4.86	lim; ann @ 1000°C	78
$HoNi_3$	4.9570	24.190	4.88	lim; ann @ 800-1000°C	65
	4.9580	24.330	4.91	am; ann 3 d @ 1000°C	72
$ErFe_3$	4.0860	24.460	4.81		27
$ErCo_3$	4.9720	24.179	4.86	am only	79
$ErNi_3$	4.9730	24.410	4.91	am; ann @ 900°C	66
	4.9430	24.210	4.90	lim; ann @ 800-1000°C	65
	4.9410	24.252	4.91	am; ann 3 w @ 900°C	80
	4.9480	24.270	4.91	am; ann 3 d @ 1000°C	65
$TmFe_3$	5.0770	24.430	4.81		27
$TmNe_3$	4.9300	24.250	4.92	lim; ann 800-1000°C	65
	4.9370	24.213	4.90	am; ann 3 d @ 1000°C	72
$YbCo_3$	4.9520	24.190	4.88	Solid state reaction for 3 w @ 800°C or melt 5 m @ 1200°C; ann 3 w 700-800°C in Mo crucible	81
	4.913	24.270	4.94	lim; ann 800-1000°C	
$LuCo_3$	4.950	24.000	4.85	lim only	62
	4.955	24.101	4.86	am; ann 5 d @ 900°C and powder 21 h @ 900°C	72
$(Lu_{1-x}Th_x)Fe_3$				im in Cu boat; ann 950°C time given in days	67
x = .1	5.088	24.463	4.81	22	
.3	5.111	24.626	4.82	22	

STRUCTURAL TYPE - $PuNi_3$ (continued)

Composition	Lattice Parameters a(Å)	c(Å)	c/a	Method of Preparation	Ref.
x = .4	5.142	24.761	4.82	24	67
.45	5.141	24.776	4.82	24	
.5	5.164	24.819	4.81	24	
.55	5.165	24.903	4.82	24	
.7	5.881	24.982	4.82	22	
.9	5.214	25.046	4.80	22	

STRUCTURAL TYPE - $CeNi_3$

Composition	Lattice Parameters a(Å)	c(Å)	c/a	Method of Preparation	Ref.
YCo_3	5.015	16.280		lim; ann 200 h @ 800°C	82
$CeNi_3$	4.980	16.540	3.32	im and slowly cooled	83

STRUCTURAL TYPE - Th_2Mn_{23}

Composition	Lattice Parameter	Method of Preparation	Ref.
Y_6Mn_{23}	12.438		84
Y_6Fe_{23}	12.078	im; ann 160 h @ 1000°C	85
Nd_6Mn_{23}	12.657		84
Sm_6Mn_{23}	12.558		
Gd_6Mn_{23}	12.532		
Tb_6Mn_{23}	12.396		
$Tb_{.167}Fe_{.633}Al_{.20}$	12.314	im; ann 200 h @ 1000°C	86
Dy_6Mn_{23}	12.361		84
Dy_6Fe_{23}	12.062	am; ann 42 @ 1250°C	17
	12.055	am; ann 200-700 h @ 900-1100°C	74
Ho_6Mn_{23}	12.324		84
Ho_6Fe_{23}	12.032	im; ann 1 d to 4 w @ 1100-1350°C	76
Er_6Mn_{23}	12.275		84
Tm_6Mn_{23}	12.226		
Yb_6Fe_{23}	11.945	Solid state reaction 3 w @ 800°C and 5 m @ 1200°C then ann 3 w @ 700-800°C	81
Lu_6Mn_{23}	12.187		84

STRUCTURAL TYPE - $CaCu_5$

Composition	Lattice Parameters a(Å)	c(Å)	c/a	Method of Preparation	Ref.
YFe_5	4.870	4.0600	.834	ns	87
YCo_5	4.937	3.9780	.806	lim and quench	88
	4.945	3.9830	.805	drawn single crystal	64
	4.940	3.9800	.806	lim	62
	4.995	3.9940	.800	am 3 times	63
	4.925	3.997	.812	am; ann 6 to 40 h @ 1000-1100°C	28
	4.935	3.9640	.804	am only	89
	4.928	3.9920	.810	ns	87
$Y_{.6}La_{.4}Co_5$	5.0128	3.9739	.793	im; ann 1 w @ 1000°C	90
$Y_{.6}La_{.4}Fe_{.5}$ $Co_{4.5}$	5.0255	3.9816	.792		
$Y_{.6}La_{.4}Fe_{.65}$ $Co_{4.35}$	5.0192	3.9864	.794		
$Y_{.7}La_{.3}Fe_{.8}$ $Co_{4.2}$	5.0056	3.9957	.798		
Yni_5	4.883	3.9670	.812	ns 83.4% Ni	87
YCu_5	4.984	4.1170	.826		
YCo_3B_2	5.033	3.038	.604		91
$YCo_{5-x}Fe_x$				am only	92
x = .5	4.935	4.000	.811		
1	4.930	4.020	.815		
$YCo_{5-x}Ni_x$				am only	
x = 0	4.940	3.975	.805		

STRUCTURAL TYPE - $CaCu_5$ (continued)

Composition	Lattice Parameters a(Å)	c(Å)	c/a	Method of Preparation	Ref.
.8	4.885	3.970	.814		92
1.0	4.885	3.960	.811		
$Y_xPr_{1-x}Co_3Ni_2$				am; ann 1/2 h @ 1000°C, 4 h @ 400°C	93
x = 0	5.04	4.000	.794		
.2	5.03	4.000	.795		
1	4.94	4.000	.810		
$Y_xPr_{1-x}Co_3Ni_2$				am; ann 1/2 h @ 1000°C, 4 h @ 400°C	
x = 0	5.00	4.000	.800		
.4	4.94	3.990	.808		
1	4.92	3.980	.809		
$Y_{1-x}Sm_xCo_5$				am several times	94
x = 0	~4.95	~3.980	.804		
.6	~4.96	~4.000	.806		
1	~4.97	~4.000	.805		
	a peaks around x = .6 and drops off while c increases gradually to x = .6 and then increases rapidly				
$LaCo_5$	5.105	3.996	.777	am only	89
	5.107	3.972	.778	am; ann 6-40 h @ 1100-1180°C	28
	5.100	3.968	.778	am; ann 3 d @ 1000°C (80% Co)	95
	5.108	3.976	.778	ns	87

STRUCTURAL TYPE - $CaCu_5$ (continued)

Composition	Lattice Parameters a(Å)	c(Å)	c/a	Method of Preparation	Ref.
$LaNi_5$	5.013	3.984	.745	ns	87
$LaCu_5$	5.184	4.112	.793		
$LaPt_5$	5.386	4.378	.815		
$LaZn_5$	5.427	4.225	.778		
$CeFe_5$	4.900	4.136	.844		
$CeCo_5$	4.926	4.020	.816	lim and quench	88
	4.920	4.030	.819	am; ann 7-14 d @ 900°C 1-3 w @ 500-1150°C	26
	4.922	4.016	.816	am only	89
Co rich	4.922	4.030	.819	am; ann 6-40 h @ 1100-1180°C	28
$CeCo_{5+x}$				am; ann 1-5 w @ 950°C for Co >80% and 1-2 w @ 1000-1100°C for Co <80% 1-5 w @ 950°C	96
x = .1 to .9	4.933	4.015	.8134		
$CeNi_5$	4.875	4.010	.823	ns	87
$CeCu_5$	5.146	4.108	.798		
$CeZn_5$	5.4163	4.2647	.787		
$CePt_5$	5.369	4.385	.817		
$CeCo_3B_2$	5.061	3.038	.600		97
	5.057	3.036	.600		91
$Ce_xLa_{1-x}Co_5$				am; ann 1-5 w @ 950°C if >80% Co; ann 1-2 w @ 1000-1100°C if <80% Co	96

STRUCTURAL TYPE - $CaCu_5$ (continued)

Composition	Lattice Parameters a(Å)	c(Å)	c/a	Method of Preparation	Ref.
x = 1	5.117	3.975	.770		96
0	4.933	4.019	.815		
$PrCo_5$	5.024	3.988	.794	lim	88
	5.010	4.000	.798	am; ann 7-14 d @ 900°C, 1-3 w @ 500-1150°C	26
	5.013	4.000	.798	am; ann 6-40 h @ 1100-1180°C	28
	5.013	3.980	.794	am only	89
	5.010	3.990	.796	ns	87
$PrNi_5$	4.958	3.980	.803		
$PrCu_5$	5.122	4.109	.802		
$PrPt_5$	5.353	4.386	.819		
$Pr_{.167}Co_{.833-x}Al_x$				im only	98
x = 0	5.012	3.998	.7977		
.05	5.027	4.013	.7984		
.10	5.041	4.039	.8012		
.15	5.062	4.059	.8011		
.20	5.084	4.059	.7984		
$Pr_xSm_{1-x}Co_5$				am only	99
x = 0	5.000	3.980	.796		
.6	5.020	4.000	.797		
1	5.020	3.980	.793		

STRUCTURAL TYPE - $CaCu_5$ (continued)

Composition	Lattice Parameters a(Å)	c(Å)	c/a	Method of Preparation	Ref.
$NdCo_5$	5.012	3.978	.794	lim	88
	5.000	3.980	.796	am; ann 7-14 d @ 900°C, 1-3 w @ 500-1150°C	26
	5.002	3.988	.797	am; ann 6-40 h @ 1100-1180°C	28
	5.020	3.977	.792	am only	89
	5.026	3.975	.791	ns	87
$NdNi_5$	4.948	3.977	.804		
	4.926	3.957	.803	am; ann @ 700°C	66
Nd_2Ni_{17}	4.922	3.963	.805	am; ann @ 900°C	
	4.886	3.987	.816	am; ann @ 1150°C	
$NdCu_5$	5.104	4.107	.805	ns	87
$NdPt_5$	5.345	4.391	.822		
$SmCo_5$	5.004	3.969	.793	am only	89
	4.989	3.978	.797	lim	88
	4.978	3.974	.798	am; ann 6-40 h @ 1100-1180°C	28
	5.004	3.971	.794	ns	87
Sm rich	4.995	3.965	.794	am only	70
Co rich	4.939	4.008	.812		
Sm rich	5.005	3.960	.791	am; ann @ 800°C cooled slowly	
Co rich	4.998	3.967	.794		
Sm rich	5.010	3.975	.793	im only	71

STRUCTURAL TYPE - $CaCu_5$ (continued)

Composition	Lattice Parameters a(Å)	c(Å)	c/a	Method of Preparation	Ref.
Co rich	4.957	4.006	.808		71
$SmCo_{4.9}$	5.003	39707	.794	am only	29
Sm_2Co_{17}	4.8561	4.0813	.840	am only	100
$SmNi_5$	4.924	3.974	.807	ns	87
$SmCu_5$	5.07	4.099	.808		
$SmCo_3B_2$	5.059	3.019	.597		91
$Sm_{.167}Co_{.833-x}Al_x$				im only	98
x = 0	4.957	3.998	.8078		
.05	4.984	4.008	.8041		
.10	5.012	4.023	.8027		
.15	5.027	4.039	.8035		
.20	5.041	4.065	.8063		
$GdFe_5$	5.000	4.100	.820	ns	87
$GdCo_5$	4.970	3.970	.799		
	4.971	3.985	.802	am; ann 6-40 h @ 1100-1180°C	28
	4.973	3.969	.798	am only	13
	4.904	4.018	.819	am; ann @ 1300°C	
	4.976	3.973	.798	lim	88
	4.973	3.969	.798	am only	89
$GdCo_x$				am; ann @ 1200°C	101
x = 4.6	4.980	3.970	.797		

STRUCTURAL TYPE - $CaCu_5$ (continued)

Composition	Lattice Parameters a(Å)	c(Å)	c/a	Method of Preparation	Ref.
5.4	4.960	3.990	.804		101
6.2	4.940	4.000	.810		
$GdCo_5$				im only	71
Gd rich	4.977	3.967	.797		
Co rich	4.960	3.989	.804		
$GdNi_5$	4.899	3.973	.811	ns	87
$GdCu_5$	5.018	4.117	.820		
$GdCo_3B_2$	5.059	3.019	.597		91
$GdCo_{5-x}Al_x$				lim only	102
x = 0	4.980	3.980	.799		
.25	5.000	3.990	.798		
1.00	5.010	4.040	.806		
1.50	5.040	4.060	.806		
1.75	5.050	4.070	.806		
$GdCo_{5-x}Cu_x$				lim only	
x = 0	4.980	3.980	.799		
.5	4.990	3.990	.800		
1.0	4.980	4.000	.803		
2.0	5.000	4.020	.804		
3.0	5.010	4.040	.806		
4.0	5.020	4.070	.811		
4.2	5.030	4.080	.811		

STRUCTURAL TYPE - $CaCu_5$ (continued)

Composition	Lattice Parameters a(Å)	c(Å)	c/a	Method of Preparation	Ref.
$TbCo_5$	4.990	3.988	.800	am only	89
	4.946	3.980	.805	lim	88
	4.947	3.982	.805	ns	87
$TbCo_{5.1}$	4.950	3.979	.804	am only	89
$TbNi_5$	4.894	3.966	.810	ns	87
$TbCu_5$	4.960	4.150	.837		
$TbCo_3B_2$	5.048	3.010	.596		97
$TbCo_3B_2$	5.048	3.005	.595		91
$DyFe_5$	4.900	4.100	.837	ns	87
$DyCo_5$	4.926	3.988	.810		
	4.933	3.983	.807	lim	88
$DyCo_{5.2}$	4.897	4.007	.819	am; 1130°C	89
$DyNi_5$	4.869	3.969	.815	ns	87
$DyCo_3B_2$	5.033	3.015	.599		97
	5.028	3.015	.600		91
$HoFe_5$	4.860	4.100	.844	ns	87
$HoCo_5$	4.910	3.996	.814		
	4.911	3.993	.813	lim	88
Co rich	4.901	4.011	.818	am; ann 6-40 h @ 1100-1180°C	28
$HoCo_{5.5}$	4.881	4.006	.821	am only	95
Ho rich	4.903	3.996	.815	held near melting point and quenched	

STRUCTURAL TYPE $CaCu_5$ (continued)

Composition	Lattice Parameters a(Å)	c(Å)	c/a	Method of Preparation	Ref.
Co rich	4.875	4.014	.823		95
$HoCo_{5.5}$	4.881	4.006	.821	am; 1150°C	89
$HoNi_5$	4.871	3.966	.814	ns	87
$HoCu_5$	4.960	4.016	.814		
$HoCo_3B_2$	5.017	3.024	.603		97
	5.026	3.029	.603		91
$Er_{.86}Co_{5.14}$	4.870	4.002	.823	am; ann 1000°C	79
$ErCo_5$	4.883	4.007	.821	lim	88
Co rich	4.883	4.015	.822	am; ann 6-40 h @ 1100-1180°C	28
$ErCo_{6.0}$	4.870	4.002	.822	am; 1150°C	89
$ErCo_5$	4.885	4.002	.819	ns	87
$ErNi_5$	4.856	3.966	.817		
	4.854	3.964	.817	am only	80
Ni rich	4.827	3.974	.823		
$ErCo_3B_2$	5.005	3.029	.604		97
	5.003	3.024	.604		91
$TmCo_5$	4.863	4.017	.826	lim	88
$TmCo_3B_2$	4.999	3.019	.604		97
	4.991	3.019	.605		91
$YbNi_5$	4.841	3.965	.819	ns	87
	4.847	3.962	.817	Solid state vapor phase reaction 3 w @ 800°C or 5 m @ 1200°C and 3 w @ 700-800°C in Mo crucible	81

STRUCTURAL TYPE - $CaCu_5$ (continued)

Composition	Lattice Parameters a(Å)	c(Å)	c/a	Method of Preparation	Ref.
$YbCo_3B_2$	4.985	3.020	.606		97
$LuCo_3B_2$	4.959	3.035	.612		91

STRUCTURAL TYPE - Th_2Ni_{17}

Composition	Lattice Parameters a(Å)	c(Å)	c/a	Method of Preparation	Ref.
Y_2Fe_{17}	temp. dependent study			lim; ann 3 d @ 950°C	94
4.2°K	8.46	8.35	.987		
300°K	8.46	8.30	.981		
900°K	8.51	8.33	.979		
Y_2Co_{17}	8.35	8.14	.975	lim only	62
Y_2Co_{17}	temp. dependent study			lim; ann 3 d @ 950°C	94
4°K	8.33	8.12	.975		
300°K	8.34	8.14	.976		
900°K	8.40	8.18	.974		
Y_2Ni_{17}	8.31	8.04	.968	lim; ann 500-800°C	103
	8.30	8.04	.969	ns	104
	8.34	8.08	.969	ns	87
Y_2Ni_{17}	temp. dependent study			lim; ann 3 d @ 950°C	94
4°K	8.29	8.01	.966		
300°K	8.30	8.04	.969		
900°K	8.37	8.09	.967		
$Y_x(Fe_{1-x}Co_x)_{17}$				lim only	105
x = 0	~8.48	~8.30	.979		
.3	~8.47	~8.30	.980		
1	~8.33	~8.15	.978		

a curves continuously downwards and c peaks near x = .3 and approximately linear between these points

STRUCTURAL TYPE - Th_2Ni_{17} (continued)

Composition	Lattice Parameters a(Å)	c(Å)	c/a	Method of Preparation	Ref.
$Y_2Ni_{17-x}Cu_x$				lim; ann 800-950°C	106
x = 0	~8.310	~8.040	.968		
5.8	~8.375	~8.130	.971		
	a and c are linear between these points				
Ce_2Fe_{17}(d)	8.490	8.281	.775	ann 2-3 w @ 900°C then 1 w @ 600°C	107
Ce_2Co_{17}	8.335	8.102	.972	lim; ann 400 h @ 800°C slowly cooled (4h)	108
Ce rich	8.378	8.148	.9726	am; ann 1-2 w	96
Co rich	8.400	8.151	.9703	@ 1000-1100°C	
Ce_2Co_{17}	8.370	8.140	.969	ns	87
Nd_2Ni_{17}	8.402	8.048	.958	am; ann @ 1250°C	66
	8.440	8.120	.962	lim; ann 500-800°C pure Ni present	103
Sm_2Ni_{17}	8.380	8.105	.967	lim; ann 500-800°C	
	8.470	8.060	.952	ns	104
Gd_2Fe_{17}	8.500	8.350	.984	lim; ann 500-800°C	103
Gd_2Fe_{17}	temp. dependent study			lim; ann 3 d @ 950°C	94
4.2°K	8.480	8.370	.987		
300°K	8.490	8.340	.982		
450°K	8.500	8.330	.980		
900°K	8.530	8.350	.979		
Gd_2Co_{17}				am; quenched from 1300°C	13
Gd rich	8.418	8.073	.959		

STRUCTURAL TYPE - Th_2Ni_{17} - (continued)

Composition	Lattice Parameters a(Å)	c(Å)	c/a	Method of Preparation	Ref.
Co rich	8.353	8.140	.975		13
Gd_2Co_{17}	8.370	8.140	.973	ns	87
Gd_2Ni_{17}	8.180	8.470	1.035		
	8.330	8.060	.968	lim; ann 500-800°C	103
	8.430	8.040	.954	ns	104
Tb_2Ni_{17}	8.300	8.040	.969	lim; ann 500-800°C	103
	8.310	8.040	.968	ns	104
$Tb_{.105}Fe_{.895-x}Al_x$				im only	5
x = 0	8.451	8.298	.984		
.05	8.465	8.320	.983		
.10	8.506	8.342	.981		
,15	8.532	8.349	.978		
Dy_2Fe_{17}	8.450	8.290	.980		82
Dy_2Fe_{17}				am; ann @ 900°C cooled slowly	17
Dy rich	8.453	8.287	.980		
Fe rich	8.446	8.291	.982		
Dy_2Co_{17}	8.335	8.102	.972	lim; ann 400 h @ 800°C cooled slowly (4h)	108
Dy_2Ni_{17}	8.290	8.020	.967	lim; ann 500-800°C	103
	8.290	8.030	.969	ns	104
$Dy_2Fe_{12}Al_5$	8.590	8.420	.980		82
Ho_2Co_{17}	8.335	8.101	.973	lim; ann 400 h @ 800°C and cooled slowly (4h)	108

STRUCTURAL TYPE - Th_2Ni_{17}-(continued)

Composition	Lattice Parameters a(Å)	c(Å)	c/a	Method of Preparation	Ref.
Ho_2Co_{17}	8.331	8.117	.974	lim; ann 72 h @ 1000°C	109
	8.320	8.113	.975	am; ann 24 h @ 1000°C	77
$HoCo_{5.5}$-Ho_2Co_{17}	8.337	8.083	.970	slowly cooled	
Ho_2Co_{17}-Co	8.319	8.115	.975		
$HoCo_{5.5}$-Ho_2Co_{17}	8.356	8.079	.967	quenched from melt	
Ho_2Co_{17}-Co	8.319	8.115	.975		
Ho_2Ni_{17}	8.280	8.020	.969	lim; ann 500-800°C	103
	8.290	8.020	.967	ns	104
Er_2Co_{17}	8.301	8.100	.976	lim; ann 400 h @ 800°C cooled slowly (4h)	108
	8.310	8.113	.976	am; ann 1000°C	79
Er_2Ni_{17}	8.287	8.017	.967	am; ann 1 w @ 1000°C	80
	8.280	8.010	.967	ns	104
	8.250	8.000	.970		
$Er_2(Co_{1-x}Fe_x)_{17}$				am only	110
x = 0	~8.330	~8.120	.975		
.8	~8.420	~8.360	.993		
1	~8.460	~8.300	.981		
	a has a slight curvature while c is linear to a peak at x = .8 then slopes downward				
$Er_2(Co_{1-x}Ni_x)_{17}$					
x = 0	~8.320	~8.120	.976		
.6	~8.330	~8.070	.969		

STRUCTURAL TYPE - Th_2Ni_{17}- (continued)

Composition	Lattice Parameters a(Å)	c(Å)	c/a	Method of Preparation	Ref.
x = 1	~8.310	~8.070	.971		110
	a curves continuously while c is linear and then flat				
Tm_2Co_{17}	8.285	8.095	.977	lim; ann 400 h @ 800°C slowly cooled (4h)	108
Tm_2Ni_{17}	8.250	8.008	.971	ns	104
	8.250	8.000	.970	lim; ann 500-800°C	103
Yb_2Co_{17}	8.309	8.096	974	Solid state reaction @ 800°C for 3 w or 5 m @ 1200°C and 3 w @ 700-800°C in Mo crucible	81
	8.250	8.005	.970	lim; ann 500-800°C pure Ni present	103
Lu_2Fe_{17}	temp. dependent study			lim; ann 3 d @ 950°C	94
4.2°K	8.380	8.340	.995		
300°K	8.380	8.290	.989		
900°K	8.450	8.320	.985		
Lu_2Co_{17}	8.247	8.093	.981	lim; ann 400 h @ 800°C slowly cooled (4h)	108
Lu_2Ni_{17}	8.210	7.995	.9730	lim; ann 500-800°C	103
$LuFe_x$				im and indirect zone melting	111
x = 7.5	8.403	8.385	.9980		
8.0	8.403	8.385	.9980		
8.5	8.401	8.386	.9980		
9.0	8.377	8.393	1.000		

STRUCTURAL TYPE - Th_2Ni_{17} - (continued)

Composition	Lattice Parameters a(Å)	c(Å)	c/a	Method of Preparation	Ref.
9.5	8.387	8.408	1.003		111
10.5	8.388	8.406	1.002		

STRUCTURAL TYPE - Th_2Zn_{17}

Composition	Lattice Parameters a(Å)	c(Å)	c/a	Method of Preparation	Ref.
Y_2Co_{17}	8.331	12.186	1.460	im; ann 200 h @ 800°C	82
$Y_2(Fe_1\ Co)_{17}$				low temperature phase	105
x = 0	~8.490	~12.390	1.460		
.3	~8.460	~12.420	1.470		
1	~8.360	~12.200	1.460		
	.3 is the approximate peak of both a and c				
$(Y\ Sm_1)_2Co_{17}$				am only	110
x = 0	~8.420	~12.220	1.450		
1	~8.370	~12.210	1.460		
	a and c are linear between the endpoints				
$Ce_2Fe_{17}(B)$	8.490	12.416	1.460	am; ann several w @ 1000°C	107
	8.335	12.153	1.458	lim; ann 400 h @ 800°C, coolec slowly (4h)	108
Pr_2Fe_{17}	8.585	12.464	1.450	am; ann 24 h @ 800°C	112
Pr_2Co_{17}	8.415	12.170	1.446	lim; ann 400 h @ 800°C cooled slowly (4h)	108
$Pr_{.105}Co_{.895-x}Al_x$				im only	98
x = 0	8.425	12.269	1.456		
0	8.411	12.213	1.452	im; ann 200 h @ 900°C	
.05	8.453	12.250	1.449		
.10	8.467	12.374	1.462		
.15	8.478	12.485	1.473		
.20	8.481	12.572	1.482		

STRUCTURAL TYPE - Th_2Zn_{17} - (continued)

Composition	Lattice Parameters a(Å)	c(Å)	c/a	Method of Preparation	Ref.
$(Pr_xSm_{1-x})Co_{17}$				am only	110
x = 0	~8.480	~12.220	1.450		
1	~8.450	~12.230	1.450		
	a and c are linear between the endpoints				
Nd_2Co_{17}	8.441	12.181	1.443	lim; ann 400 h @ 800°C cooled slowly (4h)	108
Sm_2Fe_{17}	8.570	12.440	1.450	am only	69
Sm_2Co_{17}	8.402	12.172	1.449	lim; ann 400 h @ 800°C cooled slowly (4h)	108
Sm rich	8.460	12.150	1.440	am only	70
Co rich	8.397	12.250	1.460		
Sm rich	8.396	12.200	1.450	am; ann 800-900°C and ccoled slowly	
Co rich	8.394	12.240	1.460		
Sm rich	8.420	12.210	1.450	im only	71
Co rich	8.434	12.170	1.440		
.30	8.717	12.713	1.458	im only	
.40	8.790	12.743	1.450		
.4475	8.817	12.768	1.448		
.50	8.846	12.841	1.452		
.50	8.834	12.831	1.452	ann 200 h @ 800°C	
$Sm_2(Co_{1-x}Fe_x)_{17}$				am only	110
x = 0	~8.400	~12.220	1.450		
1	~8.570	~12.460	1.450		

STRUCTURAL TYPE - Th_2Zn_{17} - (continued)

Composition	Lattice Parameters a(Å)	c(Å)	c/a	Method of Preparation	Ref.
	a is linear while c is linear to x = .6 then increases more slowly				110
$Sm_{.105}Co_{.895-x}Al_x$				im only	98
x = 0	8.411	12.022	1.430		
0	8.411	12.022	1.430	ann 200 h @ 900°C	
.05	8.439	12.067	1.430		
.10	8.467	12.241	1.450		
.15	8.495	12.288	1.450		
.20	8.509	12.413	1.460		
$(Sm_{1-x}Gd_x)_2Ce_{17}$				am only	110
x = 0	~8.400	~12.220	1.450		
1	~8.370	~12.230	1.460		
	a and c are linear between endpoints				
Gd_2Co_{17}	8.361	12.159	1.453	lim; ann 400 h @ 800°C cooled slowly (4h)	108
	8.377	12.198	1.460		109
Gd rich	8.379	12.203	1.460	im only	71
Co rich	8.387	12.194	1.450		
	8.367	12.186	1.460	am; ann 3 d @ 1000°C	13
Tb_2Co_{17}	8.341	12.152	1.457	lim; ann 400 h @ 800°C cooled slowly (4h)	108
Dy_2Co_{17}	8.335	12.153	1.458		
$Dy_2Fe_9Al_8$	8.770	12.640	1.440		19
$Dy_2Fe_{11}Al_6$	8.640	12.570	1.440		

STRUCTURAL TYPE - Th_2Zn_{17} - (continued)

Composition	Lattice Parameters a(Å)	c(Å)	c/a	Method of Preparation	Ref.
Ho_2Fe_{17}	8.438	12.465	1.480	im; ann 1 d to 4 w @ 1100-1350°C	76

Appendix II Crystal Structure Data of the Present Work

Legend and Abbreviations

1) am indicates arc melt
2) im indicates induction melt
3) lim indicates levitation induction melt
4) ann XX time @ XX°C indicates annealing followed by duration in minutes (m) or hours (h) or days (d) or weeks (w) and temperature in degrees Centigrade (°C).
5) Compositions are given as presented by authors and are all atomic percent or stoichiometric figures.
6) ~ indicates approximate value and taken from graphs
7) If the method of preparation column is left blank the previously referred to procedure holds also for this compound.
8) ns indicates not stated

STRUCTURAL TYPE - $PuNi_3$

Composition	Lattice Parameters a(Å)	c(Å)	c/a	Method of Preparation
$Dy_{.25}Fe_{.75-x}Al_x$				im only
x = 0	5.118	29.54	4.79	
.05	5.133	24.54	4.78	
.10	5.147	24.50	4.78	

STRUCTURAL TYPE - $CeNi_3$

Composition	Lattice Parameters a(Å)	c(Å)	c/a	Method of Preparation
$Dy_{.25}Fe_{.75-x}Al_x$				im only
x = .175	5.177	16.584	3.20	
.20	5.191	16.639	3.21	
.225	5.204	16.652	3.20	
.25	5.212	16.707	3.21	
.30	5.227	16.790	3.21	

STRUCTURAL TYPE - Th_6Mn_{23}

Composition	Lattice Parameters	Method of Preparation
$Dy_{.207}Fe_{.793-x}Al_x$		im; ann 200 h @ 1000°C
x = 0	12.0564	
.05	12.0801	
.10	12.1023	
.15	12.1275	
.20	12.1494	

STRUCTURAL TYPE - $CaCu_5$

Composition	Lattice Parameters a(Å)	c(Å)	c/a	Method of Preparation
$Ce_{.167}Co_{.833-x}Al_x$				im only
x = 0	4.916	4.012	.816	
.05	4.929	4.022	.816	
.10	4.938	4.032	.816	
.15	4.999	4.079	.816	
.20	5.008	4.088	.816	
$Sm_{.167}Co_{.833-x}Si_x$				im only
x = .05	4.957	4.003	.808	
.15	4.959	3.984	.803	
.20	4.984	3.936	.790	

STRUCTURAL TYPE - $CaCu_5$

Composition	Lattice Parameters a(Å)	c(Å)	c/a	Method of Preparation
$Sm_{.167}Co_{.683}Ni_{.15}$	4.892	4.037	.825	
$Sm_{.167}Co_{.683}Ag_{.15}$	4.852	4.068	.839	
$Sm_{.167}Co_{.683}In_{.15}$	4.852	4.075	.840	
$Sm_{.133-x}Zr_xCo_{.833}$				im only
x = .034	4.921	4.016	.816	
.067	4.912	3.988	.812	
.0833	4.881	3.975	.814	
.1	4.885	3.936	.806	
.117	4.870	7.951	.811	
.134	4.873	3.872	.795	
$Tb_{.167}Co_{.833-x}Al_x$				im only
x = .10	4.963	3.947	.795	
.15	5.006	4.040	.807	

STRUCTURAL TYPE - Th_2Ni_{17}

Composition	Lattice Parameters a(Å)	c(Å)	c/a	Method of Preparation
$Sm_{.105-x}Zr_xCo_{.895}$				
x = .01	8.402	8.166	.972	im only
.02	8.352	8.163	.977	
.03	8.352	8.144	.975	
.04	8.284	8.116	.980	
$Dy_{.105}Fe_{.895-x}Al_x$				im only
x = .20	8.572	8.386	.978	
.25	8.618	8.394	.974	

STRUCTURAL TYPE - Th_2Zn_{17}

Composition	Lattice Parameters a(Å)	c(Å)	c/a	Method of Preparation
$Sm_{.105}Fe_{.895-x}Al_x$				im only
x = 0	8.545	12.477	2.460	
.05	8.681	12.509	1.441	
.05	8.581	12.477	1.454	ann 200 h @ 800°C
.10	8.608	12.531	1.456	im only
.20	8.671	12.537	1.446	
.20	8.657	12.607	1.456	ann 200 h @ 800°C
.30	8.717	12.713	1.458	im only
.40	8.790	12.743	1.450	
.4475	8.817	12.768	1.448	
.50	8.846	12.841	1.452	
.50	8.834	12.831	1.452	ann 200 h @ 800°C
$Gd_{.105}Fe_{.895-x}Al_x$				im only
x = .4	8.758	12.698	1.450	
.5	8.820	12.794	1.451	
$Dy_{.105}Fe_{.895-x}Al_x$				im only
x = 0	8.455	12.463	1.474	
.05	8.480	12.496	1.471	
.10	8.507	12.510	1.456	
.15	8.538	12.540	1.456	
.30	8.663	12.611	1.449	
.4475	8.769	12.702	1.450	

APPENDIX III

MAGNETIC DATA OF OTHER RESEARCHERS

Legend and Abbreviations

1) T_c indicates Curie temperature given in degrees Kelvin
2) T_p indicates compensation point temperature given in degrees Kelvin
3) H_c/H_a indicates coercive field and or anisotropy field given in kiloOersteds
4) M_s indicates saturation magnetization given in Bohrmagnetons per formula unit
5) Type indicates type of ordered state;
   a) F represents ferromagnetic
   b) F_i represents ferrimagnetic

$PuNi_3$ Isotypes: General Magnetic Data

Composition	T_c	T_p	H_c/H_a	M_s	Type	Ref.
YCo_3	310			1.62	F_i	62
	301			1.4	F_i	64
$Y_{1-x}Th_xFe_3$						67
x = .00	490					
.10	531					
.30	536					
.35	521					
.40	517					
.45	516					
.50	515					
.70	499					
.90	462					
1.00	437					
$CeCo_3$	78			.2	F	113,14
$PrCo_3$	349			3.8	F	
$PrNi_3$	20			1.57	F	
$NdCo_3$	395			5.6	F	
$HoNi_3$	27			1.88	F	
$GdFe_3$	725	615		1.6	F_i	27
$GdCo_3$	612			2.2	F_i	113,14
			36.5			13

$PuNi_3$ Isotypes: General Magnetic Data (continued)

Composition	T_c	T_p	H_c/H_a	M_s	Type	Ref.
$GdNi_3$	118			6.50	F_i	114
$TbFe_3$	655	595		3.6	F_i	27
$Tb_{.25}Fe_{.75-x}Al_x$					F_i	5
x = 0				2.62		
.05				3.44		
.10				3.77		
.15				4.23		
.20				5.06		
.25				5.48		
$TbCo_3$	506			3.4	F_i	113,14
$TbNi_3$	98			6.84	F_i	115
$DyFe_3$	605	545		4.6	F_i	27
$DyFe_{3-x}Ni_x$					F_i	116
x = .5	478	388		4.70		
1.0	401			5.60		
2.0	385			6.63		
2.5	276			7.05		
3.0	66			7.10		
$Py_{1-x}Th_xFe_3$						68
x = 0	609	560				
.1	605	470				
.2	588	420				

$PuNi_3$ Isotypes: General Magnetic Data (continued)

Composition	T_c	T_p	H_c/H_a	M_s	Type	Ref.
.5	555			5.9		115
1.0	513			5.30		
2.0	203			6.80		
2.5	165			7.50		
3.0	65			8.54		
$HoCo_3$	418			5.6	F_i	113,14
$HoCo_{3-x}Ni_x$					F_i	115
X = 0	418			5.3		
.5	142			6.6		
1.0	98			7.74		
1.5	79			8.20		
2.5	71			8.14		
$HoNi_3$	66			7.84	F_i	114
$ErFe_3$	555	250		3.5	F_i	27,119
$ErCo_3$	401			3.9	F_i	113,14
$ErNi_3$	62			5.77	F_i	114
	66			6.4		62
$TmFe_3$	535			1.6	F_i	27
$TmCo_3$	370			3.0	F_i	113,14
$TmNi_3$	43			3.86	F_i	114,118
$Lu_{1-x}Th_xFe_3$						67

$PuNi_3$ Isotypes: General Magnetic Data (continued)

Composition	T_c	T_p	H_c/H_a	M_s	Type	Ref.
.3	573	290				68
.4	564					
.5	511					
.6	534					
.7	526					
.8	513					
.9	484					
1.0	437					
$DyCo_3$	450			4.3	F_i	113,14
$DyCo_{3-x}Ni_x$					F_i	115
x = 0	455			3.78		
$DyCo_{3-x}Ni_x$					F_i	
x = .5	303			5.00		
1.0	155			5.25		
1.5	111			5.80		
2.0	84			5.85		
$DyNi_3$	69			7.0	F_i	117,118
$HoFe_3$	566	383		4.2	F_i	73
	575	395				27
$HoFe_{3-x}Ni_x$					F_i	115
x = 0	565	350		4.8		

$PuNi_3$ Isotypes: General Magnetic Data (continued)

Composition	T_c	T_p	H_c/H_a	M_s	Type	Ref.
x = 0	535					67
.1	531					
.3	535					
.4	531					
.45	531					
.5	530					
.55	530					
.7	502					
.9	464					
1.0	437					
$LuCo_3$	362			1.80		62

Th_6Mn_{23} Isotypes: General Magnetic Data

Composition	T_c	T	H_c/H_a	M_s	Type	Ref.
Y_6Fe_{23}	484			37.8	F	120
Y_6Mn_{23}	486			12.4		121,122
Nd_6Fe_{23}	492				F_i	15
Nd_6Mn_{23}	437			9.6	F_i	123
Sm_6Mn_{23}	439			3.0	F_i	121,123
Gd_6Fe_{23}	468					120,115
Gd_6Mn_{23}	473			50.2	F	121,123
Tb_6Fe_{23}	574					15
Tb_6Mn_{23}				45.0	F_i	123
Dy_6Fe_{23}	524					15
Dy_6Mn_{23}	443			51.6		123
Ho_6Fe_{23}	501					15
Ho_6Mn_{23}	434			49.8	F_i	15,121,123
Er_6Fe_{23}	493			7.2	F_i	15,123,124
Er_6Mn_{23}	415			46.2	F_i	121,123
Tm_6Fe_{23}	475					15
Tm_6Mn_{23}				31.8		123
Lu_6Fe_{23}	471					15
Lu_6Mn_{23}				9.2		123

$CaCu_5$ Isotypes: General Magnetic Data

Composition	T_c	T_p	H_c/H_a	M_s	Type	Ref.
YCo_5	978			7.9		125
			2.6/130	7.5		89
	921		6.7/130			
	977			6.8		88
$Y_{.6}La_{.4}Co_5$	923					
$Y_{.6}La_{.4}Fe_{.5}Co_{4.5}$	923					
$Y_{.6}La_{.4}Fe_{.65}Co_{4.35}$	948					
$Y_{.6}La_{.3}Fe_{.8}Co_{4.8}$	948					
$LaCo_5$	840		3.6/175	7.1		126
$CeFe_{.5}Co_{3.8}Cu_{.9}$			7			127
$CeCo_5$	647		2.8/190			126
	737					88
			2.8/180	5.5		89
	673			6.6		125
$Ce_{.167}Co_{.633}Al_{.2}$			1			
$PrCo_5$	885		5.8/177			126
	912			9.9		88
$PrCo_5$	921			10.4		125
			5.8/145	9.0		89
$Pr_{1-x}Dy_xCo_5$						128
$x = 0$	912			10.0		

$CaCu_5$ Isotypes: General Magnetic Data (continued)

Composition	T_c	T_p	H_c/H_a	M_s	Type	Ref.
.2	955			8.0		128
.4	955			5.7		
.6	960			3.3		
.8	975			1.4		
1.0	966			1.6		
$NdCo_5$	913			10.4		125
	910			9.5		88
			.7/230	9.1		89
$Nd_{1-x}Gd_xCo_5$						128
x = 0	910			11.7		
.2	950			8.5		
.4	965			7.0		
.6	1000			5.6		
.8	1000			3.2		
1.0	1008			1.3		
$Nd_{1-x}Dy_xCo_5$						
x = .2	920			8.6		
.4	930			7.8		
.6	940			7.3		
.8	950			1.6		
.85				.8		
.9				.5		

$CaCu_5$ Isotypes: General Magnetic Data (continued)

Composition	T_c	T_p	H_c/H_a	M_s	Type	Ref.
$Nd_{1-x}Gd_xNi_5$						129
x = 0	14			2.2		
.2	16			1.3		
.3				1.2		
.4	28			1.3		
.5	29			2.4		
.6	28			3.1		
.8	31			4.8		
1.0	33			6.7		
$Hd_{1-x}Ho_xNi_5$						
x = 0	63			2.2		
.2	63			3.2		
.4	68			3.1		
.6	66			4.7		
.8	69			6.4		
1.0	73			8.8		
$SmCo_5$	1000					130
	997		25/250			126
				7.8		131,115,117
				7.8		
			713/210	7.2		89

$CaCu_5$ Isotypes: General Magnetic Data (continued)

Composition	T_c	T_p	H_c/H_a	M_s	Type	Ref.
$Sm_{.167}Co_{.833-x}Al_x$						4
x = .15						
.20						
$GdCo_5$	1008		23.5	1.2		88
	1013			1.4		132
			13/270	2.6		89
$GdCo_{5-x}Al_x$						102
x = 0				1.6		
.25				1.1		
1.0				2.2		
1.5				4.0		
1.8				4.9		
$GdCo_{5-x}Cu_x$						
x = 0				1.6		
.5				1.7		
1.0				1.5		
2.0				2.5		
3.0				4.4		
4.0				6.3		
4.2				6.4		
$Gd_xDy_{1-x}Co_5$						128
x = .2	1000			.9		

$CaCu_5$ Isotypes: General Magnetic Data (continued)

Composition	T_c	T_p	H_c/H_a	M_s	Type	Ref.
.4	1000			.5		128
.6	1000			.5		
.8	1005			1.1		
$Gd_xHo_{1-x}Co_5$						
x = 0	1000			1.9		
.2	1010			1.0		
.4	1010			1.3		
$Gd_xHo_{1-x}Co_5$						
x = .6	1015			1.4		
.8	1010			1.6		
$GdNi_5$	28			6.9		133,134
	33			6.8		135
$Gd_xDy_{1-x}Ni_5$						129
x = 0	29			8.9		
.2	26			8.4		
.4	31			8.3		
.6	32			7.5		
.8	37			7.1		
1.0	32			6.7		
$Gd_xHo_{1-x}Ni_5$						
x = 0	23			8.3		
.2	19			8.0		

$CaCu_5$ Isotypes: General Magnetic Data (continued)

Composition	T_c	T_p	H_c/H_a	M_s	Type	Ref.
.4	25			7.8		129
.6	28			7.4		
.8	34			7.2		
1.0	30			6.7		
$TbCo_5$	980			.6		88
	987			.7		132
$TbCo_{5.1}$			2.1	1.7		89
$DyCo_5$	966			.7		88
	998			1.7		132
$DyCo_{5.2}$			1.0/25	3.2		89
$HoCo_5$	1036			2.1		132
	1000			1.1		88
$HoCo_{5.5}$			4.3/135	4.6		89
$ErCo_5$	1066			1.7		132
	1000			1.1		88
$ErCo_6$			5.5/100	5.6		89
$ErNi_5$	12			7.7		80
$TmCo_5$	1020			1.9		88
$TmNi_5$	22			6.7		135

Th_2Ni_{17} Isotypes: General Magnetic Data

Composition	T_c	T_p	H_c/H_a	M_s	Type	Ref.
Y_2Fe_{17}	244			34.2	F	14,62
Y_2Co_{17}	1167			26.9	F	103
Y_2Ni_{17}	621			4.67	F	106
$Y_2Ni_{17-x}Cu_x$						
x = 0	610			4.70		
.38	600			4.25		
1	550			2.15		
2	470			1.00		
2.5	415			.85		
3	310			.70		
3.8	210			.30		
4.75				.10		
Ce_2Fe_{17}	270			30.6		107
Ce_2Co_{17}	1083			26.1		14
Pr_2Fe_{17}	290					119
Nd_2Fe_{17}	326					
Sm_2Co_{17}	1190			20.1		14
Sm_2Ni_{17}	641			5.25		103
Gd_2Fe_{17}	466			21.2	F_i	
Gd_2Co_{17}	1209			14.4	F_i	14
Cd_2Ni_{17}	623	140		9.36	F_i	103

Th_2Ni_{17} Isotypes: General Magnetic Data (continued)

Composition	T_c	T_p	H_c/H_a	M_s	Type	Ref.
Tb_2Fe_{17}	408			16.8	F_i	103
$Tb_{1.105}Fe_{8.895-x}Al_x$					F_i	136
x = 0				18.8		
.05				14.1		
.10				13.3		
.15				9.9		
Tb_2Co_{17}	1180			10.7		14
Tb_2Ni_{17}	615	125		12.2	F_i	103
Dy_2Fe_{17}	380			15.9	F_i	17
Dy_2Co_{17}	1152			8.3		14
Dy_2Ni_{17}	604	101		14.7		103
Ho_2Fe_{17}	325			15.0		
Ho_2Co_{17}	1173			7.7		14
$Ho_2Co_{17-x}Mn_x$						137
x = 0	1173			9.3		
1				8.9		
2				8.5		
3				7.15		
4				3.6		
5				1.8		
6				6.2		

Th_2Ni_{17} Isotypes: General Magnetic Data (continued)

Composition	T_c	T_p	H_c/H_a	M_s	Type	Ref.
$H_2Co_{17-x}Ru_x$						137
x = 0	1173					
1						
2	933					
3	763					
4	593					
5	433					
6	298					
Ho_2Ni_{17}	611	70		13.8		103
Er_2Fe_{17}	299			18.0	F_i	16
$Er_2(Co_{1-x}Fe_x)_{17}$				16.2	F_i	110
x = 0	1200			21.5		
.2	1150			23.7		
.4	1050			25.9		
.5				27.7		
.6	900			28.0		
.8	650			27.6		
.9				22.6		
1.0	300			16.8		
Er_2Co_{17}	1186			10.1	F_i	14
$Er_2(Co_{1-x}No_x)_{17}$						110

Th_2Ni_{17} Isotypes: General Magnetic Data (continued)

Composition	T_c	T_p	H_c/H_a	M_s	Type	Ref.
x = 0	1200			21.5		110
.1	1180			19.1		
.2	1100			17.4		
.3				16.0		
.4	1000			14.3		
.5				12.4		
.6	640			11.2		
.8	400			7.6		
1.0	0			2.4		
Er_2Ni_{17}	602	51		11.00		103
Tm_2Fe_{17}	233					16
Tm_2Co_{17}	1182			11.3		14
Tm_2Ni_{17}	603	20		7.31		103
Tm_2Co_{17}	1182			11.3		14
Lu_2Fe_{17}	238			33.8		
	263					
Lu_2Co_{17}	1192			30.6		62
Lu_2Ni_{17}	601			5.0		103

Th_2Zn_{17} Isotypes: General Magnetic Data

Composition	T_c	T_p	H_c/H_a	M_s	Type	Ref.
$Y_2Co_{17-x}Mn_x$						137
x = 0	1167			27.8		
1				28.3		
2				27.0		
3	838			23.5		
4	663			19.0		
5	483			14.3		
6	358			9.4		
$Y_2Co_{17-x}Ru_x$						
x = 0	1167			27.8		
1				24.9		
2	893			22.0		
3	753			18.8		
4	623			15.4		
5	423			11.5		
6	298			8.0		
$(Y_xSm_{1-x})_2Co_{17}$						110
x = .00	1200			26.1		
.25	1200			27.3		

Th_2Zn_{17} Isotypes: General Magnetic Data (continued)

Composition	T_c	T_p	H_c/H_a	M_s	Type	Ref.
x = .50	1200			27.1		110
.75	1200			26.9		
1.00	1200			26.8		
Pr_2Co_{17}	1171			31.0		14
$(Pr_xSm_{1-x})_2Co_{17}$						110
x = 0	1200			26.1		
.2	1200			27.2		
.4	1200			28.0		
.6	1200			29.3		
.8	1200			30.0		
1.0	1200			30.6		
Nd_2Co_{17}	1150			30.5		14
$Sm_2(Co_{1-x}Fe_x)$						110
x = 0	1200			26.1		
.1	1200					
.2	1190			29.6		
.3	1180			32.0		
.4	1170			33.9		
.5				35.2		
.6	1000			35.9		
.7	900			35.8		

Th_2Zn_{17} Isotypes: General Magnetic Data (continued)

Composition	T_c	T_p	H_c/H_a	M_s	Type	Ref.
x = .8	800			35.6		110
.9	600					
1.0	400			33.1		
$(Sm_{1-x}Gd_x)_2Co_{17}$						
x = 0	1200			26.1		
.25	1210			23.4		
.5	1220			21.1		
.75	1230			18.3		
.9				16.9		
1.0	1240			16.0		
Gd_2Co_{17}	1209			14.4	F_i	13

$PuNi_3$ Isotypes: Specialized Magnetic Data

$HoFe_5$ Crystallographic site moments (neutron diffraction data) Ref. 73

Site	M @ 77°K	M @ 297°K
A	8.76	5.07
C_2	9.01	5.42
B	1.88	1.41
C_1	1.43	1.12
H	1.61	1.52

$Dy_{3-x}Ni_x$ Hyperfine fields and Curie temperatures (Mossbauer data) Ref. 75

x	Fields (kOe) @ 4.2°K	Fields (kOe) H Site @ 300°K	Fields (kOe) B and C @ 300°K	T_c
0	238.43	216.94	201.21	612
.25	244.63	213.72	200.72	
.5	247.72	212.10	211.88	478
1	247.72	191.10	200.23	401
1.5	241.53	173.94	178.07	
2	216.86	126.10	129.10	285
2.5	190.44	0	0	276
2.75	179.60	0	0	
3				66

$PuNi_3$ Isotypes: Specialized Magnetic Data (continued)

YCo_3 Crystallographic site moments (neutron diffraction data) Ref. 64

Site	M @ 4.2°K		M @ 90°K	M @ 215°K
$-(A+C_2)$	-.35±.19		-.30±.22	-.07±.10
C_1	.55±.04	.55±.03	.49±.04	.18±.03
H	.83±.05	.79±.04	.78±.06	.34±.03
B	.40±.02	.40±.01	.37±.02	.17±.01
M_s	1.30±.27	1.51±.04	1.22±.33	.59±.16

Ref. 138

Composition	T (°K)	A	C_2	B	C	H
$PrCo_3$	4.2		2.4±.2	1.2±.4	.9±.2	
	295		1.1±.1	.3±.1	.5±.1	
$NdCo_3$	4.2		2.4±.4	.9±.3	1.2±.2	
	295		.8±.1	.7±.5	.7±.2	
$TbCo_3$	4.2	8.5±.5	8.1±.4	-1.9±.6	-.9±.4	-1.2±.3
	295	5.7±.2	4.8±.2	-1.3±.2	-1.4±.2	-1±.1
$HoCo_3$	4.2	10.0±.4	9.6±.3	-1.8±.4	-1.2±.3	-1.2±.2
	295	2.1±.2	3.4±.2	-.4±.2	-1.5±.3	-.6±.1
$ErCo_3$	4.2	8.2±.8	7.5±.6	-2.0±.6	-1.1±.7	-1.3±.6

$DyNi_3$ Crystallographic site moments (Mossbauer data) Ref. 117

Site	M @ 4.2°K
A	10
C_2	10

Th_6Mn_{23} Isotypes: Specialized Magnetic Data

Y_6Fe_{23} (Mossbauer Data) Ref. 85

Crystallographic Site	Hyperfine Field (kOe)
34f	300
4b	277
24d	268
32f	249

$CaCu_5$ Isotypes: Specialized Magnetic Data

YCo_5 Crystallographic Site Moments (neutron diffraction data) Ref. 64

Site	With Y Moment	Without Y Moment
A	-.40±.30	
C	1.68±.04	1.66±.04
G	1.67±.04	1.66±.04
M_s	7.97±.34	8.30±.15

$TbCo_5$ Crystallographic Site Moments (neutron diffraction data) Ref. 59

T(°K)	A Site	C Site	G Site	M_s
4.2	8.35±.55	1.55±.2	1.7±.1	.1±1.2
78	8.15±.55	1.55±.25	1.67±.25	.0±1.8
293	6.30±.55	1.35±.25	1.55±.25	1.2±1.8
348	5.75±.35	1.30±.35	1.55±.3	1.6±2.0
403	4.80±.50	1.40±.30	1.55±.3	2.7±2.0
423	4.50±.50	1.40±.30	1.50±.3	2.8±2.0
453	4.10±.55	1.45±.35	1.45±.3	2.9±2.0

$NdCo_5$ Crystallographic Site Moments (neutron diffraction data) Ref. 59

T(°K)	A Site	C and G Site	M_s
4.2	2.45±.30	1.45±.20	9.7±1.3
78	2.15±.10	1.50±.10	9.65±.6
273	1.50±.20	1.50±.15	9.00±.9
295	1.20±.10	1.50±.10	8.70±.6
340	1.10±.15	1.50±.10	8.60±.6

APPENDIX IV

MAGNETIC DATA OF THE PRESENT STUDY

Legend and Abbreviations

1) T_c indicates Curie temperature given in degrees Kelvin
2) T_p indicates compensation point temperature given in degrees Kelvin
3) H_c/H_a indicates coercive field and or anisotropy field given in kiloOersteds
4) M_s indicates saturation magnetization given in Bohrmagnetons per formula unit
5) Type indicates type of ordered state;
   a) F represents ferromagnetic
   b) F_i represents ferrimagnetic
6) * indicates powdered material

$PuNi_3$ Isotypes: General Magnetic Data

Composition	T_c	T_p	H_c/H_a	M_s	Type
$Dy_{.25}Fe_{.75-x}Al_x$					F_i
x = 0			2.32	4.64	
.05			7.06	5.08	
.10			9.43	5.08	
.125			11.8		
$CeNi_3$ Isotype for the remaining $Dy_{.25}Fe_{.75-x}Al_x$ compounds					
x = .15			10.14	5.64	
.175			10.02	5.92	
.20			9.31	5.12	
.225			10.61	5.52	
.25			11.0		
.30			9.43	8.32	

Th_6Mn_{23} Isotypes: General Magnetic Data

Composition	T_c	T_p	H_c/H_a	M_s	Type
$Dy_{.207}Fe_{.793-x}Al_x$					F_i
x = 0			1	17.98	
.05			1	22.62	
.10			3	24.07	
.15			5	25.52	
.20			5.4	26.10	

Th_2Ni_{17} Isotypes: General Magnetic Data

Composition	T_c	T_p	H_c/H_a	M_s	Type
$Sm_{.105}Zr_{.105-x}Co_{.895}$					
x = .01			.2/366	24.43	
.02			.15/232	26.15	
.03			.1/181	27.98	
.04			.1/158	28.23	
$Dy_{.105}Fe_{.645}Al_{.250}$			1.84	6.7	F_i

Th_2Zn_{17} Isotypes: General Magnetic Data

Composition	T_c	T_p	H_c/H_a	M_s	Type
$Y_{.105}Fe_{.895-x}Al_x$					
x = .4			2	9.14	
.5			2	7.66	
$Sm_{.105}Fe_{.895-x}Al_x$					
x = .00	363		.1	35.5	
.05	473		.1	31.2	
.10	482		.2	24.5	
.20	499		.2	25.7	
.30	395		.4	20.1	
.40	197		7.0	14.3	
.4475	144		13.5	10.3	
.50	129		15.0	10.1	

Th_2Zn_{17} Isotypes: General Magnetic Data

Composition	T_c	T_p	H_c/H_a	M_s	Type
$Dy_{.105}Fe_{.895-x}Al_x$					
x = 0			.5	16.3	
.05			2.6	15.8	
.10			3.7	11.0	
.15			4.9	9.9	
.30			0	3.2	
.4475			62.5	3.0	

APPENDIX V

EXPERIMENTAL PROCEDURES AND ERROR ANALYSES

The rare earth materials used for these studies were from Michigan Chemical Corporation. They were 99.9% pure with respect to the other rare earths and were better than 99.5% pure overall. The transition metals and other elements were better than 99.999% pure and came from American Scientific and Chemical of Portland.

All alloys were prepared by combining their preweighted constituents to within ± 0.00025 grams. They were then melted in an induction furnace under a flow of high purity Argon. The heavy rare earth alloys were melted in quartz crucibles while the light rare earth alloys were melted in magnesia crucibles. A few of the alloys were remelted as many as three more times to insure homogeneity of the material. These alloys were then surface cleaned and fractured. Some of the fragments were subsequently annealed in an evacuated quartz ampule on a piece of magnesia in a muffle furnace. The accuracy of these furnace temperatures was approximately ± 3% of the temperature setting. The ampules were then quenched by immersion in an ice bath. The resulting fragments were then surface cleaned before further studies were performed.

Debye-Scherrer diagrams were taken with V-filtered Cr and Fe-filtered Co radiations and calibrated by means of NaCl. The lattice parameters were determined in most cases from high angle

reflections. In a few cases computer least squares fit programs were used to determine the lattice parameters. The precision of lattice parameters are within ± 0.005 Å.

Magnetic studies were carried out on a Princeton Applied Research Foner magnetometer, which was calibrated with Ni. The saturation moments (Ms) were extrapolated from plots of the magnetic moment versus reciprocal applied field. In a few cases magnetic moments at maximum field are reported. The magnetic fields were determined within 2.5% (rated field uniformity) accuracy. Temperatures were measured with a calibrated Ge crystal to within ± .1°K. The samples were contained in fabricated nylon holders.

Curie temperature plots were obtained in a special oven with a Chromel-Alumel thermocouple. The fields for such studies were transverse to the specimen between poles of a water cooled magnet of ± 0.5% stability. The sample holders were of boron-nitride to withstand the high temperatures. Since temperature sensors were not at the sample site a temperature lag was noted especially on increasing temperature and therefore the higher accuracy was noted on cooling the specimen. The majority of the Curie temperatures were taken as the inflection points of the magnetization versus temperature on decreasing temperature. In a few cases the more accurate method as described by McGuire and Flanders[139] was used to compare with the other results. This procedure is referred to as the method of Arrott plots.

VITA

Duane Ray McNeely was born 20 December 1944, in St. Paul, Minnesota. In May of 1970 he received his Bachelor of Science degree in Physics with departmental honors at the University of Puget Sound.

In June of 1970 he began his graduate studies at the Oregon Graduate center where he received his Master of Science degree in Physics in April of 1972. In September of 1972 he was awarded a National Science Foundation Graduate Traineeship and he became a Wilson W. Clark Fellow in 1973. In October of 1976 the requirements for the degree Doctor of Philosophy were completed.

LIST OF PUBLICATIONS

1. Z.F. Danes and D. R. McNeely, "Possibility of a Layered Moon" Icarus 15, 314 (1971).

2. H. Oesterreicher and D. R. McNeely, "Low Temperature Magnetic Hardness in Substituted Samarium-Cobalt ($SmCo_5$) American Institute of Physics Conference Proceedings 24, 678 (1974).

3. H. Oesterreicher and D. R. McNeetly, "Low-Tempterature Magnetic Studies on Various Substituted Rare Earth (R)- Transition Metal (T) Compounds RT_5" J. Less-Common Metals 45, 111 (1976).

4. D. R. McNeely and H. Oesterreicher, "Structural and Low-Temperature Magnetic Studies on Compounds Sm_2Fe_{17} with Aluminum Substituted for Iron" J. Less-Common Metals 44, 183 (1976).

5. L. W. Swanson, J. T. Dickinson and D. R. McNeely, "Fabrication and Surface Characteriation of Composite Refractory Compounds Suitable for Thermionic Converters" NASA Contractor Report NASA CR-2668 (1976).